October 2019

Cold Spray Deposition of Polymers – Characterization and Optimization

Zahra Khalkhali
University of Massachusetts Amherst

COLD SPRAY DEPOSITION OF POLYMERS – CHARACTERIZATION AND OPTIMIZATION

A Dissertation Presented

by

ZAHRA KHALKHALI

Submitted to the Graduate School of the
University of Massachusetts Amherst in partial fulfillment
of the requirements for the degree of

DOCTOR OF PHILOSOPHY

SEPTEMBER 2019

Mechanical and Industrial Engineering

COLD SPRAY DEPOSITION OF POLYMERS - CHARACTERIZATION AND OPTIMIZATION

A Dissertation Presented

by

ZAHRA KHALKHALI

Approved as to style and content by:

_____

Jonathan P. Rothstein, Chair

_____

Jae Hwang Lee, Member

_____

Jessica Schiffman, Member

_____

Sundar Krishnamurty, Department Head

ACKNOWLEDGMENTS

I would like to express the deepest appreciation to my advisor and the committee chair, Professor Jonathan P. Rothstein, who has continually and kindly conveyed a spirit of enthusiasm to this research. Without his guidance and persistent help this research would not have been possible.

I would like to thank Professor John Klier, and my committee members, Professor Jae-Hwang Lee and Professor Jessica Schiffman, who enriched my research with their supportive advice and having their students do collaborative researches with me.

In addition, I would like to thank Dr. Yuan Lui, Guozhen Yang, Wanting Xie, Zimu Zhou who collaborated with me and helped me add more dimensions to my research. I thank KU LEUVEN for providing me with polymer powders. I would also want to thank Trenton P. Bush for his significant contribution to this project and Samrat Sur for his kind assistances, and Feyza Dundar for providing me with various types of polymer particles for the cold spray studies.

This research was accomplished through a cooperative research agreement with the US Army Research Laboratory.

ABSTRACT

COLD SPRAY DEPOSITION OF POLYMERS - CHARACTERIZATION AND OPTIMIZATION

SEPTEMBER 2019

ZAHRA KHALKHALI
B.Sc., IMAM KHOMEINI INTERNATIONAL UNIVERSITY, QAZVIN, IRAN
M.Sc., IRAN UNIVERSITY OF SCIENCE AND TECHNOLOGY, TEHRAN, IRAN

Directed by: Professor Jonathan P. Rothstein

The use of a supersonic gas flow to accelerate solid particles to form bonding upon impact on a substrate is known as "cold spray deposition". The kinetic energy of the impacting particles dissipates in the form of heat resulting in the thermal softening and plastic deformation of the particles. This extensive interfacial contact leads to strong bonds and entanglements between the particle and the substrate surface. The cold spray process has been commercialized for some metallic materials, but further research is required to unlock the exciting potential material properties possible with polymeric particles. In this research, a laboratory-scale cold spray system with the capability of accelerating 10 – 200 μm polymer particles up to Mach 2 was used to study the deposition behavior of a series of polymers on polymeric substrates. By systematically varying the particle temperature and impact velocity, the deposition window was developed for each particle and substrate combination in order to understand the cold spray processing conditions necessary to form coatings. Additionally, a study of deposition efficiency revealed the optimal process parameters for each particle/substrate pair yielding a deposition efficiency close to 10% for high-density polyethylene powder and providing insights into the physical mechanics responsible for bonding. The deposition efficiency approached to 57% for a polymer particle with a particular core-shell structure at specific spray conditions. For the purpose of 3-dimensional (3D) printing and conformal coatings on 3D objects, the critical angle for deposition were also analyzed for the polymer particles studied in this project depositing on an LDPE substrate. The microstructural properties of the coatings were studied using a scanning electron microscopy and the mechanical properties including nano-hardness, elastic modulus, adhesion/cohesion strength and the toughness of the cold sprayed coatings were analyzed according to the pertinent standards. A series of laser-induced single particle impact experiments was also implemented under specific conditions to mimic the cold spray process. Ultrafast photography was used to track particle flight, impact and rebound from the substrate as they were accelerated up to 500 m/s. Single particle impact studies provide a wealth of information about the particle impact dynamics including the plastic deformation of a successfully deposited particle and the coefficient of restitution of a rebounding particle

that cannot be monitored during cold spray. All studied polymer particles exhibited deposition on LDPE in the micro-ballistic single particle impact experiments at critical velocities slightly above those we obtained from the cold spray for the same pairs of particles and substrates. For all particles, the like-on-like deposition was successful in the cold spray process whereas in the laser-induced single particle impact experiments, only polyurethane particles deposited on alike substrates. The later result suggests multiple particle impacts and/or surface roughness can play a major role in the effectiveness and efficiency of the cold spray deposition process for polymers. The addition of certain amounts of sacrificial glass beads with certain particle size to the polymer particle batch was found to increase the deposition efficiency and expand the deposition window to lower particle temperatures and lower impact velocities without interfering with the coating qualities.

TABLE OF CONTENTS

Page

LIST OF TABLES

LIST OF FIGURES

Figure Page

CHAPTER 1

INTRODUCTION

1.1 Problem Statement

Cold spray is a solid-state coating process that uses a high-speed gas jet to accelerate solid powder particles toward a substrate. Upon impact with the substrate, the particles plastically deform and form strong chemical and/or mechanical bonds with the substrate to form a strong, homogeneous coating with properties comparable to the original powder and little to no porosity. The main advantage of this process over other additive manufacturing techniques like plasma spray, High Velocity Oxygen Fuel (HVOF), or laser cladding is that melting is avoided in this method which minimizes chances of oxidation and evaporation and hinders miss-matches between microstructure, expansion and other properties [1, 2]. Additionally, a technical advantage of cold spray process is that the spraying gun can be held by a robot arm and the substrate can be mounted on a three-dimension (3D) printing platform to form complex structures [3]. Cold spray has evolved into a viable additive manufacturing solution, especially for an increasing number of non-traditional applications. Additionally, as environmental, health and safety regulations are becoming progressively more stringent, interest in cold spray has grown as a potentially greener alternative because no solvent is used in this additive manufacturing process.

Since the onset of cold spray application in mid-1980s, copper, aluminum, nickel, iron, zinc, tin, and alloys of these elements have been studied extensively [1, 4, 5, 6]. There are also many studies of metallization of polymer substrates using cold spray technique, including tin cold-sprayed onto the surface of polystyrene, polyamide-6, and polypropylene or aluminum cold-sprayed onto carbon reinforced Polyether ether ketone (PEEK) [3] and copper onto Polyvinyl chloride (PVC) and other polymers [7, 8, 9]. However, investigations on the cold spray deposition of polymer particles on polymer substrates are very sparse and few [10, 11, 12, 13]. One obstacle that researchers face in their investigations on polymers, is the low deposition efficiency obtained in this process. For example, in the work of Y. Xu et al. less than 1% of the polymer particles were found to adhere to the surface [12]. This is quite different from the observations in metal cold spray where close to 100% deposition efficiency is achieved [6]. Thus, one of the main challenges in the studies of the polymer cold spray is the low deposition efficiency which wastes a great proportion of the sprayed powder material.

In metallic cold spray, it has been argued that the strong shear flow formed at the interface between the impacting particle and the substrate can remove the oxide layer from the particle/substrate interface allowing for a strong metallurgical bond to form between the freshly exposed surfaces. A variety of other bonding mechanisms have been reported for metallic deposition including mechanical interlocking [3], crack filling [14], particle/substrate modulus difference [15], interfacial flow instability [16], and adiabatic shear instability [17]. The adiabatic shear instability is regarded as the dominant bonding mechanism when significant plastic deformation occurs during impact [17]. The adiabatic assumption hypothesizes that the heat generated from the impact-induced plastic deformation does not diffuse from regions of high deformation and subsequently the high shear rate of the order of 10^9 S^{-1} can dramatically increase the interfacial temperature between the particle and the substrate material [18]. For plastic particles this adiabatic assumption is reasonable due to the low thermal conduction of the polymer. The elevated temperature, in turn, leads to thermal softening which allows for more plastic deformation and energy dissipation. Additionally, the adiabatic shear instability can lead to mechanical interlocking between the particle and the substrate resulting in particle adhesion [19]. Topochemical reactions and mechanical interlocking are considered as bonding mechanisms for metals and ductile materials [20, 21, 22, 23, 24] whereas for brittle materials like ceramics, activating the substrate surface with impinging particles has been regarded as a key reason for the bonding development [23]. Hussain et al concluded that both mechanical interlocking and metallurgical bonding contribute to the bond strength while polished and annealed surfaces of the metal particles can lead to stronger bonding mechanisms like metallurgical bonds [24]. Although, metallurgical bonds are not available in most polymers, the peening effect caused by successive impacts of subsequent particles can enhance the plastic deformation and eliminate the pores between the deposited particles [25, 26]. Closer examination of the interface between the substrate and the adhered particle is still needed to conclusively determine the dominant bonding mechanism in the cold spray deposition of polymers. Monitoring the evolution of the flattening ratio and the crater depth during impact is also a meaningful examination. Unfortunately, these experiments are quite difficult because of the large number of particles depositing during cold spray and the peening effect of the subsequent successful and unsuccessful particle impacts. Here, single particle impact studies can lead to insights into the impact and adhesion of particles during the cold spray process.

1.2 Background and Motivation

Developed first in the mid-1980s by Papyrin et al. [27], cold spray is a well-established additive manufacturing technique for coating and depositing a wide range of metallic materials. This technique

utilizes a high-pressure gas stream to carry metallic powder particles through a converging-diverging de Laval nozzle where they are accelerated to supersonic velocities before impacting on a solid substrate [12, 28, 29, 30].

Xu et. al [12] studied the cold spray deposition of large (D = 150 – 250 μm) HDPE particles on an HDPE sheet and obtained a critical velocity of 100 m/s which was an order of magnitude smaller than that of most metals. They couldn't localize melting at the particle/substrate interface and reported a deposition efficiency less than 0.5%. Alhulaifi et al. [10] studied smaller HDPE particles (D = 53 – 75 μm) cold sprayed on an aluminum substrate using a diffuser nozzle to reduce the particle velocity and reported a critical velocity of 190 m/s. Sagar's simulation showed that the deposition would get easier once the first layer of polymeric particles are adhered to a hard substrate like copper due to the enhanced plastic deformation and energy dissipation that a thin soft layer can encourage [19]. Ravi et al. [11] studied cold spray deposition of ultra-high molecular weight polyethylene (UHMWPE) onto both aluminum and polypropylene substrates. They added up to 4 wt.% alumina nanoparticles to facilitate inter-particle bonding. They also found out that only the adhered particles displayed evidence of melt crystallization after examining the thermal history of rebound, adhered, and unsprayed UHMWPE powder by Differential Scanning Calorimetry (DSC). The finite element simulations of Shah et al. [19], showed that the addition of metallic nanoparticles to the polymer particle improved the deposition by increasing the particle's density and its impact kinetic energy for a fixed impact velocity.

The critical velocity needed for deposition of metals is calculated from the following equation [28, 12]:

$$v_{cr} = \sqrt{F_2 c_p \left(T_m - T_p\right) + F_1 \frac{4\sigma}{\rho}\left(\frac{T_m - T_p}{T_m - T_{ref}}\right)}. \qquad \text{(Eq. 1)}$$

Here, F_1 and F_2 are empirical fitting constants, T_m is the melt temperature of the particle, T_p is the temperature of the particle at impact, T_{ref} is the temperature at which particle material properties were measured, σ is the tensile strength of the particle, ρ is the density of the particle, and c_p is the specific heat of the particle. The critical velocity model of Eq. 1 is a weighted combination of two different models used to understand the dynamics of particle impact and adhesion [28]. In the first part of Eq. 1, the critical impact velocity is associated with a certain fraction, F_2, of the impact kinetic energy being converted entirely into thermal energy

$$\frac{1}{2}\rho_p v_{cr}^2 = F_2 \rho_p c_p \left(T_m - T_p\right). \qquad \text{(Eq. 2)}$$

The second part of Eq. 1 is a dynamical model that correlates the ground pressure resulting from the ballistic impact of the particle to the tensile strength of the particle with a correlation coefficient, F_1, such that

$$\frac{1}{8}\rho v_{cr}^2 = F_1 \sigma \left(\frac{T_m - T_p}{T_m - T_{ref}} \right). \quad \text{(Eq. 3)}$$

Here, the tensile strength of the particle is modified using the Johnson-Cook equation to account for thermal softening. For metal cold spray, a wide range of materials have been studied and it has been shown that the critical impact velocity data from across all these materials can be collapsed when $F_1 = 1.2$ and $F_2 = 0.3$ [28] resulting in an empirical formula for the critical impact velocity for adhesion that becomes

$$v_{cr} = k \sqrt{c_p \left(T_m - T_p \right) + \frac{16\sigma}{\rho_p} \left(\frac{T_m - T_p}{T_m - T_{ref}} \right)}. \quad \text{(Eq. 4)}$$

For metal-on-metal deposition, the fitting parameter in Eq. 4 has been found to be $k = 0.55$ [3]. Using the material properties of HDPE and the fitting coefficient from metal cold spray, a critical impact velocity of approximately 400m/s is expected at room temperature. This is equivalent to a Mach number in air of $Ma = 1.16$ which is significantly lower than what is needed for metals due to the lower specific heat and tensile strength of HDPE as compared to even soft metals such as copper. As a result, the converging-diverging nozzle design for polymer cold spray can be designed with a much smaller area ratio than a typical metal cold spray nozzle.

1.3 Objectives and Scope

This project seeks five major goals: (1) developing cold spray deposition windows for polymer particles with various applications on polymeric and non-polymeric substrates, (2) optimizing process conditions to maximize the deposition efficiency for each powder/substrate combination, (3) understanding bonding mechanisms in polymer cold spray in comparison to comprehensively studied metallic cold spray, (4) characterizing the microstructure and mechanical properties of the deposited coatings, (5) Examining the feasibility of creating conformal coating on 3D objects and 3D printing with the cold spray system.

The study of the deposition windows for high-density polyethylene, polyurethane, polyamide, polystyrene, and ultra-high molecular weight polyethylene (UHMWPE) showed that process parameters

like temperature and impact velocity play key roles in the deposition process. The substrate material and temperature, the stand off distance, the particle size, and the nozzle design proved effective in increasing the deposition efficiency. A specific core-shell particle maximized the deposition efficiency to about 57% in depositing on a galvanized steel substrate. The materials characterization methods including SEM studies, nano-indentation and adhesion/cohesion strength investigations demonstrated a equivalent set of properties in the cold sprayed samples compared to those of melt-cast materials. The laser-induced single particle impact experiments revealed the important role of a low glass transition temperature and the successive collisions from incoming particles in making deposition possible in the cold spray process. In consistency with the results from the micro-ballistic single particle impact experiments, the addition of 10 wt.% glass beads with the same range of particle size of the depositing polymer particle, was found to notably increase the deposition efficiency and expand the deposition windows. The feasibility and criteria of a high-quality 2D conformal coating on a 3D object and 2D coating onto an angled surface was finally explored through experimental processes.

CHAPTER 2
MATERIALS AND TECHNIQUES

2.1 Materials

In Table 1, materials properties are provided for the studied polymer particles in comparison to copper cold spray deposition on copper. Included in this table are also the critical velocity fitting constant, k for each material in the case of deposition on LDPE using Eq. 4. The studied powder particles included HDPE (BYK Ceraflour 916), composites of copper nano-particle/HDPE, polyurethane, polyamide-12, and polystyrene, and ultra-high molecular weight polyethylene (UHMWPE). The fitting constant was also calculated using Eq. 1 and applying the experimental critical velocity results to this equation. The resulted values are also listed in Table 1. Each of these polymers has a different molecular architecture which leads to variation in density, Young's modulus, yield strength, melt temperature and glass transition temperature amongst other properties. All the particles used were roughly the same diameter, D = 50 μm, with the exception of UHMWPE which had a diameter of D = 20 μm. The particles were, however, very different in shape as seen in SEM images in Figure 1. Some particles like PS were quite spherical, while many others like PU which were formed through cryo-milling were like flat disks. The shape was found to have a large impact on the ability to provide a uniform flux of particles from the hopper. Spherical particles were found to be much easier to work with than the disk-shaped particles.

Cold-spray deposition of the powder particles was studied on a series of both polymeric and inorganic substrate materials. These include: high density polyethylene (HDPE) (Vycom Hitec), polyvinylchloride (PVC) (Vycom Vintec 1, T_g = 85 °C, T_m = 240 °C), polyoxymethylene (POM) (Quadrant Acetron GP Acetal, T_g = -60 °C, T_m = 175 °C), melt-cast BYK Ceraflour 916, and low-density polyethylene (LDPE) (McMaster-Carr) with T_m = 110 °C, and T_g = -90 °C, and melt-cast samples of each of the studied materials.

Table 1 – Material and Empirical Fitting Properties. Copper on copper properties are provided for reference. Material properties marked with (*) are estimates for general material types. All others are from manufacturer data sheets.

Materials	T_g (°C)	T_m(°C)	D (µm)	Yield Strength [MPa]	Density [kg/m^3]	Source	Fitting Constant, k
HDPE	-90	128	48 ± 18	20	990	BYK Ceraflour	0.187
HDPE/ 1wt.%Cu	-90	128	48 ± 18	20	1070	PS&E	0.175
HDPE/ 2.5wt.%Cu	-90	128	48 ± 18	20	1190	PS&E	0.170
HDPE/ 20wt.%Cu	-90	128	48 ± 18	20	2584	PS&E	0.158
Polyurethane	-30	92	50 ± 11	24	450	KU Leuven	0.147
Polyamide 12	97	180	50 ± 25	50	1010	KU Leuven	0.191
Polystyrene	100	175	44 ± 4	34	1040	KU Leuven	0.189
UHMWPE	-150	130	20 ± 7	22	949	Mipelon ™	-
PEEK	143	343	50 ± 20	92	1320		-
Copper on Copper	N/A	1085*	50*	50-85*	8960*	-	0.548

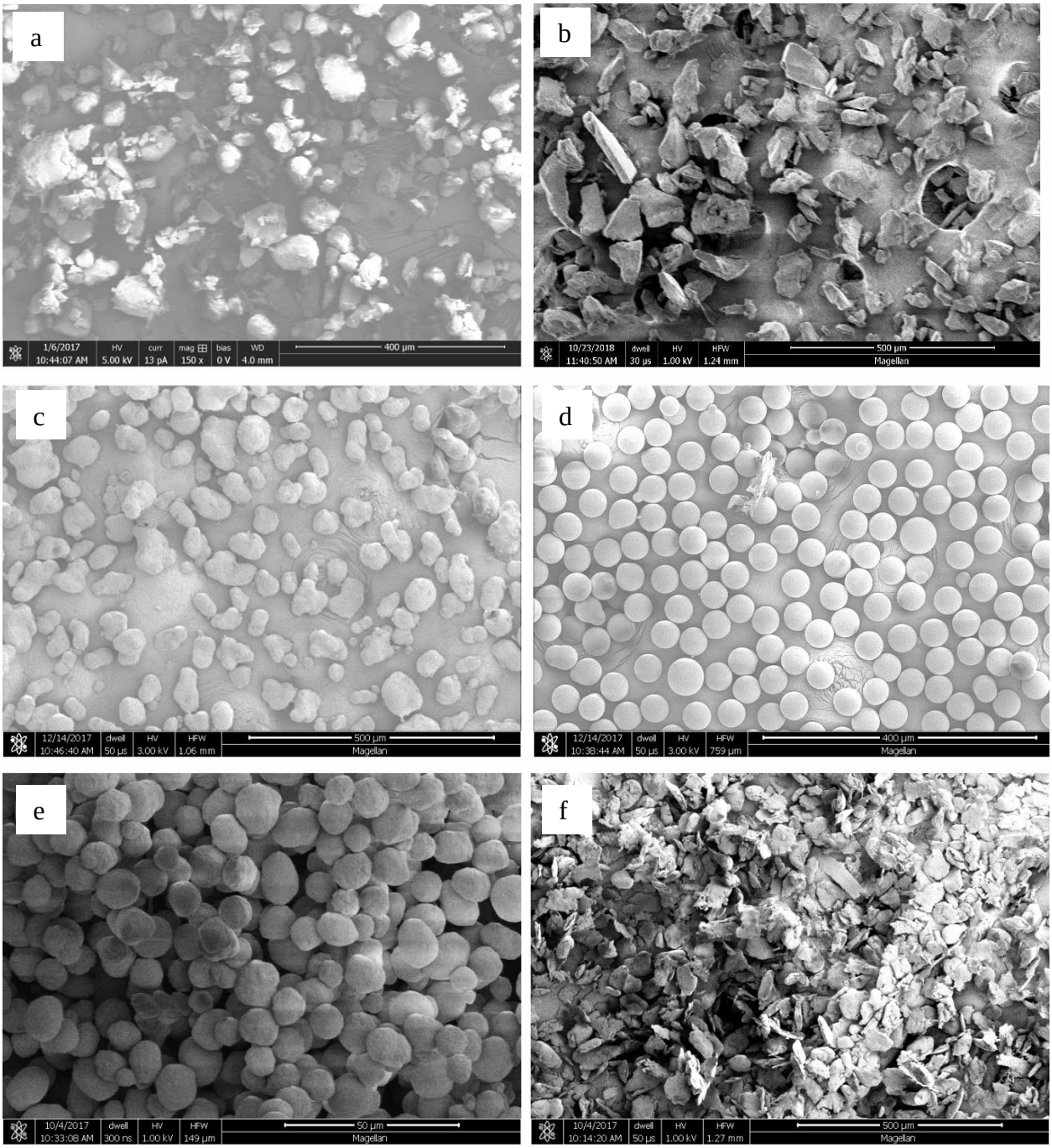

Figure 1 – SEM imaging of the feedstock powder particles (a) HDPE, (b) polyurethane, (c) polyamide 12, (d) polystyrene, (e) UHMWPE, (f) polyether ether ketone.

2.2 Cold Spray Technique

The cold spray setup used in my work was designed and built by Trenton P. Bush under supervision of Professor Jonathan P. Rothstein after computational and experimental studies of different nozzle designs. A schematic diagram of the cold spray setup is shown in Figure 2a, alongside a picture of the actual cold spray system in Figure 2 b. As described in the introduction chapter, due to the lower anticipated critical impact velocity, it was possible to run this polymer cold spray system either using a compressed nitrogen cylinder or a 1.85kW, consumer-grade single-stage air compressor capable of producing a pressure of 6.2 bars at 8.5 m^3/hr. The compressed air traveled through filters and a pressure regulator before entering a heated pressure vessel which housed the powder feeder. The hot gas/powder mixture then exited the vessel and passed through the nozzle. This spray system emphasizes powder preheating with a linear system design. The powder and process gas are heated together and mixed well upstream of the nozzle. Unlike many commercial systems, there is no parallel routing of cold powder-conveyor gas that must be mixed at the nozzle entrance.

The aluminum pressure vessel was heated with three 500W band heaters (Omega MB-1). The temperature of the pressure vessel was monitored with an internal bore thermocouple (Omega BT) inserted through a radial pressure fitting near the bottom of the barrel and was controlled with a PID temperature controller (Omega CN2110). The inner diameter of the pressure vessel was 38mm and it had a total length 27cm. Nozzle inlet conditions were monitored via a thermocouple and a pressure transducer (Omega PX309-300GV) inserted just upstream of the nozzle as seen in Figure 2b. At the mass flow rates employed by this cold spray system in this study, the residence time of the air within the heated pressure vessel was sufficient to heat the air up to the controlled temperature of the pressure vessel which could easily exceed 150^{o}C. The measured inlet temperature and pressure conditions were used as inputs to the CFD code to simulate the nozzle flow field so that the particle impact conditions could be calculated, and the data presented as a function of particle and not gas temperature and velocity.

Powder feed was accomplished by routing the carrier air around a vibratory powder dispenser contained in the pressure vessel. A pneumatic vibrator (Cleveland Vibrators VM-25) was mounted on a connecting rod above the pressure vessel. The connecting rod ran through a slip-fit bushing and into the vessel, where it transmitted vibration to an attached aluminum tube that contained the powder to be deposited. The bottom of the tube was capped with coarse wire mesh, which allowed agitated powder to fall into the surrounding carrier gas. Finally, a spring was mounted on the vibrating assembly in order to prevent pressurized air from pushing the connecting rod out of the pressure vessel. The hopper design is

capable of delivering a wide range of particle feed rates depending on the mesh size chosen and the intensity of the vibratory agitation.

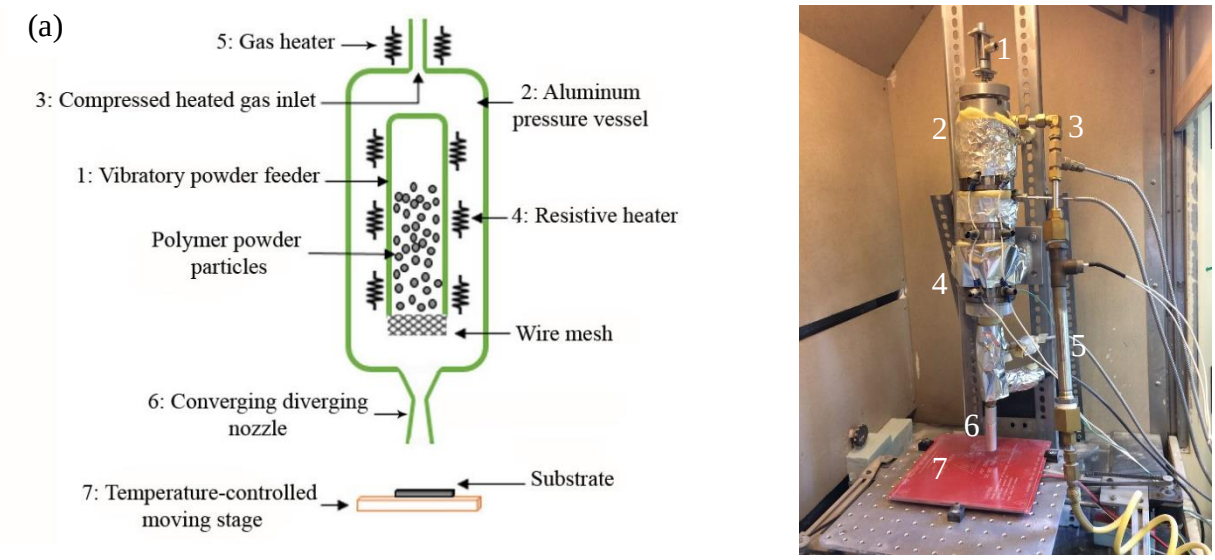

Figure 2 - (a) A schematic diagram of the cold spray setup, b) a picture of the cold spray setup used in these experiments.

The "Max Velocity Match" Nozzle which was used most frequently in my experiments had a 4.19 cm long constant-area extension section in addition to a 2.99 cm long converging section and a 0.3 cm long diverging section. The inlet, throat and exit diameters were 0.95, 0.16, and 0.19, respectively. The constant-area extension was added to maximize particle residence time and thus velocity. This geometry produces Fanno flow conditions, resulting in a normal shock in the constant area extension that decelerated (and heated) the gas back to sonic conditions. In this design, the particles are rapidly accelerated by supersonic flow, then are conveyed by warmer sonic gas, and the substrate is not subjected to shock phenomena as in standard converging-diverging nozzles. This design is similar to that of the diffuser nozzle created by Alhulaifi et al. [10], but without the complications of a second throat.

A 2D xy-stage was fabricated and controlled by an Arduino operated by an open source software package designed for 3D printing (Repetier-Host). A PCB heater was placed on top of this stage to enable controlled substrate heating up to 120^{o}C during deposition. The desired deposition patterns were inputted into the software as STL files. The stage speed could be varied from 1 to 20mm/s to change the thickness and height of the deposited cold-sprayed lines.

A one-dimensional (1D) inviscid model of gas and particle dynamics created by Champagne et al. [31] was used for rapid prototyping and as the basis for a numerical optimization routine with which three of the nozzles were designed. The model uses 1D compressible gas dynamics theory to calculate the velocity, temperature, and pressure variations through the nozzle [32]. In a converging-diverging nozzle, the gas is accelerated to the speed of sound at the throat and then supersonic, $Ma > 1$, in the diverging section of the nozzle by converting the enthalpy of the gas into kinetic energy. As a result, as the velocity increases, the pressure and temperature of the gas decrease in a known way that is easily calculated from theory [32]. The particle velocity is determined by first assuming the particles do not disturb the flow field and then calculating the drag force using a simple drag law. For ease of calculations, we chose to use the lumped capacitance model in both 1D theoretical predictions of nozzle performance and the 2D CFD simulations which were run to validate the 1D model and finalize the nozzle designs. For the purposes of particle impact simulations, a more precise 3D temperature profile across the particle upon impact might be critical to accurately model the temperature distribution within the particle during impact. The velocity and temperature evolution for the mean particle size was calculated as a function of position along the converging-diverging Laval nozzle to determine the impact temperature and velocity of each polymer powder. For simplicity, the powders were assumed to be spherical which is clearly not always the case and the temperature was assumed to be uniform across their cross-section or that they are Lumped. Both assumptions and the errors they introduce are discussed in detail in Bush et al. [13]. The flight of the HDPE particles was recorded using a Phantom VEO high speed camera S 640 at the framerate of 19,000 fps, resolution of 512 × 320, and the exposure time of 50 μs.

2.3 Laser Induced Single Particle Impact Experiments

In order to directly and precisely examine the flight, impact, and deposition or rebound of the particles, a series of micro-ballistic single particle impact experiments were conducted using four of the polymeric materials studied in this project. In these experiments, an ablation laser pulse (5–8 ns pulse duration, 1064 nm) was created by using a neodymium-doped yttrium aluminum garnet, Nd:YAG laser (Quanta-Ray INDI-40-10-HG, Spectra-Physics) to accelerate an individual polymer particle placed near the focal point of the laser ablation on a polydimethylsiloxane (PDMS)/Au/glass substrate as shown schematically in Figure 3 a [33]. The particle was subsequently accelerated by the rapid expanding motion of an 80 μm thick elastomeric film made of cross-linked PDMS. Combining a femtosecond laser source with three electro-optic modulators, this Laser Induced Projectile Impact Test (LIPIT), can provide up to 40 million frames per second. A photonic crystal fiber (SCG-800, Newport) was used to convert the gated laser pulses to

white light, resulting in an image like the one seen in Figure 3a, containing multiple exposure of the particle in flight as it approaches and rebounds off the substrate. The particle diameter was measured from the ultrafast photography [33].

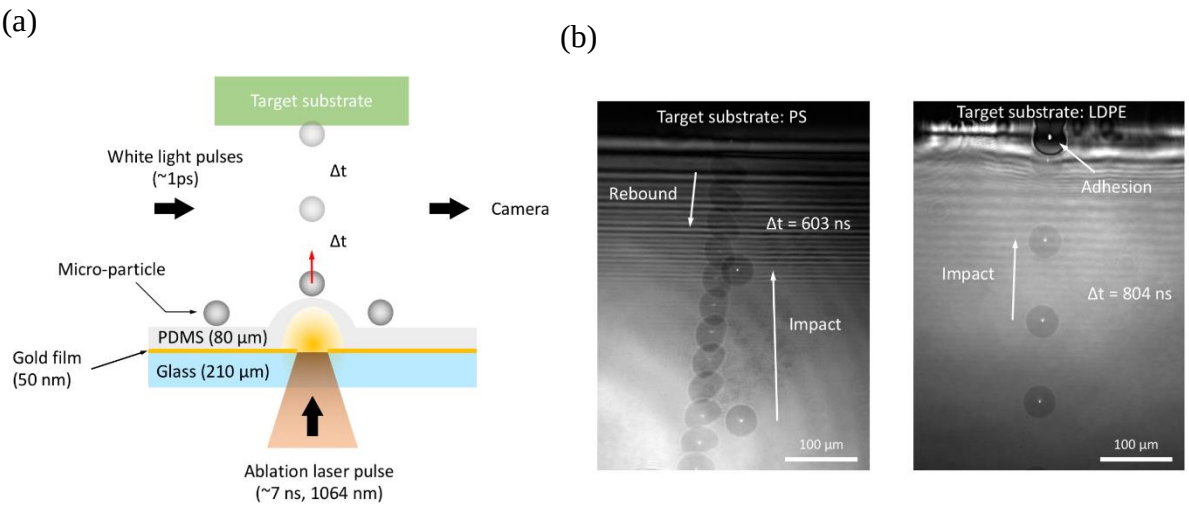

Figure 3 – (a) A schematic diagram of the single particle impact setup and b) sample ultrafast images of particles approaching and impacting different target substrates – Image provided by W. Xie.

CHAPTER 3

WINDOW OF DEPOSITION STUDIES

A series of experiments were performed in order to study how a number of key parameters affect the cold-spray deposition of the feedstock powders on to a number of different substrates. These parameters included: particle temperature, size and impact velocity, substrate composition and temperature as well as stand-off distance between the nozzle exit and the substrate. The effect of parameter variation on cold-spray deposition were quantified by (1) determining whether deposition occurred or not, (2) by measuring the deposition efficiency and by characterizing the quality of the deposition through scanning electron microscopy (SEM) images, and (3) quantification of the porosity of the deposition and measurements of the properties of the deposited material through nano-indentation hardness measurements.

3.1 High-density polyethylene (HDPE)

The first sets of experiments performed were designed to set a baseline for future comparisons by studying the deposition of HDPE powders on a variety of substrates including a melt-cast surface of the same HDPE powder, LDPE, POM, PVC, 6061 aluminum and quartz glass. In these experiments, the Max Velocity Match nozzle described in the introduction section was utilized, the nozzle stand-off distance was set to 10 mm and the substrate was held at T_s= 100 °C. A number of different hopper temperatures were utilized between 20°C and 80°C and pressures between 1 and 4.8 bars resulting in particle velocities that ranged from 75m/s to 275m/s. In Figure 4, the resulting windows of deposition for like-on-like deposition of the HDPE powder as well as those of deposition on LDPE, POM and PVC are shown for a nozzle stand-off distance of 10 mm and at substrate temperature of T_s= 100 °C. As is typical in the cold spray literature, the data are presented as particle temperature against particle impact velocity. In the cases of like-on-like deposition and deposition on LDPE, only the lower boundaries of the deposition window are visible. Experiments at velocities high enough to determine the upper boundary were not performed for this powder/substrate combination. However, in depositing on PVC and POM, upper velocity limitations are also detectable in addition to lower velocity boundaries. Note that the particles were found to become tacky at temperatures above 80°C. As a result, the particles were found to jam in the hopper, thus setting the maximum operating temperature of the pressure vessel for this powder.

As expected, the critical particle impact velocity decreases with increasing hopper and particle temperature. Here we observe a reduction from V_{cr} = 100 m/s at T_p = 20 °C to V_{cr} = 90 m/s at T_p = 80 °C. However, note that the critical impact velocity at room temperature predicted by Eq. 4 exceeds the observed value by a factor of 3. As we will show with other polymer powders, the data in Figure 4 can still be well fit by the model in Eq. 4 if the fitting parameter, *k*, is modified from k = 0.55, which has been shown to work for metals, to k = 0.19 for this HDPE powder. This finding of significantly reduced critical impact velocity is consistent with previous studies of polyolefin deposition [10, 12]. Clearly the mechanics that govern adhesion in metal cold spray differ considerably from the polymer case. Taken in the context of the adiabatic shear instability mechanism, low thermal diffusivity is one possible explanation for the reduced critical velocity seen in polymers. Thermal diffusivity can be a thousand times lower in polymers than metals. As a result, temperature buildup at the interface may be more localized in a polymer than a metal particle [34]. This can be observed in the numerical simulations of Shah et al. who investigated the impact polymer particles on different substrates [19]. Localization of the temperature rise could result in a reduction of the amount of total energy needed to be released through plastic deformation of the particle to obtain the interfacial temperature necessary for adhesion.

The resulting deposition maps are presented in Figure 4. Successful cold-spray deposition of HDPE was achieved on all four of these polymeric substrates. This is in stark contrast to our deposition attempts on inorganic substrates like aluminum and glass, for which successful deposition was not possible under these deposition conditions. As a result, the deposition map for aluminum and glass is not presented in Figure 4. As will be shown in the following section, cold-spray deposition of HDPE was possible on aluminum and glass but required heating of the substrate up to the melting temperature of the HDPE powder to be successful.

In Figure 4a – d, cold-spray deposition maps of the HDPE particles are presented on the studied substrates including LDPE, HDPE, PVC and POM. As seen in Figure 4, the result of the mismatch in modulus between the particle and the substrate was a reduction in the critical impact velocity across the entire temperature range of approximately 15%. As an example, at T_p = 20°C the critical impact velocity was reduced from V_{cr} = 140m/s on HDPE to V_{cr} = 120m/s on LDPE. This change is similar to what was observed for cold-spray deposition of metals [28] and is consistent with trends in energy dissipation predicted for the impact of polymer particle on surfaces with mismatched moduli [15]. Similar critical impact velocities to the one deposited on HDPE substrate, were also observed for both POM and PVC substrates. However, the bonding mechanism between these very different polymers and the impacting HDPE particle is not entirely clear. It is important to note that all the data in Figure 4 can still be well fit by the model in Eq. 4, if the fitting parameter *k*, is modified from k = 0.55, a value which has been shown to

work for metals. The resulting values of the fitting parameter, k, are given in Table 1 and were found to range between $0.15 < k < 0.19$ with a mean value of $k = 0.174$ for all seven of the polymer particles studied so far in this project. As a result, on average, the critical impact velocity for deposition of the studied powder materials is 3.3 times smaller than expected for a metal particle with the same material properties, or expressed differently, deposition of polymer particles requires 11 times less kinetic energy than for a similar metal.

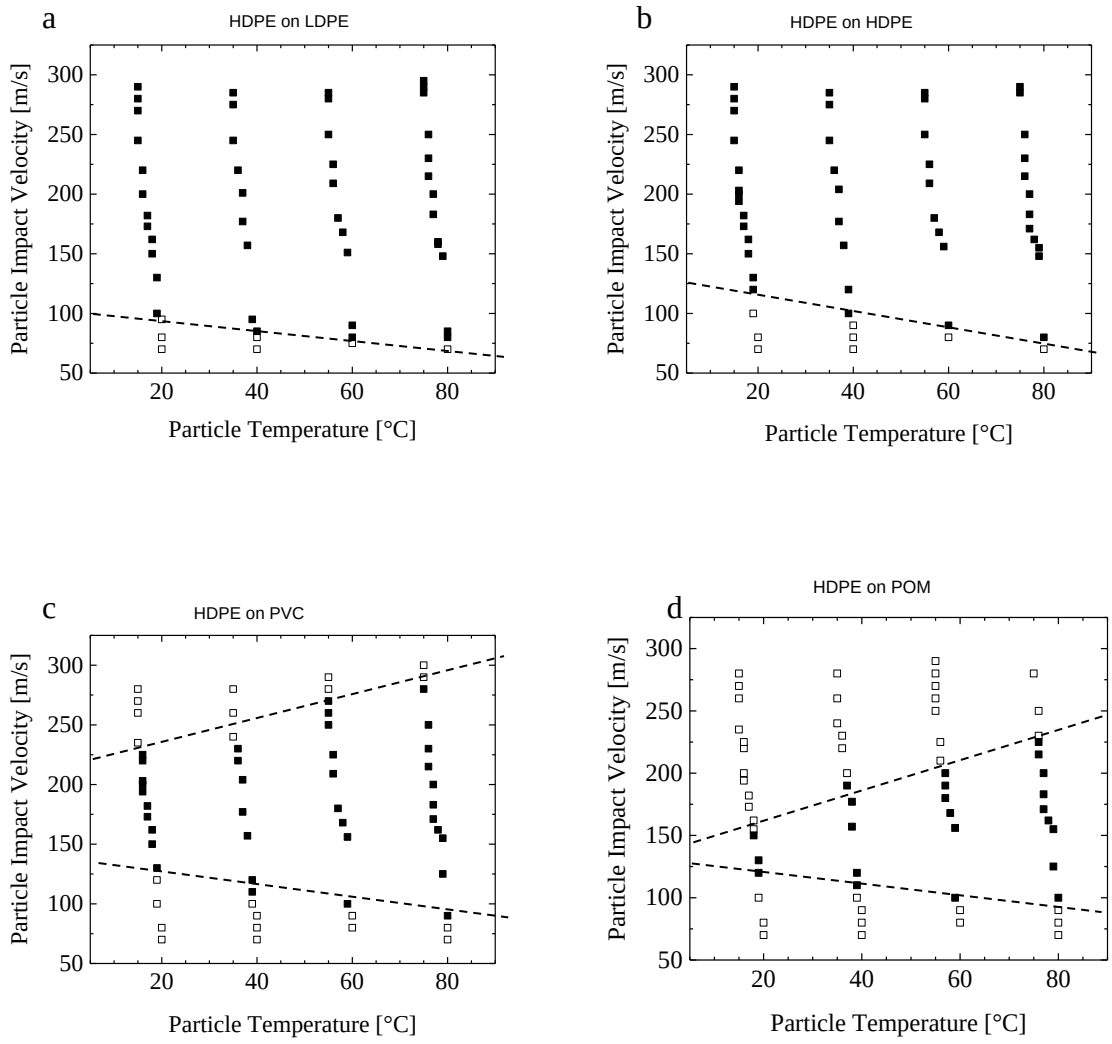

Figure 4 – Deposition window of (a) HDPE-on-LDPE, (b) HDPE-on-HDPE, (c) HDPE-on-PVC and (d) HDPE-on-POM in cold spray experiment showing the transition from no deposition, (□) to deposition, (■). In all cases, the substrate was held fixed at T_s= 100 °C and the stand-off distance was 10 cm.

The most notable difference between the like-on-like case and the different polymeric substrates that one can observe from the data in Figure 4 is the appearance of an upper deposition boundary for the POM and PVC substrates. In the case of POM, erosion of the deposition was observed to occur through an interesting mechanism. During spraying at high impact velocities and pressures, a deposit appeared to form, build up, and then delaminate from the surface, repeating one or two times per second. At low temperatures, where this delamination effect was observed, deposition was not possible above $V_p > 150$m/s resulting in a very narrow deposition window. This observation suggests that for HDPE deposition on POM, that once a threshold deposit size is attained, shear forces from the carrier gas can grow larger than the adhesion strength of the deposit. It also indicates that the adhesion strength between the HDPE and the POM is not optimal and suggests that the substrate material should be properly chosen to maximize adhesion strength of the subsequent deposition. Conversely, the failure of deposition of the HDPE particles on the PVC surface at high velocities occurred through a more commonly-observed mechanism, which is the impact-induced ablation of the substrate. This observation suggests that, in this case, deposition was not possible due to a cohesive failure of the substrate material rather than an adhesive failure between the particles and the substrate.

3.2 Polyurethane (PU)

In Figure 5, the deposition window of PU on a variety of substrates including LDPE, PVC, and POM is shown. The substrate temperature was fixed at $T_s = 100$ °C and the particle flowrate was kept between 45 – 55 g/min in all experiments. The critical impact velocity was found to decrease with increasing particle temperature. For the case of deposition on LDPE for instance, a reduction from $V_{cr} = 100$ m/s at $T_p = 20$ °C to $V_{cr} = 90$ m/s at $T_p = 80$ °C can be seen in Figure 5. These results are consistent with our previous cold spray results for HDPE particles deposited on LDPE [13]. As was seen in Bush et al. [13], the critical velocity was a factor of four or five smaller than what would be predicted for metal particles based on the critical velocity equation of Schmidt et al. [28]. Deposition of PU powders on a melt cast PU substrate was found to shift the critical velocity for adhesion to larger velocities especially at lower temperatures. For example, at room temperature, $T_p = 20$°C, the critical impact velocity for adhesion increased from $V_{cr} = 100$ m/s on LDPE to $V_{cr} = 135$ m/s on PU. Like-on-like deposition of PU was also found to be more sensitive to particle temperature than deposition on LDPE. Here, the critical impact velocity for adhesion drops to $V_{cr} = 90$ m/s at a particle temperature of $T_p = 80$ °C. This is most likely because in the case of deposition of particles on LDPE most of the deformation takes place in the soft substrate which is not changing with particle temperature. While for like-on-like deposition, much of the deformation needed for adhesion is occurring on the impacting particle which gets softer and more mobile as the temperature approaches T_{melt}. Deposition of PU particles on the harder POM and PVC substrates were similar to like-on-like deposition

on PU. The main difference was that the PU particles were found to exhibit an upper bound on velocity at which successful deposition was possible. Within the studied velocity ranges, deposition was not found to have an upper velocity limit on PU or LDPE. However, on the POM and PVC substrates, it is clearly evident. Above these maximum deposition velocities, deposition was found to fail through an adhesive failure of the deposition after an initial build up. For PU deposition on PVC, the upper velocity for successful deposition starts at V_{cr} = 225 m/s at T_p = 20 °C and grows with particle temperature to V_{cr} = 275 m/s at T_p = 80 °C. The deposition window is significantly narrower for PU deposition on POM. These results show that adhesion strength is strongly dependent on the particle/substrate combinations chosen. The upper limit for deposition of polyurethane on POM and PVC was also observed for HDPE particles [13, 25].

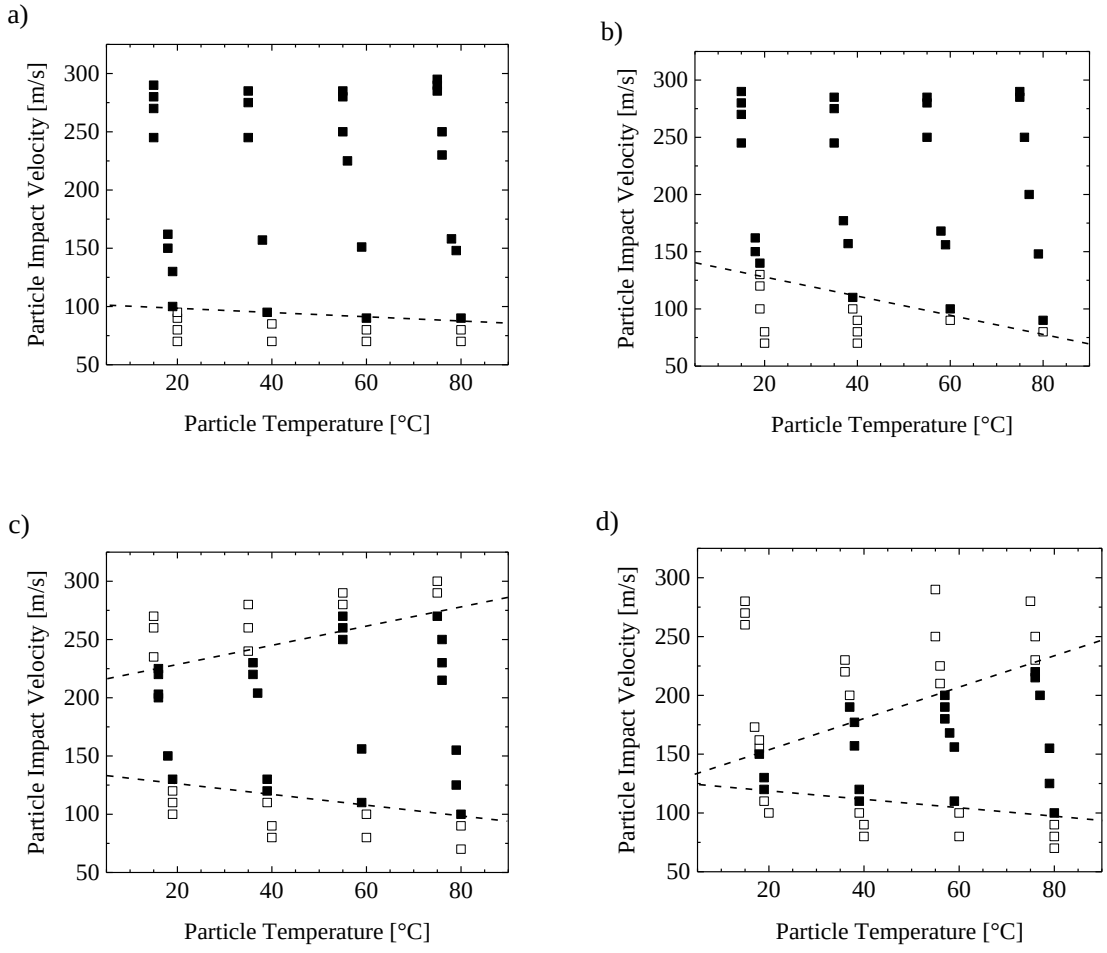

Figure 5 – Cold spray deposition window for PU particles on substrates of (a) LDPE, (b) PU, (c) PVC and (d) POM. Data include experiments showing successful deposition (■), and no deposition (□). In all cases, the substrate was held fixed at T_s = 100 °C and the stand-off distance was 10 mm. The dashed lines are not meant to be quantitative but are simply there to guide the reader's eye.

3.3 Polyamide 12

In Figure 6, the cold spray deposition windows of PA particles on a variety of substrates including LDPE, PVC, and POM are shown. Deposition of PA was significantly more different than PU. A critical velocity of V_{cr} = 170 m/s was required for PA on LDPE and 180 m/s was needed to deposit PA on a melt cast PA at 20°C. That is nearly a two-fold increase in the critical velocity for PU on LDPE. This large difference is likely due to the increase in the glass transition temperature for PU, T_g = –63 °C meaning even at room temperature the PU particles are quite mobile. In contrast for PA, T_g = 97 °C and as a result both the PA particle and substrate are glassy at the temperature tested. Only in the thin region in the impact crater

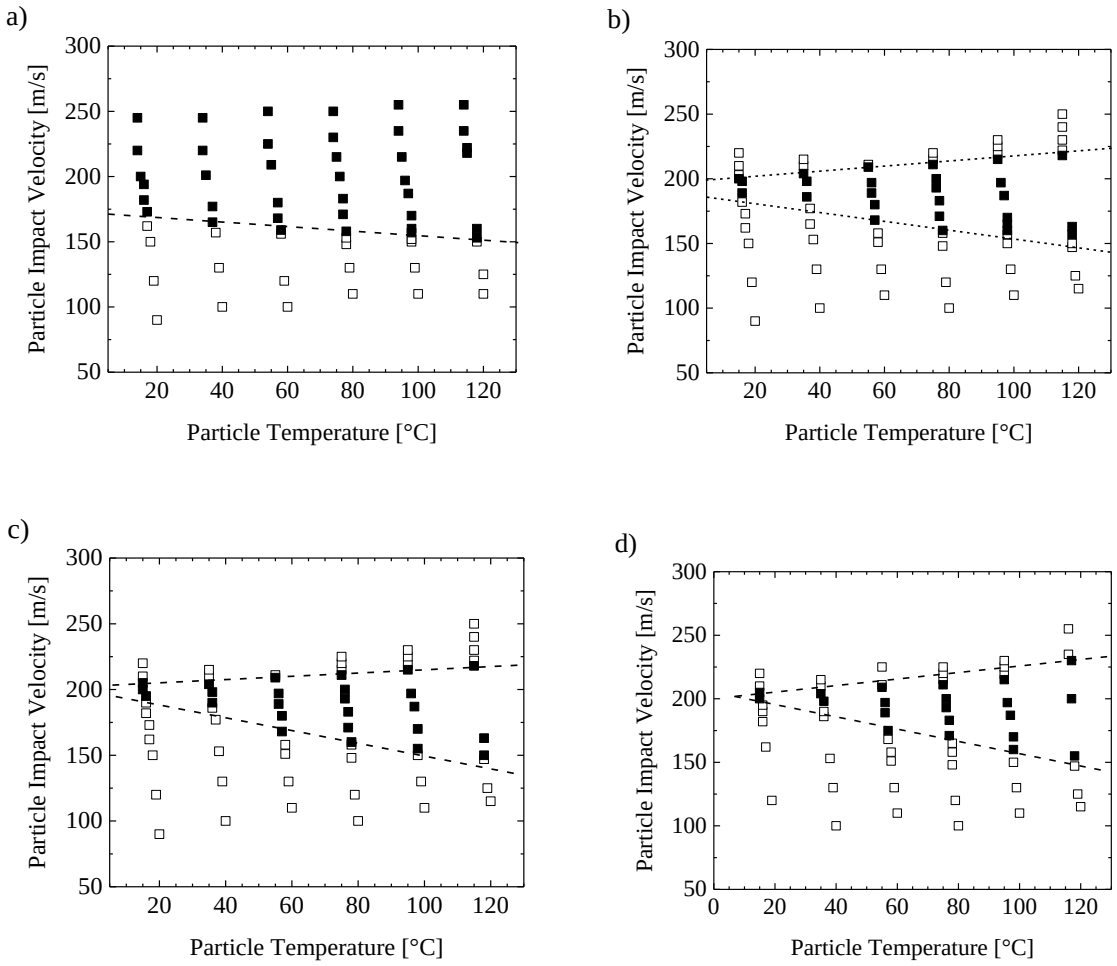

Figure 6 – Cold spray deposition window of PA particles on (a) LDPE, (b) PA, (c) PVC and (d) POM substrates showing the transition from no deposition (□) to deposition (■). In all cases, the substrate was held fixed at Ts= 100 °C and the stand-off distance was 10 mm. The dashed lines are not meant to be quantitative but are simply there to guide the reader's eye.

where the kinetic energy of the particle is transformed into thermal energy with the temperature rise large enough for the particle to rise above its T_g and begin to flow [19]. As a result, more kinetic energy is needed to initiate sufficient plastic deformation to result in particle adhesion. Additionally, although deposition on LDPE shows no upper velocity limit, like-on-like deposition showed an upper velocity limit which resulted in a very narrow deposition window especially at the lower temperatures tested. At room temperature, deposition was only possible in a narrow window between 195 and 205 m/s. The deposition map was found to get even narrower in the case of depositing on PVC and POM. PVC (T_g = 85 °C) has a higher glass transition temperature than LDPE (T_g = –110 °C). POM, on the other hand, has a low glass transition temperature of its amorphous component (T_g = –60 °C) [35], it is highly crystalline and as such has a high fraction of a rigid phase that remains frozen up to the melting temperature (T_m = 175 °C) which is well beyond the temperature expected to be achieved during particle impact. this makes deposition almost impossible at room temperature on POM. The deposition window does, however, expand to between 150 m/s and 225 m/s on PA, PVC, and POM as the particle temperature is increased to 120 °C, well above its T_g. Improved results would likely possible for like-on-like deposition if the substrate temperature could be raised well beyond the glass transition temperature, but unfortunately, we were limited experimentally to a maximum substrate temperature of T_S = 100 °C.

3.4 Polystyrene

In Figure 7, the deposition windows of PS on a variety of substrates including LDPE, PS, PVC, and POM are shown. The observations are similar to the results for PA except that an upper velocity limit for successful deposition was found to emerge in all cases even for the deposition of PS on LDPE. The effect of substrate was less significant. The deposition was roughly 255 wider for PS on LDPE than PS, PVC or POM. Replacement of LDPE with PS, for example, increased the minimum critical velocity for particle adhesion from V_{cr} = 160 m/s to 180 m/s for PS particles and decreased the maximum velocity for particle adhesion from 225 m/s to 215 m/s at room temperature.

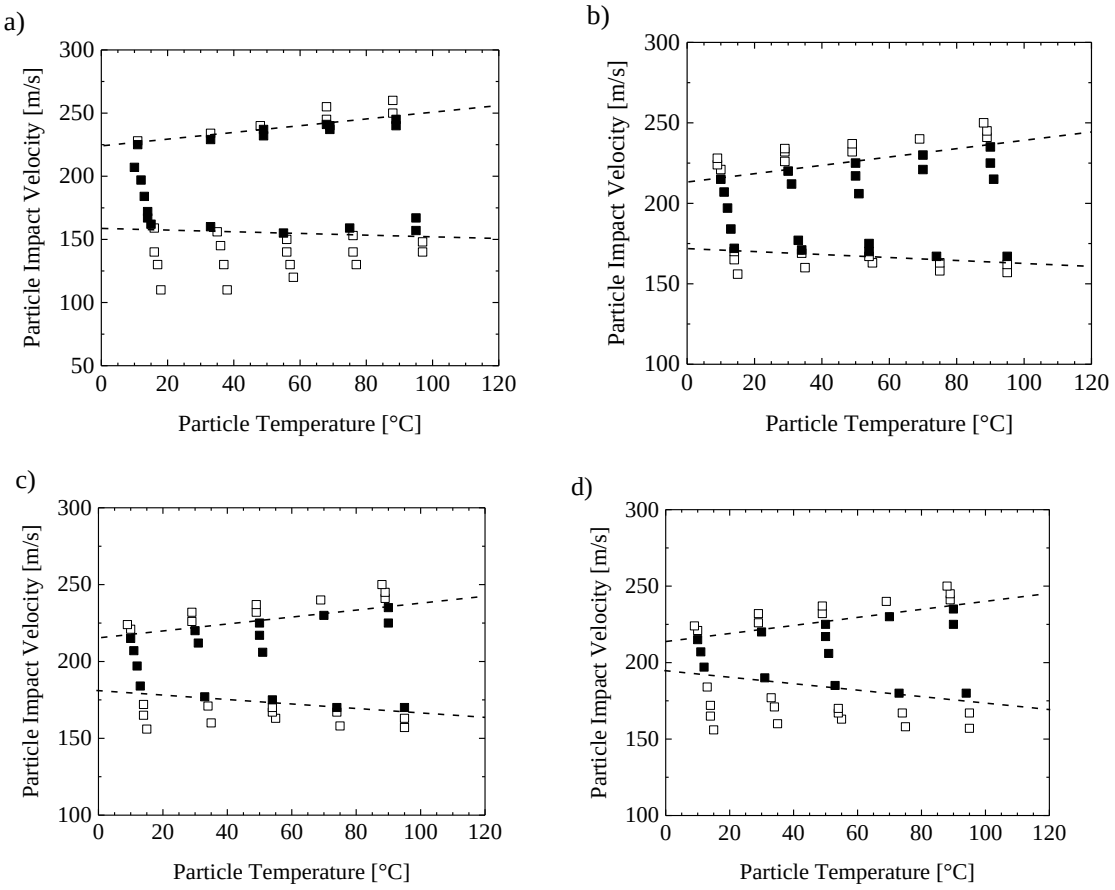

Figure 7 – Cold spray deposition window of PS particles on (a) LDPE, (b) PS, (c) PVC and (d) POM in cold spray experiment showing the transition from no deposition (□) to deposition (■). In all cases, the substrate was held fixed at T_s = 100 °C and the stand-off distance was 10 mm. The dashed lines are not meant to be quantitative but are simply there to guide the reader's eye.

3.5 UHMWPE

UHMWPE is utilized in the applications demanding high wear resistance, high impact resistance and high cavitation erosion resistance. UHMWPE is a comparably efficient (high strength to weight ratio), inexpensive and an easily procurable option to hard alloys and intermetallic compounds which are often used in such applications [36]. In Figure 8, deposition windows over the particle temperature and particle velocity space are demonstrated for both of the cold spray deposition of UHMWPE particles on an LDPE substrate and deposition of UHMWPE on a melt cast UHMWPE substrate. Compared to all the previously studied materials, the deposition window for UHMWPE was found to shift to much larger values of both particle temperatures and particle velocities. Deposition windows for UHMWPE on PVC and POM are not

shown because successful deposition was never achieved. On LDPE, deposition of UHMWPE was not possible for particle temperature below T_p = 60°C. Even beyond 60°C, an impact velocity of 280 m/s was needed to deposit UHMWPE on LDPE. Compared to HDPE, this is an increase in V_{cr} of more than 150 m/s or more than a two-fold even though the materials have similar physical properties including melt and glass transition temperatures. The higher molecular weight of the UHMWPE clearly impacts its mobility upon particle impact, reducing the plastic deformation, flow, and mixing between the particle and substrate that is necessary for adhesion. Interestingly, no upper limit was found even as the particles were accelerated well past Ma = 1. For the case of deposition of UHMWPE on UHMWPE, deposition required T_p > 80°C and velocities beyond V_{cr} = 300 m/s. Interestingly, for HDPE, these same impact velocities cause particles to be stripped from the interface and mild abrasion of the substrate [13].

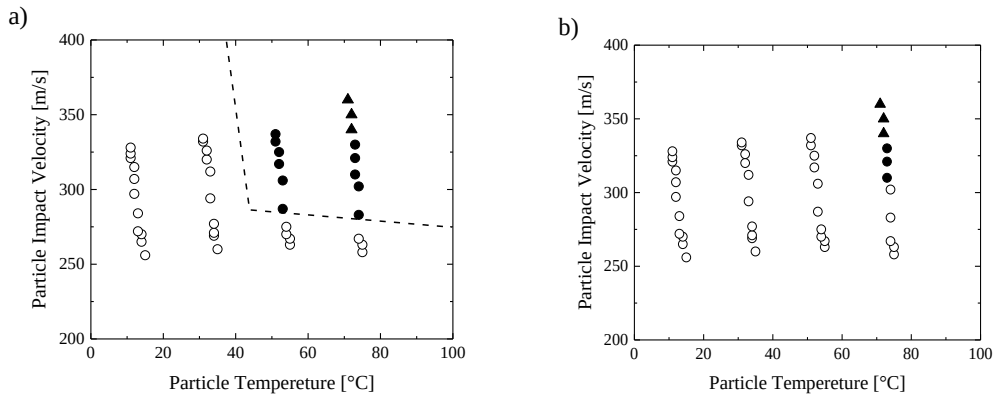

Figure 8 – Cold spray deposition window of UHMWPE particles on (a) LDPE, and (b) UHMWPE showing the transition from no deposition (o) to deposition (●, ▲). The solid triangle symbols (▲) correspond to the results from using the supersonic nozzle. In all cases, the substrate was held fixed at T_s = 100 °C and the stand-off distance was 10 mm.

Ravi et al. [36] studied the deposition of UHMWPE on 1100 grade aluminum. To obtain deposition, they added up to 10% fumed nano-alumina (FNA) particles to the feedstock powder to enhance surface activity of UHMWPE particles. These hydrophilic polar nano-alumina particles make possible the formation of H-bonds at the polymer particle/aluminum substrate interface which improved deposition and increased the deposition efficiency from 0.06% for UHMWPE+0% FNA to 1.4% for UHMWPE+10% FNA at 500 °C gas temperature. Ravi et al. [36] also showed that increasing particle velocity and gas temperature can have a positive effect on deposition efficiency of UHMWPE on aluminum substrates. As will be discussed in following sections, increasing temperature and impact velocity were also found to increase the deposition efficiency of UHMWPE on LDPE and UHMWPE substrates.

CHAPTER 4

MATERIALS CHARACTERIZATIONS

4.1 Microstructural Studies

Surface topology was examined via optical microscopy and scanning electron microscopy (SEM) (FEI Magellan 400 XHR-SEM). Several deposition conditions were examined from a top view, and 45 and 90-degree tilt to view the cross section. A small subset of these images is presented in Figure 9. As can be seen from Figure 9, a smooth continuous line was deposited of the HDPE particles on an LDPE substrate for inspection through SEM. Both in the optical images and the SEM images, no obvious grain boundaries between individual particles could be observed. For the size of the particles deposited, D = 48μm, and the scale of the SEM images, each image should show impact craters of multiple particles. However, no evidence of individual particles is apparent from either the optical images or the SEM images in Figure 9. Instead, the resulting HDPE deposition was found to be uniform and dense with little to no observable porosity or voids. The deposition was also found to be quite smooth with an average surface roughness of less than 10μm, which is well below the diameter of the impacting HDPE particles. One possible explanation for the high quality of the deposition is that, as we will describe below, the deposition efficiencies were less than 10%. As a result, the particles that didn't adhere may have been responsible for peening the deposition into a dense and smooth formation.

Various compositions of the copper/HDPE composite including 1 wt.% Cu/HDPE, 2.5 wt.% Cu/HDPE, and 20 wt.% Cu/HDPE were cold sprayed at various particle impact velocities. In Figure 10, optical and SEM imaging of cold-sprayed deposits of two of the composites on LDPE substrates are shown. As we will see in the following section, a dense and uniform microstructure was always founded to be associated with a deposited layer with a high deposition efficiency. The HDPE/Cu composite particle yielded the highest deposition efficiency of about 10% among other polymer materials studied in this project. As can be seen from Figure 10, a dense microstructure of the deposited polymer composite is obvious for the copper nano-particle infused HDPE powder.

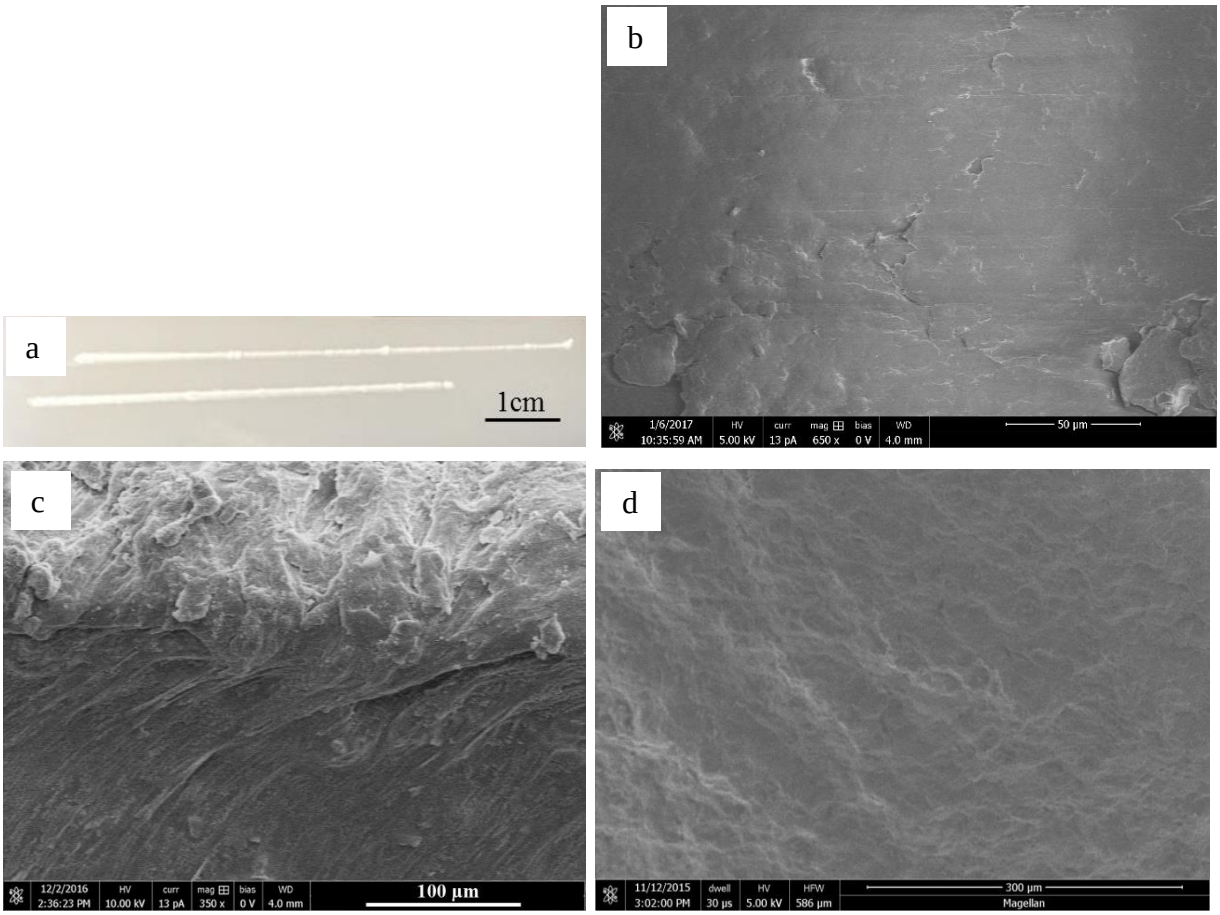

Figure 9 – SEM imaging of cold-spray deposits of HDPE particles on an LDPE substrate. In (a) an optical image of a 1D line of HDPE deposited at T_{pi} =19°C at V_i =197m/s is shown. In (b) an SEM image of the top of the deposition in (a) is shown. In (c), the deposit in (a) was cut and imaged using SEM at a 45° angle to reveal the cross section of the deposit. In (d) an SEM image of the melt cast HDPE is shown for comparison with the cold-sprayed deposits.

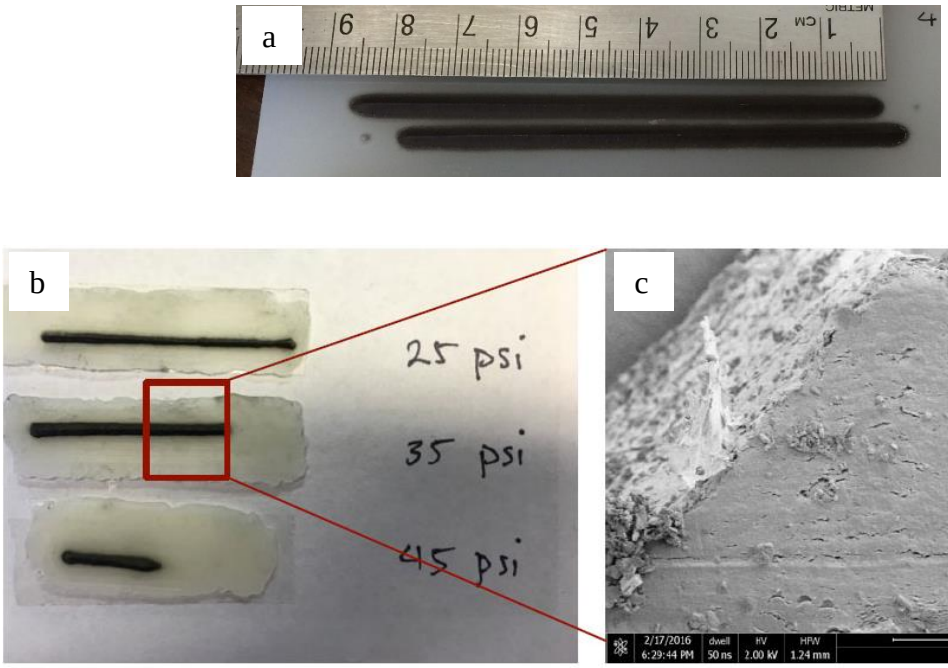

Figure 10 – Optical and SEM imaging of cold-sprayed deposits of Cu nanoparticles / HDPE composite on an LDPE substrate, (a) an optical image of cold-sprayed 20 wt.% Cu/HDPE on LDPE at T_{pi} =20°C at V_i =160m/s, (b) an optical image of cold-sprayed 2.5 wt.% Cu/HDPE on LDPE at T_{pi} =20°C at different impact velocities ranging between V_i = 120m/s – 160m/s, (c) an SEM image of the cross section of the deposited line in (b). All experiments were at room temperature.

A subset of the cold-sprayed coatings of 2D patterns are presented in Figure 11. The height of the coatings was found to depend on the traverse speed and the deposition efficiency of the depositing particles. For example, at a given traverse speed of 33 mm/s, HDPE particles were found to build up a 3 mm height coating on an LDPE substrate when being accelerated to 270 m/s at particle temperature of T_p = 60 °C and substrate temperature of T_s = 100 °C.

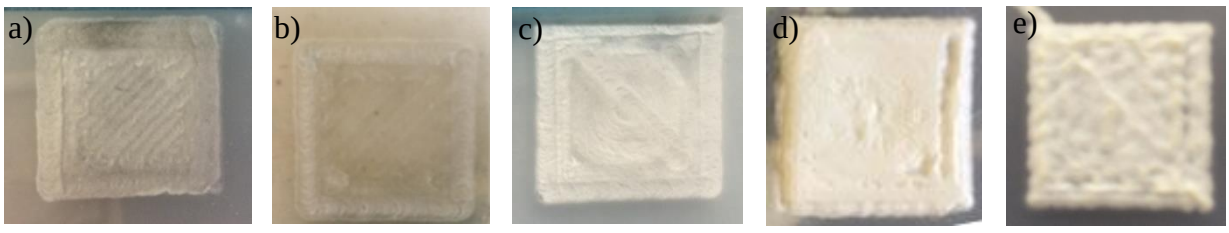

Figure 11 – Cold-sprayed coatings of 2D patterns including polyurethane (a) on LDPE and (b) on polyurethane substrates, (c) polyamide on LDPE, (d) polystyrene on LDPE, and (e) UHMWPE on LDPE.

The surface topology of the cold sprayed samples was examined via scanning electron microscopy (SEM) (FEI Magellan 400 XHR-SEM). Several deposition conditions for each of the polymer powders were examined from a top view, 45° tilt angle and 90° tilt angle to view the cross section and observe the boundary between the substrate and the deposited layer. A small subset of these images is presented in Figure 12. In all cases, the deposits were very similar. It is clear that for the processing parameters for which particles adhere well to the substrate, no voids or obvious grain boundaries between individual particles or between the particles and the substrate could be observed. In fact, little difference can be seen between a melt cast and a cold sprayed surface. The microstructure of the melt cast polymers can be seen in the third image in each row in Figure 12 as the substrate. Given that, the average size of the particles deposited was between 20 μm and 50 μm, at the magnification of the SEM images, impact craters of unadhered particles or evidence of individual particles should be visible if present. multiple particles. However, no evidence of individual particles was apparent from the SEM images in Figure 12. Instead, the resulting particle depositions were found to be uniform and dense with little to no observable porosity or voids. The deposition was also found to be quite smooth with an average surface roughness of less than 10 μm for both the 1D and 2D depositions. This is well below the diameter of the impacting particles. One possible explanation for the high quality of the deposition is that, as we will describe below, the deposition efficiencies for all of these powders were less than 10%. As a result, the particles that did not adhere may have been responsible for peening the deposition into a dense and smooth formation.

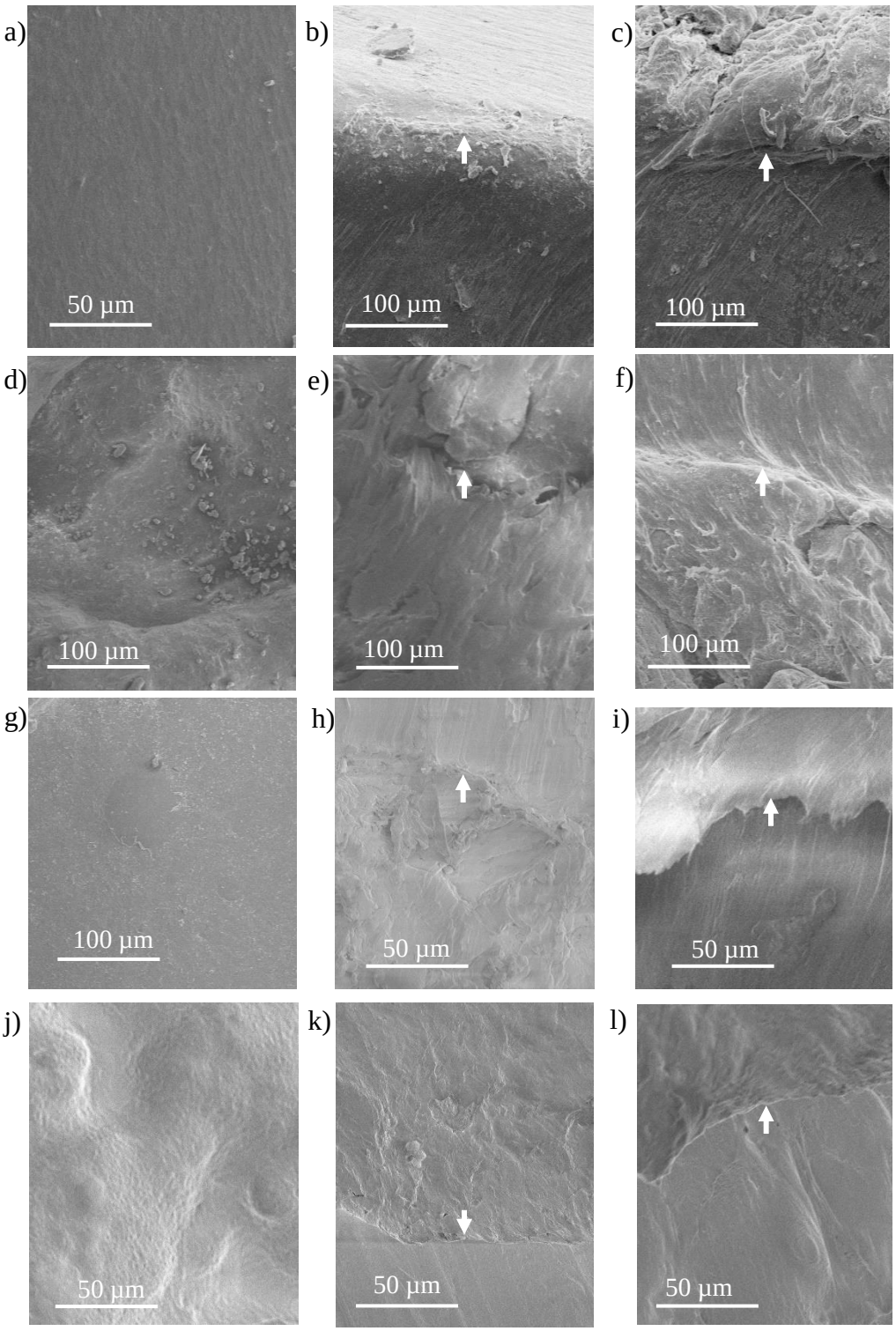

Figure 12 – SEM imaging of cold-sprayed deposits of (a, b, c) PU, (d, e, f) PA, (g, h, i) PS, and (j, K, l) UHMWPE. In each row, the sequence of the images is the top view, cross-sectional view of the deposited particles on LDPE and cross-sectional view for the like-on-like deposition. Cold spray parameters included T_p = 20 °C and V_i = 130 m/s for PU, T_p = 20 °C and V_i = 170 m/s for PA12, T_p = 20 °C and V_i = 200 m/s for PS, and T_p = 80 °C and V_i = 310 m/s for UHMWPE. In the cross-section views, an arrow is used to indicate the boundary between melt-cast (bottom) and cold-sprayed (top) polymer.

In Figure 13, an SEM image of a weakly deposited like-on-like deposition of the PS particle at V_i =165 m/s is shown. This poorly deposited layer was subsequently stripped off the PS melt cast substrate after being initially deposited. In some cases like this, the high shear stresses applied to the deposited layer from the airflow and the incoming particles can delaminate on initially deposited layer. Figure 13, also shows the bottom view of a deposited PS layer after being stripped off the melt cast PS substrate. The honey comb structure of the delaminated layer in Figure 13b clearly shows evidence of individual particles. Under these conditions, the particles deposit to form a close-packed hexagonal lattice upon impacting the substrate. Although some deformation is clear at the boundaries between particles, these particles have not undergone the significant plastic deformation observed in well-adhered and non-porous depositions in Figure 12. The reduced plastic deformation is likely due to the large T_g of the PS particles. Plastic deformation is clearly isolated to areas of high shear formation where temperatures are known to rise significantly, and the particle can melt and flow. Subsequent peening from non-adhesive particles clearly does not have as large as an impact in this case as the PS requires significant additional heating to get above T_g and flow. Once the particle has initially adhered, requires higher impact velocities, larger surface and particle temperatures, and perhaps multiple sequential impacts to peen the particles. This may also explain the lower deposition efficiencies observed for PS and other high glass transition temperature polymers that will be discussed in the following section.

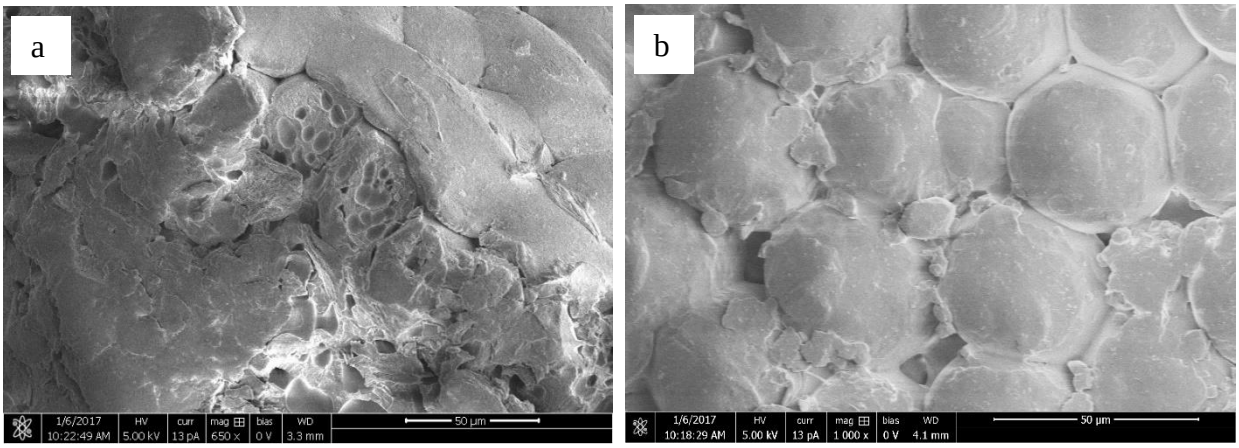

Figure 13 – SEM imaging of a poorly deposited PS on a melt cast PS substrate showing (a) the cross section and (b) bottom view of the delaminated. This surface was deposited at V_i = 165 m/s and T_p = 20 °C.

4.2 Mechanical Properties

Surface hardness measurements were performed using a nano-indentation instrument, Hysitron piezo controller IV-A equipped with a standard Berkovich indenter with a 300 nm three-sided pyramidal tip and a maximum displacement range of 2 mm. The displacement resolution and the loading resolution were 0.01 nm and 50 nN, respectively. The maximum testing load was 50 μN and the indentation depths were within 10% of the coatings' thickness, thus minimizing substrate effects. All studied samples were ground mechanically using SiC sandpaper to ensure a smooth surface. The loading and its corresponding displacement were recorded as a function of time during the experiment. The surface hardness of cold sprayed surfaces was compared to that of a melt cast sample of that polymer material serving as the 'bulk' material reference. The small scale of nano-indentation allows a spatial map of hardness to be generated. Knowledge of spatial variation in hardness is important to understand the uniformity of the coating. About 20 measurements were made over an area of 4 mm^2 to determine the uniformity of surface properties. Special attention was given to the region at the interface between the substrate and the first layer of the cold spray deposited particles.

4.2.1 Nano-Hardness and Elastic Modulus

Nanoindentation is a widely-used technique to measure the mechanical properties of materials, especially thin films. In nanoindentation experiments, a rigid probe is pressed into the polished surface of a sample, and the transducer records the in-situ force and displacement responses. According to the Oliver-Pharr method, the elastic modulus can be obtained from the slope of the initial portion of the unloading curve and the hardness can be calculated by dividing the maximum indentation load with the contact area [37]. Using the Finite Element Method in conjunction with nanoindentation experiments, elastic and plastic properties of the tested samples can also be estimated by fitting experimental loading/unloading curves [37, 38]. However, these traditional methods typically assume that the materials behave as elastic-plastic materials and do not take into account any viscoelastic properties. This is true for many solid materials such as metals and ceramics which exhibit minimum viscoelastic behavior at room temperature, but for polymer materials, viscoelasticity is very important.

In this work, we applied the trapezoidal loading function with 5 s peek holding time and 5 s for loading/unloading for all experiments. The loading and its corresponding displacement were recorded as a function of time during the experiment. For each test, the procedure was repeated for 20 times in various positions and the average value along with its standard deviation is reported in Table 2.

From a comparison between the nano-hardness and elastic modulus of the cold-sprayed samples and those of the melt cast samples in Table 2, a remarkable consistency between the values of nano-hardness was observed for each of the materials studied. A general reduction of 5 – 10% was observed for most cold sprayed samples, however, this variation is clearly well within the experimental uncertainty.

Table 2 – Mechanical properties of the cold-sprayed coatings in comparison to the melt cast samples.

	Nano-hardness (MPa)	
	Melt Cast	Cold Sprayed
LDPE	210 ± 10	-
HDPE	260 ± 20	220 ± 20
PU	200 ± 20	200 ± 20
PS	390 ± 20	380 ± 20
PA	270 ± 20	260 ± 20

4.2.2 Adhesion/Cohesion Strength

Adhesion strength was measured according to ASTM-C633 standard [39] which is generally used for both thermal sprayed and cold sprayed samples [40]. The tests are based on linear elastic fracture mechanics approach, and consist of subjecting assembly of coating, substrate and fixtures to a tensile load (normal to the plane of the coating). Melt cast specimens of each of the five polymer materials were prepared using a vacuum hot press machine to ensure removal of the voids from the melt. 2×5×5 mm rectangular cubes were cut out of the melt cast samples which were then used as substrates. Polymer powders were cold sprayed onto corresponding melt-cast samples to create 1-2 mm thick deposition on the substrates. Thickness of the coatings was adjusted by the traverse speed. Then, using an epoxy resin glue (polyamide-epoxy FM 1000), the coating/substrate assemblies were glued to separated ends of a dog-bone sample of melt-cast polyamide 12 as shown in Figure 14. The dog bone samples were left for 16 h at room temperature for the glue to be cured.

A servo-hydraulic Dartec machine with a 20 kN load cell connected to an Instron controller was employed to carry out the tests. The dog bone specimens were clamped at both ends. One end was fixed while the other was displaced at a pre-defined velocity of 0.033 mm/s, which corresponds to the strain rate of 10^{-3} s^{-1}. The length, width and thickness of all specimens were measured with a sliding caliper prior to the testing. The force-displacement curves were converted to stress-strain curves for each testing after dividing the force by the cross-sectional area and dividing the displacement by the initial length of the samples. Two parallel tests were performed for specimens of each polymer material, and the resulted curves were compared to ensure repeatability of the results. All tensile tests were carried out at room temperature, $T \approx 20$ °C.

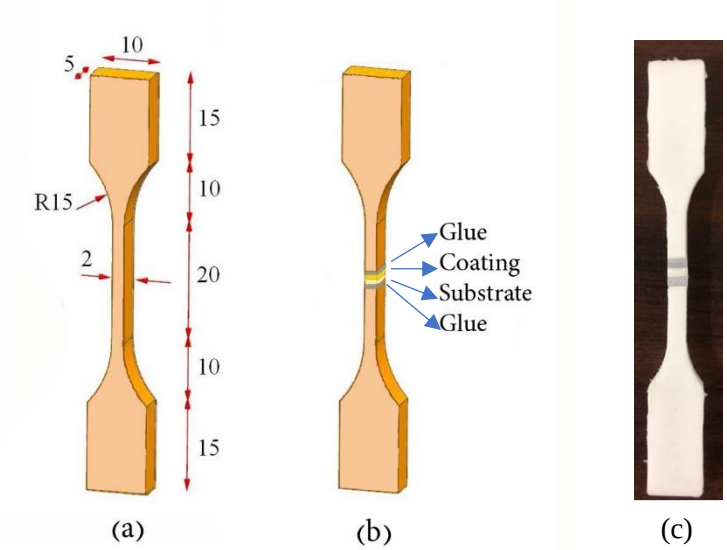

Figure 14 – (a) Dimensions of the standard polyamide 12 dog bone used for the adhesion/cohesion strength testing, (b) schematic diagram of how the coating/substrate were glued into the dog bone, (c) example of a dog bone before testing.

The stress/strain curves for each of the polymer powders tested here are presented in Figure 15. All the materials tested in this study exhibited a cohesive failure with the fracture occurring within the cold sprayed coating. These studies confirm the high adhesive strength between the cold-sprayed particles and the melt-cast substrate.

Looking at Figure 15, one can observe that the scatter between multiple repeated test results are reasonably small and that quantitative agreement was achieved between the tensile tests of the cold sprayed samples and the melt-cast specimens of the same material. Analyzing these curves in more detail can provide insight in how the deposition technique can affect the solid-state properties of a coating.

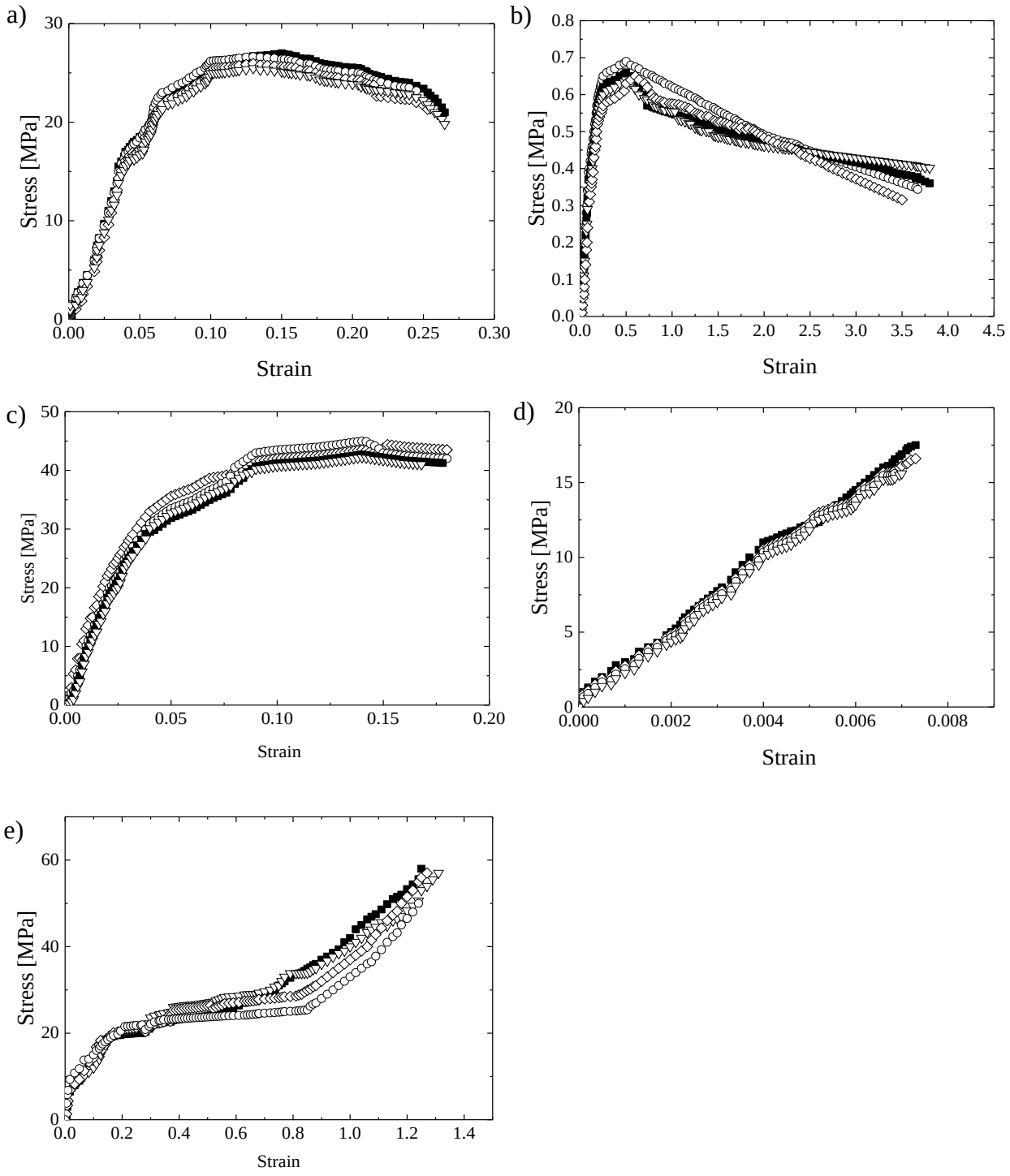

Figure 15– Stress-strain curves produced from tensile testing until failure of (a) HDPE, (b) PU, (c) PA, (d) PS, (e) UHMWPE. Data for melt-cast samples are represented by solid symbols and cold sprayed samples by hollow symbols.

For instance, elongation to failure is a characteristic of the ductility of a material and is measured as the maximum strain of a material at failure in tensile testing. From Table 3, little difference can be observed between the cold-sprayed and melt-cast samples. Cold spraying polymer powder does not embrittle a coating even though flow induced stresses are frozen in during deposition, they appear to be small enough not to affect the polymer ductility or perhaps they are worked out through the peening of subsequent, non-adhering particles. The toughness of each sample was calculated as the area under the strain-stress curves and is indicative of the ability of polymer to absorb plastic deformation without failing. Little to no deviation from that of melt-cast samples can be seen in Table 3 for the toughness results of cold-sprayed samples. This is especially important for the UHMWPE samples as its enhanced toughness is one of its more desirable characteristics. Here the cold-sprayed UHMWPE sample showed a modest decrease in toughness although the change was well within the uncertainty of the data and as a result it should not be considered significant. Similar results were also observed for the ultimate tensile strength.

Table 3 – Mechanical properties including ultimate tensile strength (UTS), elongation at failure, and fracture toughness for both like-on-like cold-sprayed samples and the corresponding melt-cast samples

	UTS [MPa]		Elongation at failure		Toughness [MPa]	
	Melt-Cast	Cold Sprayed	Melt-Cast	Cold Sprayed	Melt-Cast	Cold Sprayed
HDPE	27	26 ± 2	0.27	0.25 ± 0.07	5.85	5.50 ± 0.09
PU	0.69	0.7 ± 0.1	3.8	3.7 ± 0.1	2.01	2.1 ± 0.2
PA	43	44 ± 4	0.18	0.17 ± 0.02	6.14	6.1 ± 0.1
PS	17.5	17.2 ± 0.8	0.0077	0.007 ± 0.0005	0.068	0.066 ± 0.003
UHMWPE	60	52 ± 8	1.3	1.2 ± 0.2	32.5	27.0 ± 8.3

4.3 Temperature Profile within the Particles

Experimental results so far, have indicated the very important role of temperature on the deposition properties. Therefore, it is critical to have a precise measure of the temperature of the particles, air and the substrate. The aluminum pressure vessel was heated with three 500 W band heaters (Omega MB-1). The temperature of the pressure vessel was monitored with an internal bore thermocouple (Omega BT) inserted through a radial pressure fitting near the bottom of the barrel and was controlled with a PID temperature controller (Omega CN2110). At the mass flow rates employed by this cold spray system in this study, the residence time of the air within the heated pressure vessel was sufficient to heat the air up to the controlled temperature of the pressure vessel which could easily exceed 150 °C. The measured inlet

temperature and pressure conditions were used as inputs to the CFD code to simulate the nozzle flow field so that the particle impact conditions could be calculated and presented as a function of inlet conditions. To calculate the particle temperature in the 1D code, the convective heat transfer coefficient was found from the particle motion and then the heat transfer rate and particle temperature were calculated as a function of position along the nozzle assuming a lumped capacitance model. A detailed description of the mechanics behind the simplified model, including a comparison to computational fluid dynamics (CFD) simulations and experimental results, is available from the original authors [31]. This assumption of uniform temperature within the particle is valid for metal particles because the Biot[1] number is quite small owing to the large thermal conductivity of the metal particle. However, this assumption breaks down for polymers as their thermal conductivity is much smaller. In Figure 16, the temperature profile is schematically shown within same sizes of an aluminum particle and an HDPE particle to display the uniform temperature within a metallic particle versus the temperature profile within a polymeric particle.

For impact velocities targeted here, the resulting Biot number was calculated to be slightly larger than lumped capacitance cutoff of $Bi \sim 0.1$ [41]. However, to ensure the accuracy of the data from the 1D code, in this section I will address the uncertainty of the data obtained from the Lumped capacitance assumption, using a finite difference method to calculate the temperature profile within a 50 μm HDPE particle as it travels along the Max Velocity Match nozzle under extreme spray conditions. With a displacement increment of $\Delta r = r/10$, and the assumption of symmetry about the center of the particle, there would be 10 unknown nodal temperatures. In Figure 17, the nodal points between the inside and the surface of an HDPE particle used to derive the finite difference equation are shown. I calculated the temperature profile under extreme spray conditions including the critical velocity, maximum velocity, room temperature and maximum temperature. I considered the following assumptions:

1. Particles are spherical with $r = 25$ μm
2. As the air is flowing intensively downstream of the nozzle, a forced convection heat transfer coefficient is assumed for the gas surrounding the particle
3. There is no internal heat generation
4. Properties of gas and particle are constant.
5. In the x direction, one dimensional conduction is assumed.
6. Four different initial conditions are assumed as follows:

[1] The Biot number is a dimensionless number indicating the heat resistance between inside and the surface of a body and is defined as: $Bi\# = L_c h/K$, where, L_c is the characteristic length, h is the convection heat transfer coefficient and K is the convection heat transfer coefficient.

a $\begin{cases} T_H = 20\ °C \\ V_P = V_{cr} = 100\ m/s \end{cases}$

b $\begin{cases} T_H = 80\ °C \\ V_P = V_{cr} = 100\ m/s \end{cases}$

c $\begin{cases} T_H = 20\ °C \\ V_P = V_{max} = 300\ m/s \end{cases}$

d $\begin{cases} T_H = 80\ °C \\ V_P = V_{max} = 300\ m/s \end{cases}$

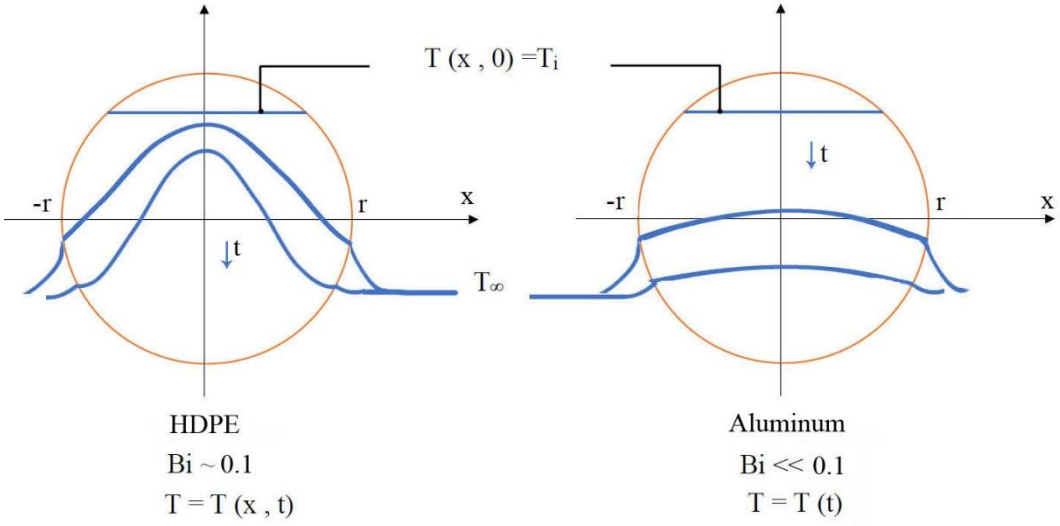

Figure 16 – Temperature profile within a same-size aluminum particle and an HDPE particle.

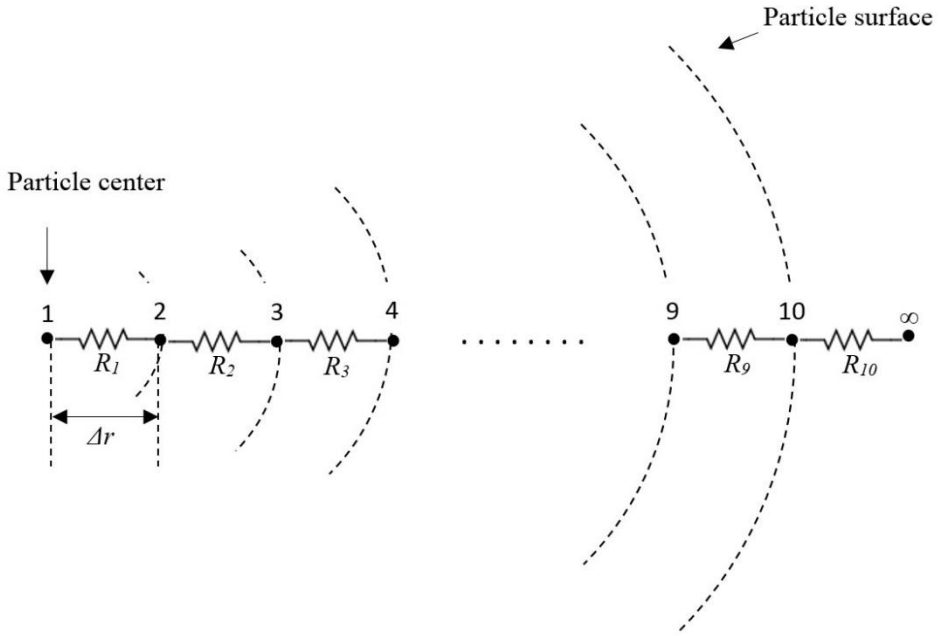

Figure 17- Nodal points used to derive a finite difference equation to determine the temperature profile between the inside and the surface of an HDPE particle

The heat transfer is through conduction between the center and the surface of the particle and convection between the particle surface and the surrounding air. Therefore, there are conductive thermal resistance inside the particle, $R_i = \Delta r/KA_i$, for $i = 1 - 9$ and convective thermal resistance between the particle surface and the air, $R_{10} = 1/hA_{10}$, where K is the conduction heat transfer coefficient of HDPE (0.47 W/mK), A_i is the surface area of the hypothetical sphere at node i defined as $A_i = 4\pi(i\Delta r)^2$ and h is the forced convection heat transfer coefficient of air. Thus, the nodal temperatures would be defined by Eq. 5 at any given time with the time increment of Δt.

$$T_i^{t+\Delta t} = T_i^t + \frac{\Delta t}{\rho c A_i \Delta r}\left(\frac{1}{R_i}\left(T_{i+1}^t - T_i^t\right) + \frac{1}{R_{i-1}}\left(T_{i-1}^t - T_i^t\right)\right) \qquad \text{(Eq. 5)}$$

The time a 48 µm HDPE particle takes to travel through this nozzle varies between 0.003s at the maximum velocity and 0.004s at the critical velocity. Therefore, a time resolution of $\Delta t = 10^{-6}$s was considered to ensure a high enough accuracy. In Figure 18, the temperature profile within an HDPE particle is shown as a function of the particle position along the nozzle using both the finite difference method and the Lumped Capacitance assumption (the 1D code) under the four described extreme spray conditions. As it can be seen from this figure, the temperature profile between the center and the surface of the particle

covers a 4.4 – 5 °C range at an impact velocity of $V_i = V_{cr}$ = 100m/s and a 6.2 – 7.8 °C range at an impact velocity of $V_i = V_{max}$ = 300m/s. In other words, from the finite difference calculation, the particle temperature was found to deviate from uniform and a modest temperature distribution of a few degrees (between 4-8 °C depending on processing conditions) was found to exist across the particle with the outer shell of the particle becoming cooler than the core during its flight through the nozzle. This detailed temperature profile was not critical to the objectives of this research and thus was neglected in subsequent studies.

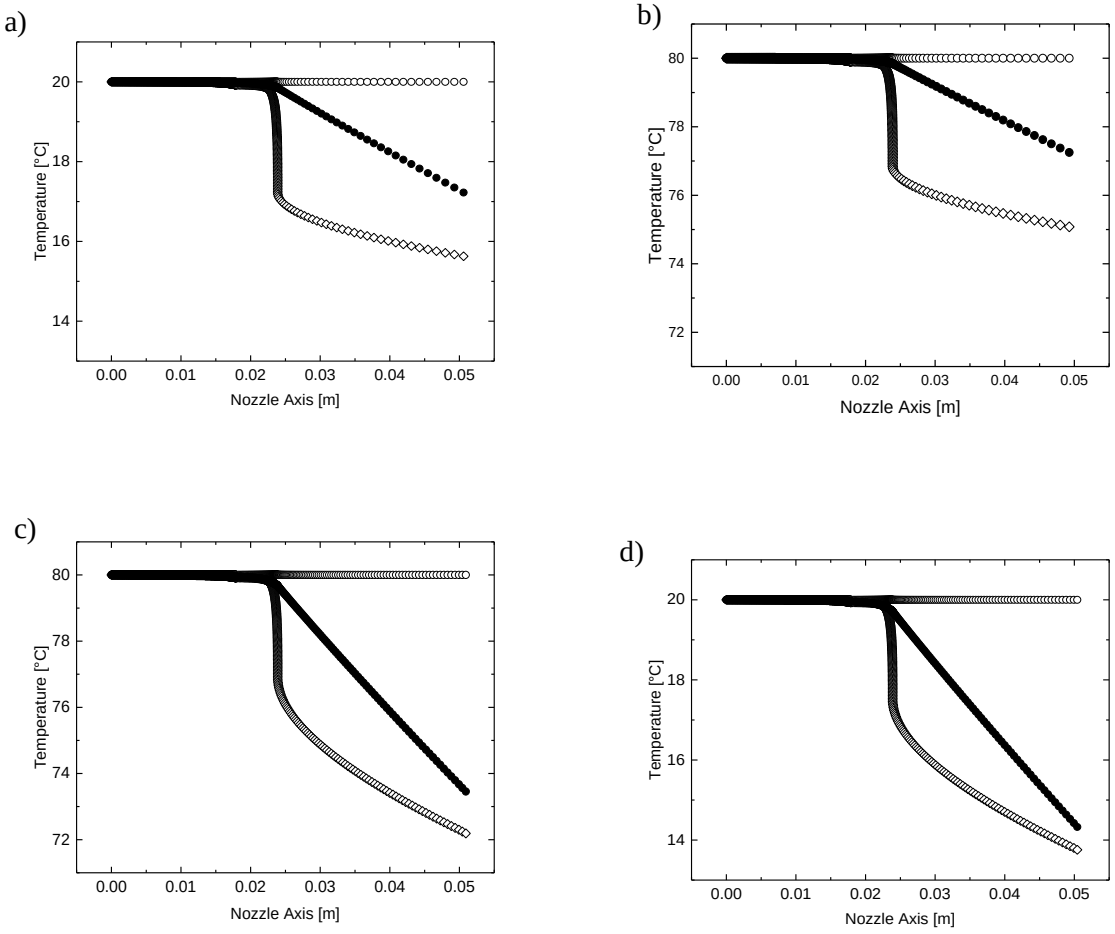

Figure 18 – Variation of the HDPE particle temperature at the core (O) and surface of the particle (◊) from the finite difference method and mean particle temperature from the Lumped Capacitance assumption (●) as a function of position of the accelerated particle along the "max velocity match" nozzle in various spray conditions (a) T_H = 20 °C and $V_P = V_{cr}$ = 100 m/s (b) T_H = 80 °C and $V_P = V_{cr}$ = 100 m/s (c) T_H = 20 °C and $V_P = V_{max}$ = 300 m/s (d) T_H = 80 °C and $V_P = V_{max}$ = 300 m/s

4.4 Rheological Characterization at High Temperatures

Rheology is the study of strain and strain rate (deformation) of materials under the influence of an applied stress revealing stress-strain relationships in materials. In rheology studies, the sample is placed in an appropriate geometric configuration, plate/plate, cone/plate, and concentric cylinders within the rheometer which applies and measures wide ranges of stress, strain, and strain rate while controlling the temperature of the sample [42].

The shear stress, τ, divided by the shear strain, γ, gives the shear modulus, G ($= \tau/\gamma$). For elastic materials over the elastic deformation regime, this shear modulus is a pure storage modulus, G', because in these materials, the energy stores in the material during deformation by extending and stretching the structure without overstretching or destroying the material and acts like a driving force to reform the structure into its original state when the stress is removed. For viscous materials, the energy does not store but dissipates in the form of friction between the components of the viscous material leading to liquid-state behaviors. For such materials the shear modulus is a pure loss modulus, G'' [42]. Therefore, while elasticity is usually the result of bond stretching along crystallographic planes in an ordered solid, viscosity is the result of the diffusion of atoms or molecules inside an amorphous material. Most polymeric materials display a time-dependent strain which is a combination of both elastic and viscous behaviors under stress and thus are called viscoelastic materials. For these, a complex modulus is defined as $G^*=\tau/\gamma$ which can be calculated from the storage and loss modulus by the Pythagoras' equation: $G^*= G'^2+ G''^2$ while $G'' = G'Tg\delta$ (Figure 19). In general, rheometers are used in two types of studies: amplitude sweep and frequency sweep. In amplitude sweep studies the objective is to describe the deformation behavior especially at the upper limits of strains. The frequency sweep aims at describing the time dependent behavior at both fast and slow motions. The geometry configuration can be adjusted to either rotate or oscillate around the sample. From the oscillatory tests, the complex viscosity can be obtained by dividing the complex shear modulus G^*, by the angular frequency ω, at a given point, $|\eta^*|= G^*/\omega$. From the rotational tests, on the other hand, the shear viscosity can be obtained by dividing the shear stress τ, by the shear rate γ, $\eta= \tau / \gamma$.

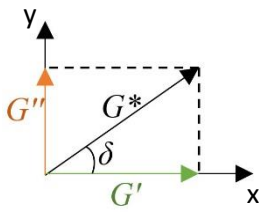

Figure 19 – complex modulus and its components as vectors

The relatively high ranges of temperatures and shear rates experienced by the particle during the cold spray process make it behave more like a liquid than a solid. This has been validated both numerically and experimentally for metals [16, 17] and polymers [19]. SEM studies in this work also confirms the existence of molten regions adjacent to particle/substrate interface. In this section, some rheological properties of the studied polymers are characterized. These studies although much below the shear rates associated with the cold spray process could eventually unfold some reasons behind the different deposition behavior of the studied powders.

Rheological properties were characterized for a melt cast sample of HDPE, PU, PA, and PS particles at four temperature steps, T_m +10 °C, T_m, T_m – 10 °C, T_m – 20 °C using a TA rheometer RSA-G2 equipped with a cone/plate geometric configuration. This instrument can apply the force range of 0.0005 – 35 N, with a force resolution of 0.00001 N, displacement resolution of 1 nm, a modulus precision of ±1% and has an isothermal stability of 0.1 °C. The separate motor and transducer of the RSA-G2 insures a pure mechanical data through independent control of deformation and measurement of stress. The force convection oven and the high-power Peltier plate system allow for precise and accurate temperature controls. The viscoelastic properties of the samples were also studied using the same instrument. The oscillating frequency sweep experiments were carried out in the linear regime to determine storage and loss moduli (G' and G'') at a strain of γ = 20% and the frequency range of 0.1–100.0 rad/s. Amplitude sweep studies were then implemented at a fixed frequency of ω = 5 rad/s over a wide range of 0.1 – 500 %.

In Figure 20, the storage modulus, G', and loss modulus, G'', are plotted against the angular frequency. The crossover points at which $G' = G''$ are also shown. HDPE with $G' > G''$ has a consistent solid structure over the low and high angular frequencies. The $|\eta^*|$ curve shows a tendency to flatten towards the plateau value of the zero-shear viscosity of η_0 = 120 kPas. PU displays liquid behavior ($G'' > G'$) at high frequencies and solid behavior ($G' > G''$) at lower frequencies. The $|\eta^*|$ curve approaches infinity in the lower frequency ranges and thus evaluating this curve is not helpful in practice for PU. Opposite to PU, PS displays liquid behavior ($G'' > G'$) at lower frequencies and solid behavior ($G' > G''$) at higher frequencies. Similar to the case for HDPE, the $|\eta^*|$ curve for PS shows a tendency to flatten towards a plateau value of the zero-shear viscosity which is equal to η_0 = 25 kPas. Like the case for PU, PA also displays liquid behavior ($G'' > G'$) at high frequencies and solid behavior ($G' > G''$) at lower frequencies and the $|\eta^*|$ curve approaches infinity in the lower frequency ranges which makes the evaluating of this curve not helpful in practice for PA. Frequency sweeps studied up to here were beneficial for describing some rheological parameters of the studied materials in this research, however, did not show any correlation to the deposition properties of the materials presented in the previous sections.

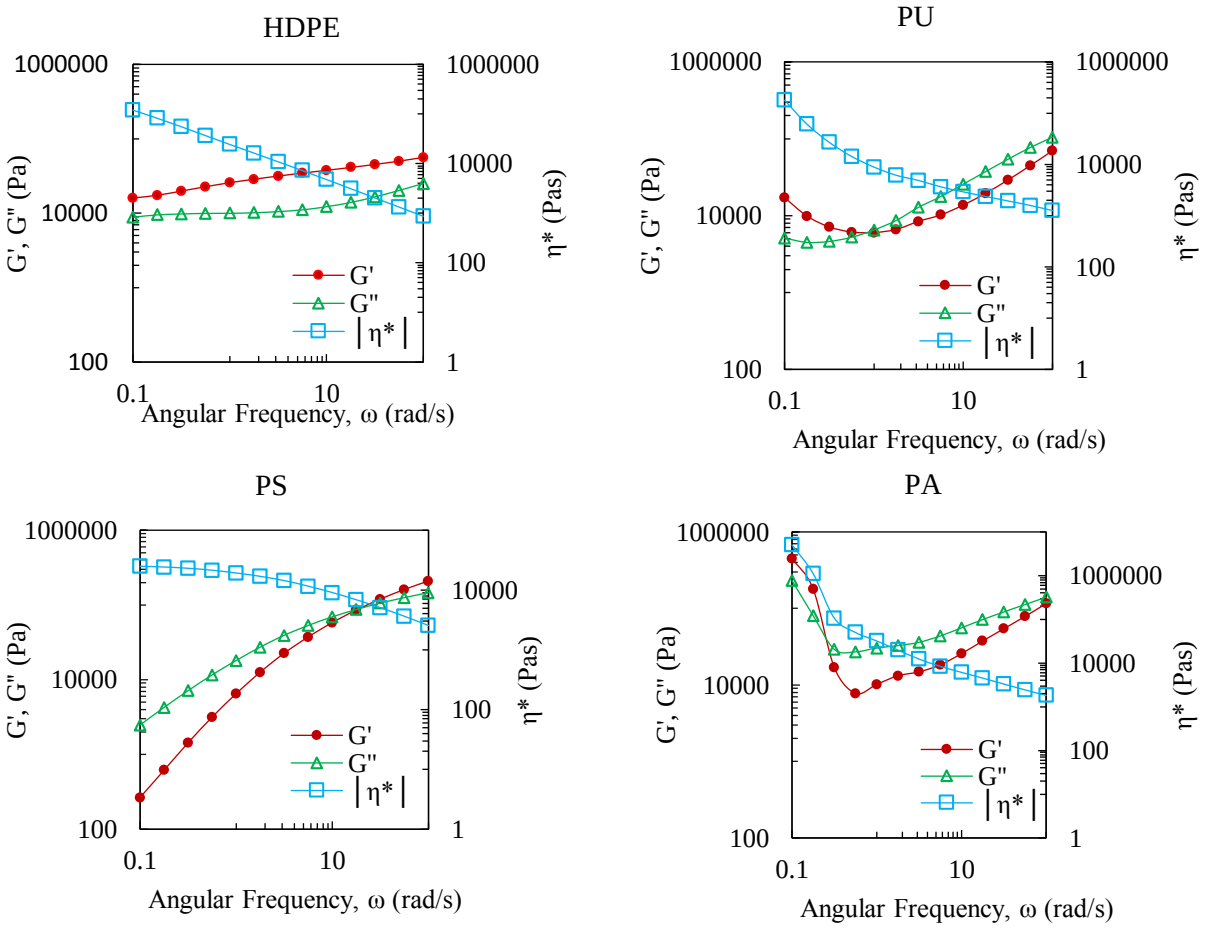

Figure 20 – Frequency sweep of the melt cast samples of the four studied materials at a strain of γ = 20% at their melting points

In Figure 21, the amplitude sweeps of HDPE, PU, PA and PS at the fixed frequency of ω = 5 rad/s are shown at their melting points. The loss to storage modulus ratio was found to be less than 1 or close to 1 for HDPE and PU over the studied strain rates up to 500%. For PS and PA, however, this ratio was found to start at values less than one but grow larger than one at about 50% strain rates for PS and 100% strain rates for PA. Towards the highest studied strain rates in this experiment, the loss modulus was found to grow to 3.3 and 2.5 times larger than the storage modulus for PS and PA, respectively. This might suggest the idea that when the loss to storage modulus ratio is much higher than one, $G''/G' >> 1$, deposition takes place and when loss to storage modulus ratio is less than one, $G''/G' < 1$, particle rebounds. Although the strain rates that particles undergo during the cold spray deposition process, ~10^6, is several orders of magnitude larger than what is this sets of rheological analysis, this high temperature rheological experiment could at least give a means of comparison between the storage and loss moduli of the studied materials to

help us further understand the causes of their different deposition behaviors. Therefore, our observations here are rather suggestive and do not lead to any certain conclusion.

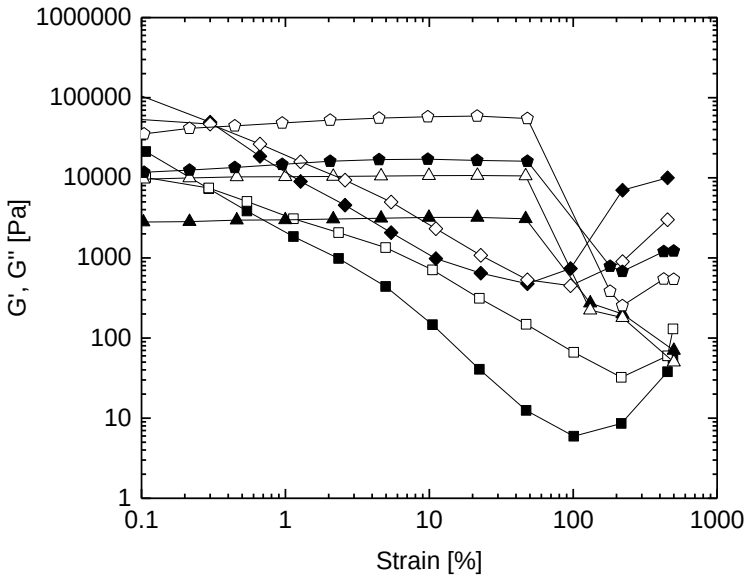

Figure 21 – Amplitude sweep of PE, PU, PA and PS at ω = 5 rad/s at their melting point, G' (—■—) and G'' (—□—) for HDPE, G' (—▲—) and G'' (—△—) for PU, G' (—⬟—) and G'' (—⬠—) for PA, G' (—◆—) and G'' (—◇—) for PS.

CHAPTER 5
DEPOSITION EFFICIENCY

As discussed in the introduction section, the critical velocity for the cold spray deposition of polymers is proven to be significantly lower than the critical velocity needed to deposit metal powders. This is true even if one factors in the differences in mechanical properties used to calculate the critical impact velocity using equation 4. Unfortunately, another major difference between HDPE and metallic particles was a dramatic reduction in the deposition efficiency. For metallic particles, deposition efficiencies can approach 100%. For polymer particles, the only efficiencies reported to date were an unspecified value below 1% [12].

Differences in bonding mechanisms likely contribute to differences in deposition efficiency between polymers and metals. As discussed in the introduction, in cold spray of metals, the formation of metallurgical bonds across the interface is often credited as a potent source of adhesion strength [12, 17, 23]. Polymeric materials, however, do not generally form such strong chemical bonds. Polyethylene, being non-polar, is particularly inert, with its cohesive strength primarily provided by chain entanglement and overlap. In order to produce chain entanglement across the interface formed between the impacting particle and the substrate, it would seem that either mechanical mixing, melt fusion, or significant diffusion must occur. The timescale of particle impacts, however, likely rules out a pure diffusive mechanism. Grujicic et al. [16] calculated that the typical metal-metal inter-diffusion distance is between 0.004 and 0.1nm at temperatures near the melting point and for the typical contact time during impact of 40ns. Because this distance is only a fraction of the inter-atomic distance, they concluded that diffusion should not be considered a dominant mechanism. For HDPE and other polymers, the lower thermal diffusivity will lead to a larger temperature gradient upon impact, lower viscosities and enhanced diffusion after the particle impact. Together, this should lead to diffusion over a greater distance in polymers as compared to metals. However, the distance requirement is much larger for polymers than for metals. For metals, the interatomic distances are on the angstrom to nanometer scale in a metal lattice. However, for a polymer the more appropriate length scale is the radius of gyration of the polymer which can be tens of nanometers or more. Diffusive processes alone are, therefore, not likely the dominant contributor to the observed adhesion in cold spray of HDPE particles.

Some amount of mechanical mixing is therefore likely needed to induce interaction and entanglement between the polymer chains in particles and the polymer chains in the substrate. As shown by the simulation of Shah et al. [19], adhesion energy alone cannot explain polymer powder deposition in the cold spray

process. At impact, the resulting shear rate can exceed $\dot{\gamma} = U_{pi} / D_p > 10^6 s^{-1}$. At these rates, the Weissenberg number, $Wi = \lambda \dot{\gamma}$, of the molten polymer within the zone of the adiabatic shear instability will be enormous resulting in huge elastic stresses and perhaps even the onset of elastic flow instabilities, like elastic turbulence [43]. These instabilities could drive mechanical mixing between the particle and substrate. Here λ is the relaxation time of the molten polymer. Although the underlying mechanism of the particle deposition and bonding cannot be precisely determined from our experiments, we can begin to develop paths towards improvement in polymer cold spray deposition efficiency by investigating the role of a number of easily modified process parameters on deposition efficiency. These parameters include: changes to particle temperature, impact velocity, and size; variation of the substrate material and temperature; and changes to the standoff distance between the nozzle and the substrate. Cold spray deposition efficiency of the HDPE particles on an LDPE substrate as a function of particle impact velocity and hopper temperature can be seen in Figure 22.

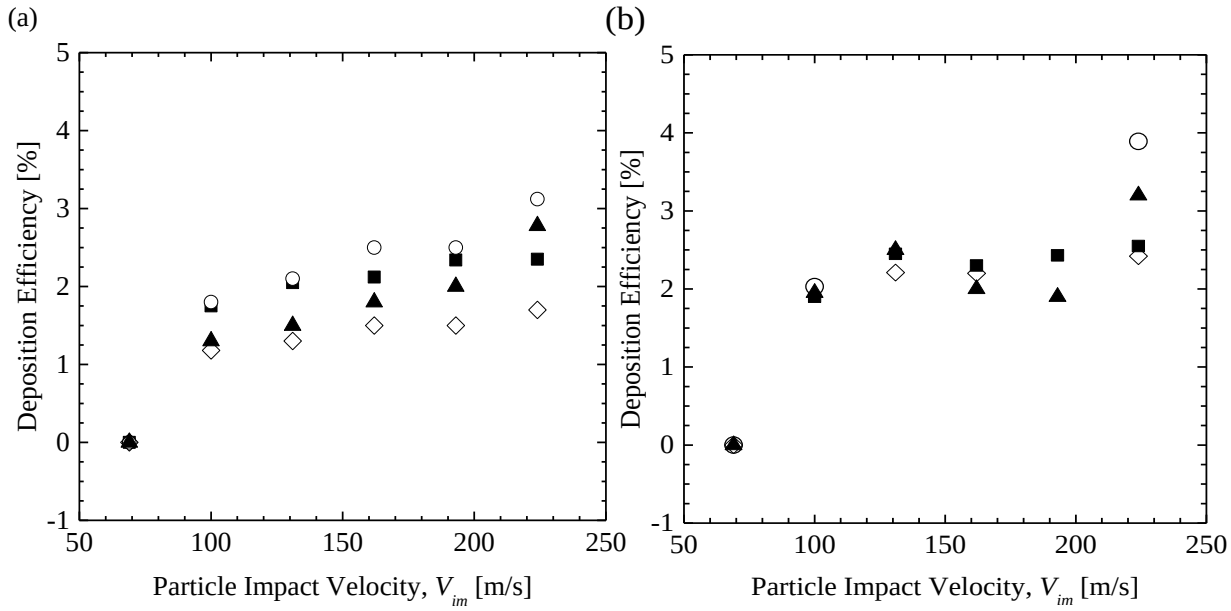

Figure 22 – Cold spray deposition efficiency of 48µm diameter HDPE particles on an LDPE substrate as a function of particle impact velocity at hopper temperatures of a) T_H = 20 °C and b) T_H = 50 °C. Data are included for standoff distances of L_{SD} = 5mm (■), L_{SD} = 10mm (○), L_{SD} = 15mm (▲) and L_{SD} = 20mm (◊).

The deposition efficiency of 48 µm diameter HDPE particles on an LDPE substrate is shown in Figure 22 as a function particle impact velocities and stand-off distance for hopper temperatures of T_H = 20 °C (a) and T_H = 50 °C (b). These two temperatures were chosen as representational to illustrate room

temperature and roughly the maximum processing temperature of the hopper. For hopper temperature much beyond $T_H > 50$ °C, the HDPE particles became tacky and began to stick to each other within the hopper, and to the walls of the hopper, making smooth continuous processing difficult or impossible. No deposition was observed for particle impact velocities below a critical velocity of approximately $V_i = 100$m/s. Beyond this critical deposition velocity, particle deposition was observed with an initial deposition efficiency of between 1% and 2% depending on the processing conditions. The deposition efficiency was observed to increase monotonically with both increasing impact velocity and increasing hopper temperature. However, neither particle impact velocity nor hopper temperature had the desired dramatic effect on deposition efficiency. Take for example the case of the particle at $T_H = 20$ °C and a nozzle stand-off distance of $L_{SD} =$ 10mm. For this case, increasing the particle impact velocity from $V_i = 100$m/s to $V_i = 225$m/s resulted in an increase in deposition efficiency from 1.8% to 3.2%. Similar increases, or near doubling, of the deposition efficiency were observed with the increase in particle impact velocities for all processing parameters studied. However, for these experiments, the maximum observed deposition efficiency was always found to be less than 4%. Increasing the hopper temperature from $T_H = 20$ °C to $T_H = 50$ °C had a modest effect, generally increasing deposition efficiency by only 0.2 to 0.5%. In both cases, the increase in deposition efficiency is likely the result of increased deformation of the particle and substrate during impact. For the case of increasing particle impact velocity, the more energetic impact likely resulted in an increase in heat dissipated during the plastic deformation of the particle and substrate during impact and a thermal softening or even localized melting of the impacting particle and substrate leading to adhesion [1]. Increasing the hopper temperature had a similar effect as the particles begin and remain hotter throughout the nozzle and, upon impact, the polymer were more mobile, deformable and closer to the melt temperature.

The effect of stand-off distance was found to be non-monotonic. As seen in Figure 22, an optimum stand-off distance between the nozzle and the substrate was found to be approximately $L_{SD} = 10$mm. With increasing stand-off distance, the HDPE particles have more time to accelerate in the high-speed jet exiting the nozzle as seen in Figure 2, but simultaneously, they have more time to cool to the temperature of the surrounding high-speed gas. These two effects are conflicting, as it is clear from Figure 8 that increasing velocity and increasing, not decreasing, temperature improve deposition efficiency. The observed optimal stand-off distance is not likely to be universal from one cold spray setup to the next but will likely depend in some way on the complex flow profile downstream of the nozzle which for supersonic flows can include oblique shocks, expansion waves and bow shocks near the substrate.

The deposition efficiency data in Figure 22a appear to increase roughly linearly with increasing particle impact velocity. As a result, if we were to extrapolate the data to say 1000m/s, which is near the limit of metal cold spray deposition, a deposition efficiency of less than 10% would still be expected. Thus,

reaching a deposition efficiency of 100% by tuning only the particle temperature and the particle impact velocity does not appear to be feasible. In Figure 23, data are presented with a substrate heated from room temperature up to T_s = 120°C. Note that the substrate temperatures quoted are measured from a thermocouple far from the deposition area, and substrate temperature is controlled using a PCB (Printed Circuit Board) heater on the moving stage. Because the high speed of the carrier gas downstream of the nozzle intensely cools down the substrate surface, the precise temperature below the impinging jet will be significantly colder than what is measured by the thermocouple and reported here. The objective of these experiments was to investigate the effect of enhancing the mobility the polymer chains within the substrate and, at the higher temperatures, using the heat from the substrate to enhance the mobility of the impacting HDPE particles. In Figure 23, results showing the cold spray deposition efficiency of 48μm diameter HDPE particles on an LDPE substrate are presented as a function of substrate temperature for a hopper temperature of T_H = 50°C and a particle impact velocity of V_i = 162m/s. A comparison between Figure 22 and Figure 23 shows that heating the substrate influences deposition efficiency more significantly than heating the powder or increasing the impact velocity. At a stand-off distance of L_{SD} = 10mm, increasing the substrate temperature from T_s = 20°C to T_s = 120°C resulted in a nearly fourfold increase in the deposition efficiency from 2.1% to 7.6%. It should also be noted that heating the substrate made it possible to deposit HDPE particles on inorganic substrates which was otherwise impossible. Under the processing conditions shown in Figure 23 and a substrate temperature of T_s = 120°C, successful deposition on glass with a deposition efficiency of 0.5% was achieved while deposition on aluminum with a deposition efficiency of 1.0% was possible. Ravi et al. [11] were also able to deposit high molecular weight polyethylene ceramic composites on aluminum only after they heated the aluminum substrate. This is thought to be because the creation of a molten layer of the polymer is a crucial step required before any low temperature adhesion to aluminum take place [19].

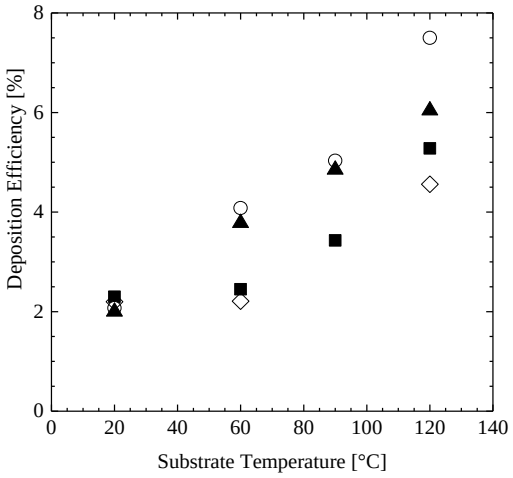

Figure 23 – Cold spray deposition efficiency of 48 μm diameter HDPE particles on a LDPE substrate as a function of substrate temperature for a hopper temperature of T_H = 50°C and a particle impact velocity of V_i = 162m/s. Data is included for stand-off distances of L_{SD} = 5mm (■), L_{SD} = 10mm (○), L_{SD} = 15mm (▲) and L_{SD} = 20mm (◊).

Finally, we investigated the effect of particle size on deposition efficiency. In Figure 24, cold spray deposition efficiency for HDPE particles with mean diameters of D_p = 48μm, 106μm and 200μm on an LDPE substrate are plotted for a hopper temperature of T_H = 50°C, a particle impact velocity of V_i = 162m/s, a substrate temperature of T_s = 20°C and a stand-off distance of L_{SD} = 10mm. Decreasing the particle size significantly improves deposition efficiency. By decreasing particle size from 200μm to 48μm the deposition efficiency was found to increase from 0.45% to 2.3%. This increase is roughly inversely proportional to the particles size, $DE \propto 1/D_p$. This observation is consistent with predictions of numerical simulations and can be understood through the development of a simple theory.

In previous numerical studies, mechanics of metal and polymeric particle impacts have been shown to strongly depend on the ratio of the kinetic energy per unit volume of the particle at the time of impact to the plastic strain energy density [19, 44, 45]. This non-dimensional parameter is expressed as $\rho U_{pi}/\sigma_Y$ where σ_Y is the substrate's dynamic yield strength. Thus, the deformation of the particles upon impact is expected to be independent of the particle diameter if the material behavior is rate-independent and the gravitational effects are negligible. The gravitational effects can be considered negligible because we are dealing with micron-sized bodies. The material properties of the particle and substrate are rate dependent; however, numerical simulations of HDPE particle impacts showed little difference in particle deformation even as the particle size was increased by an order of magnitude from 50μm to 500 μm [19]. The net result was

more than 90% of the kinetic energy of the impacting particle dissipated as heat due to the plastic deformation of the particle and the substrate. Unfortunately, even though the same fraction of kinetic energy was dissipated for all particle sizes, the kinetic energy upon impact, and thus the non-dissipated kinetic energy remaining in the particle after impact, will grow like the mass or volume of the particle, $KE_{ND} \propto D_p^3$. For the particle to deposit on the substrate, the work of adhesion between the particle and substrate must be larger than the remaining kinetic energy in the particle, $W_{PS} > KE_{ND}$. The work of adhesion will grow with the cross-sectional area of the impact crater formed between the impacting particle and the substrate which is proportional to the square of the particle diameter, $W_{PS} \propto D_p^2$. Thus, for the same processing conditions, decreasing particle size is expected to make deposition more likely as the relative importance of work of adhesion to non-dissipated impact kinetic energy grows inversely proportional to particle size, $W_{PS} / KE_{ND} \propto 1/D_p$, just as deposition efficiency was observed to do. These observations would suggest that a possible path towards more efficient deposition would involve the use of even smaller particles. However, it is expected that at some small diameter the reduction in particle mass and inertial will allow them to be deflected away from the surface by the bow shocks and pressure gradients near the substrate where the impinging jet stagnates. Future studies are planned to test the lower limit of particle size.

In order to better understand cold-spray deposition of HDPE powders, deposition experiments were performed on both polymeric and non-polymeric substrates. For deposition of HDPE on non-HDPE polymeric substrates, adhesion can still be promoted by polymer mixing and entanglement. However, for successful deposition on non-polymeric substrates like aluminum and glass, particle adhesion will have to rely on energy dissipation due to plastic deformation of the particle and a large growth in the interfacial energy resulting from significant deformation and spreading of the impacting particle on the substrate. It is known that a large mismatch in the modulus of the particle and the substrate can lead to enhanced particle or substrate deformation and higher likelihood of adhesion [19, 46]. Bae et al. [46] performed a combined FEA and experimental study of metallic deposition and demonstrated that critical velocity decreases both when the substrate is harder and when it is softer than the impacting particle. They showed that when the particle was softer than the substrate, the particle experienced most of the plastic deformation, which created a greater contact area and higher interface temperature compared to the matched-hardness case. When the particle was harder than the substrate, the substrate underwent the more severe deformation, but again produced greater contact area and higher interface temperature compared to the matched-hardness case [46]. Similar results were found by Shah et al. [19] who simulated the impact of polymer particles on both polymeric and metallic substrates with various elastic moduli.

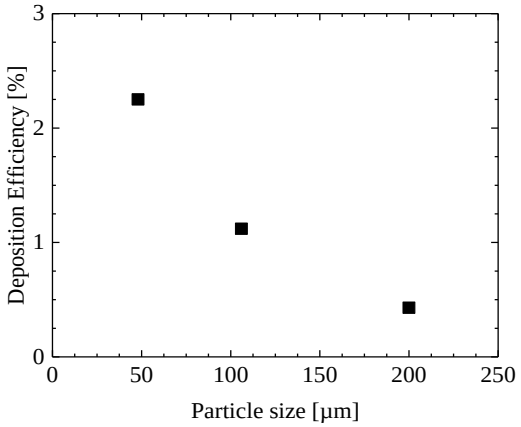

Figure 24 – Cold spray deposition efficiency on an LDPE substrate as a function of HDPE particle size for processing conditions involving a hopper temperature of T_H = 50°C, a particle impact velocity of V_i = 162m/s, a substrate temperature of T_s = 20°C and a stand-off distance of L_{SD} = 10mm.

The cold spray deposition efficiency, *DE*, of all studied particle/substrate pairs for both cases of deposition on LDPE and on melt-cast surfaces of the same polymer are plotted against particle impact velocity in Figure 25. The deposition efficiency of the HDPE particles [13] was found to be significantly larger than all the other polymers tested. Its maximum deposition efficiency was found to be more than 8% on LDPE and 5% on a melt-cast surface of HDPE. None of the other polymer tested achieved an efficiency of more than 6%. The deposition efficiency of the polyurethane particles was found to be larger than either the polyamide 12 and polystyrene particles for both the case of cold spray deposition on LDPE and the case of like-on-like deposition. The deposition efficiency of UHMWPE particles was found to be extremely low at less than 3%. These differences are likely due to the differences in their glass transition temperatures and variations of their mechanical and viscoelastic properties at elevated temperatures and at these extremely high deformation rates. In Figure 25, a monotonic increase in the deposition efficiency is observed with increasing impact velocity for all the particles in both like-on-like deposition cases as well as in cases of deposition on LDPE. With increasing impact velocity, however, the deposition efficiency was not found to increase past 10% for any of the velocities or any of the studied particle-substrate combinations. For metals like copper and aluminum, on the other hand, the variation of deposition efficiency with particle impact velocity is reported to be quite different [1]. They resemble more like a step function rather than a continuous trend observed here. In metal cold spray, at impact velocities just above the critical velocity, a deposition efficiency of *DE* = 25% is observed, but then it abruptly increases to *DE* = 75 – 100% at impact velocities higher than $1.2V_{cr}$ [1]. A similar trend was not observed here or for HDPE depositions in the past. Also, interestingly, there is no reduction of deposition efficiency at the highest velocities at which

deposition was possible. Instead, the data abruptly goes from 3 or 4% deposition efficiency to 0%. This is because at these high velocities, deposition is initially achieved, but due to the poor adhesion between the particle and the substrate, large sheets of deposited material are stripped off by the shear stresses generated by high speed gas as the impinging jet is translated across the substrate.

The temperature of both particle and substrate was found to play a key role in contributing to the deposition efficiency. For instance, at room temperature ($T_p = T_s = 20$ °C), the deposition efficiency of *DE* = 2.1% was achieved for polyurethane particles deposited on an LDPE substrate at the impact velocity of $V_i = 270$ m/s. As can be seen in Figure 25, polyurethane particles deposited at the deposition efficiency of *DE* = 5.2% at the same impact velocity, but particle temperature of $T_p = 80$ °C and substrate temperature of $T_s = 120$ °C. This means a 59% increase in the *DE* as a result of a 60 °C increase in particle temperature (from 20 to 80 °C) and 100 °C in the substrate temperature (from 20 to 120 °C). For polyamide particles depositing on LDPE, *DE* was found to increase from 2.5% to 4% as the particle temperature increased from $T_p = 20$ °C to 120 °C at the impact velocity of $V_i = 190$ m/s. At a same impact velocity and a fixed particle temperature of $T_p = 80$ °C, *DE* of polyamide particles was found to increase from 2.5% to 4% with increasing the substrate temperature from $T_s = 20$ to 120 °C. Similar trends in *DE* were observed as the particle and substrate temperatures varied for polystyrene particles cold sprayed onto LDPE substrates. UHMWPE did not deposit at room temperature on either LDPE or melt-cast surface of UHMWPE. Only after the substrate was heated above $T_s = 100$ °C and the particles above $T_s = 60$ °C, did the UMMWPE start depositing. The *DE* for UHMWPE depositing on LDPE was found to increase from 1.5 % to 1.8% as the particle temperature increased from $T_p = 60$ to 80 °C at a fixed substrate temperature of $T_s = 100$ °C. Bush et al. [13] showed a 29% increase (from 1.5% to 2.1%) in *DE* for HDPE particles deposited on LDPE at the impact velocity of $V_i = 162$ m/s as a result of an increase in particle temperature from $T_p = 20$ °C to 50 °C at a fixed substrate temperature of $T_s = 20$ °C. They also demonstrated a 46% increase (from 2% to 3.75%) in *DE* for HDPE particles deposited on LDPE at the impact velocity of $V_i = 162$ m/s this time as a result of an increase in substrate temperature from $T_p = 20$ °C to 50 °C at a fixed particle temperature of $T_s = 50$ °C.

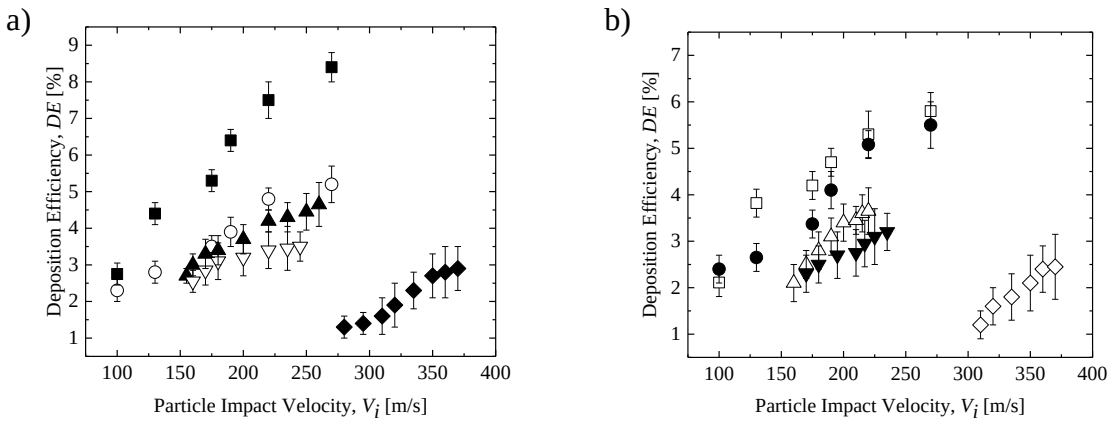

Figure 25 – Variation of deposition efficiency with the particle impact velocity for both (a) deposition on LDPE and (b) like-on-like depositions in the cold spray experiments. (■ , ▫) HDPE, (● , o) polyurethane, (▲ , △) PA12, (▼, ▽) PS, and (◆, ◊) UHMWPE. Particles of HDPE, polyurethane and UHMWPE were at T_p = 80 °C and polystyrene and polyamide 12 particles were at T_p = 120 °C. Substrate temperature was kept at T_s = 100°C for all experiments.

Table 4 – Maximum deposition efficiency percentage measured for various particle/substrate pairs under optimized conditions.

Particles / Substrate	HDPE	PU	PA12	PS	UHMWPE
LDPE	8.4	5.2	4.65	3.5	2.9
HDPE	5.8	–	–	–	–
PU	–	5.5	–	–	–
PA12	–	–	3.65	–	–
PS	–	–	–	3.2	–
UHMWPE	–	–	–	–	2.45

Studies of the deposition efficiency in the cold spray process for any studied particle/substrate combinations revealed the optimized process conditions to include the particle impact velocity in the range of (1.17 – 2.8) times the critical velocity, $V_i = (1.17 – 2.8)\ V_{cr}$, the particle impact temperature in the range of (0.6 – 0.75) times the particle melting point, $T_{pi} = (0.6 – 0.75)T_m$, and the substrate temperature at T_s =100 °C. Other observation from these studies as shown in Figure 25 and Table 4 is that the maximum deposition efficiency was assigned to HDPE cold sprayed onto an LDPE substrate and the minimum deposition efficiency was found to refer to the cold spray deposition of UHMWPE on a melt-cast sample of UHMWPE under above-described deposition conditions.

CHAPTER 6
CONFORMAL COATINGS ON 3D OBJECTS

In 3D printing, crack sealing, coating repair and generally in additive manufacturing processes, it is worthwhile to define the maximum impact angle at which the sprayed particles deposit on a substrate. Knowing this critical angle will allow for the determination of the feasibility of creating a uniform thin coating that conforms to substrates that are not flat but have surface roughness and specific topographical features.

In the experiments that follow, the cold-spray nozzle was kept stationary and the substrate was tilted at angles between $\alpha = 0°$ and $\alpha = 90°$ from the horizontal as shown in Figure 26. The tilted substrate simulates the conditions of a particle impacting a rough surface either due to its surface finish or the accumulation of previous particles deposited through cold spray. It is important to note that even for a substrate held perpendicular to the gas/particle stream, cold-sprayed particles impact the substrate at a wide range of impact angles due to the turbulence in the air and the associated drag forces and the collisions from other particles and walls of the nozzle. On average, the particles move in the direction of the gas flow. Generally, in the cold spray process, the data will demonstrate that particles deposit most efficiently when they impact normal to the substrate surface. Increasing the tilt angle reduces the normal component of the impact kinetic energy, $\frac{1}{2}m_p V_i^{\,2}\cos^2\alpha$, available to heat and deform the impacting particle while simultaneously increasing the tangential component of the impact velocity leading to shear stresses that can strip off poorly adhered particles. An LDPE substrate was attached to a tilting stage attached to the moving stage. Because a separate tilting stage was used, the printed circuit board plate could not be used to heat the LDPE substrates. As a result, all experiments were performed with a room temperature target substrate. Additionally, the 1D motion of the stage was aligned normal to the tilting direction, so that the stand-off distance was held fixed during stage motion.

In Figure 27, the maximum tilting angle at which successful cold spray deposition was possible on an LDPE substrate is shown for HDPE, PU, PA and PS particles as a function of both particle temperature and velocity. Increasing either particle temperature or impact velocity was found to result in an increase in the maximum tilting angle for substrate. For instance, increasing the PU particle temperature from $T_p = 20$ °C to 80 °C resulted in an increase in the maximum substrate tilt angle from 20° to 60°. Similar increases were observed for the other particles with temperature and velocity increases from $V_i = 150$ m/s to 300 m/s. For each data point in Figure 27, The vertical component of the impact velocity, $V_i \cos\alpha$, was found to be roughly equal to the critical velocity for $\alpha = 0°$ and the same deposition conditions. For $\alpha = 0°$, the critical impact velocity for HDPE, PU, PA and PS are $V_{crit} = 150$ m/s, 160 m/s, 180 m/s and 185 m/s, respectively.

In Figure 28, $V_i \cos \alpha$ data are plotted against V_i for the four polymer particles studied. It is seen from this figure that $V_i \cos \alpha$ data range is roughly constant around 150 m/s for HDPE and PU but grows slowly from 167 to 213 m/s with increasing particle impact velocity for PA and PS. In fact, the results from deposition on tilted substrates suggest that only the normal component of the velocity is important in particle adhesion. The slow increase in the normal component of the critical impact velocity might be due to the increase in shear stress from the air flow and glancing collisions from non-adhesive particles with increasing gas flow velocity and substrate angle. This is more obvious for the high-T_g polymers which show significantly less deformation upon impact [25] than the low-T_g particles and are as a result less strongly adhered upon initial deposition and as a result more susceptible to being removed by shear stress.

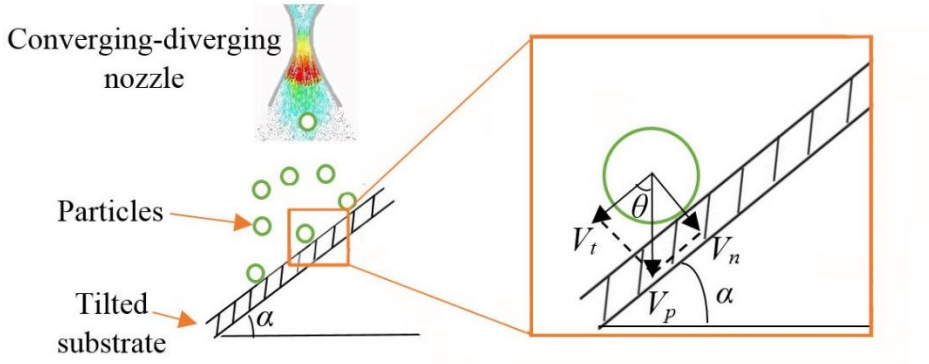

Figure 26 – Cold sprayed particles impacting a tilted angled substrate.

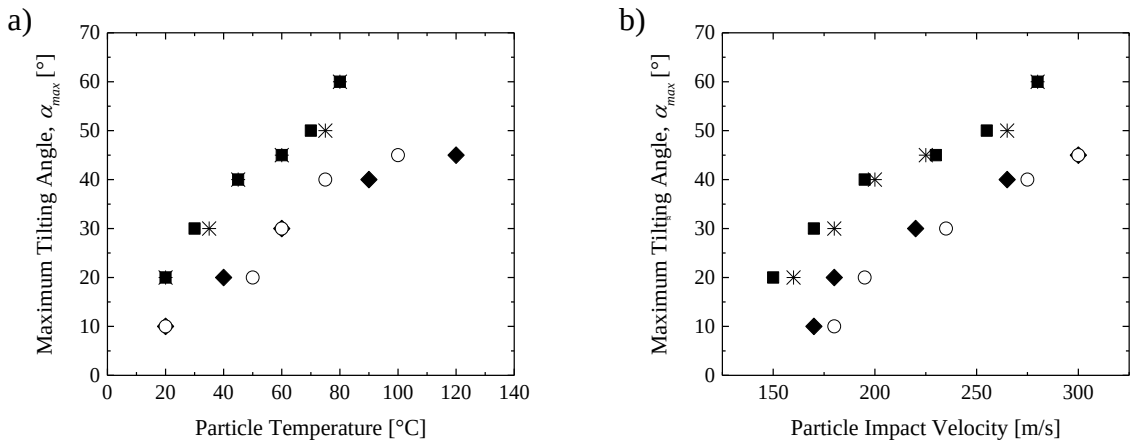

Figure 27 – Maximum tilting angle for successful deposition on an LDPE substrate as a function of (a) particle temperature and (b) impact velocity. The particle impact velocity was V_i = 170 m/s for all the experiments in (a) and the particle temperature was kept at T_p = 50 °C for all experiments in (b). The

substrate was at room temperature and the standoff distance was kept at 10 mm. the data include (■) HDPE, (*) PU, (♦) PA, and (○) PS.

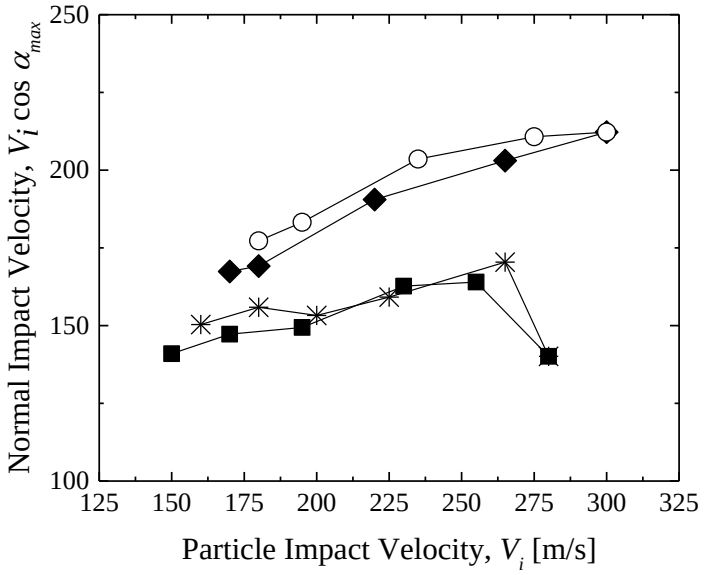

Figure 28 – Normal component of the critical particle impact velocity, $V_i \cos \alpha_{max}$, at the maximum substrate tilt angles for successful deposition on LDPE as a function of the measured critical particle impact velocity. In all cases, the substrate was maintained at room temperature and the particles were at T_p = 50 °C. The data include: (■) HDPE, (*) PU, (♦) PA, and (○) PS.

These results also suggested that deposition could be improved if we repeated some of the previous cold spray experiments at higher traverse speeds in order to allow for a larger proportion of the accelerated particles to impact the smooth surface of the substrate rather than bumpy surface of already deposited particles. These results also suggest that a line deposited using cold spray should obtain a triangular cross section with a side angle that corresponds to the critical deposition angle at the operating condition being used. These triangular cross-sections have been seen here and were documented by Bush et al. [13]. Once the triangular cross-section has been deposited with a base width of the impinging jet diameter, no additional deposition is possible and as a result the deposition efficiency will go down. There is thus an optimal particle flow rate and substrate traverse speed that should optimize deposition efficiency. For the

deposition of HDPE particles on an LDPE substrate, as the traverse speed was increased by a factor of two, the deposition efficiency was found to increase from 6.5% to 9% for an impact velocity of V_i = 250 m/s and a particle temperature of T_p = 80 °C. The coating thickness was simultaneously reduced by only 30% even as the speed was doubled. This result suggests that surface roughness can play a large role in the overall deposition efficiency. Understanding the role of surface topography can lead to even higher deposition efficiency in the future.

The study of the maximum tilting angle for successful deposition, also reveals that when the particle impacts take place on a tilted substrate, the normal component of the impact velocity on the substrate surface should equal or surpass the critical velocity obtained from deposition on a flat substrate. This finding indicates that in creating a conformal coating on 3D objects, it is essential that the robotic arm holding the nozzle continuously changes its position with regard to the 3D object to ensure a high enough normal component for the particle impact velocity.

CHAPTER 7
SINGLE PARTICLE MICRO-BALLISTIC IMPACT EXPERIMENTS

This chapter is a collaborative work with Professor Jae-Hwang Lee's research group. Wanting Xie implemented all the laser induced single particle impact experiments in Professor Jae-Hwang Lee's lab and the cold spray depositions and SEM studies were done by me in the Non-Newtonian Fluid Dynamic Lab. In this study, cold spray deposition and single particle impact experiments of some of the polymeric materials for both cases of like-on-like deposition and deposition on low-density polyethylene were performed to further explore the adhesion process of polymer particles impacting a polymer substrate. The laser-induced micro-ballistic single particle impact studies provided some valuable insights into the particle deposition process and highlighted intriguing differences between single particle and multiple particle impacts.

A Laval nozzle capable of accelerating particles to Mach number of $Ma = 2$ was used in the cold spray system showed in Figure 2. The nozzle's dimensions and the details of how the particle velocities were calculated for a given processing conditions can be found in Bush et al. [13]. The stand-off distance between the nozzle exit and the substrate was kept at 10 mm for all experiments. At this stand-off distance, the maximum deposition efficiency was observed in our previous experiments [13]. A temperature-controlled 2D xy-stage operated by an open source software package designed for 3D printing (Repetier-Host) was used to move the substrate underneath the nozzle exit at controlled speeds to create deposition patterns consisting of 1D lines and 2D patterns. Here all 2D deposition patterns were 2cm × 2cm squares that required multiple passes to deposit with 25% overlap between sequential lines (the overlap percentage is true for specific conditions of particle size, velocity and flowrate of about 50 μm, 150 m/s and 35 g/min, respectively).

7.1 High Speed Camera Velocity Measurements

As described in the introduction section, the particle impact velocity reported in this work were calculated through the 1D analytical method for inviscid gas flow. The measurement error for the results of this analytical method was obtained to be below 20 m/s. In order to further study the accuracy of the velocity calculation of this method, a high-speed camera was used as described in section 2. The impact velocity was too large to be captured with the high-speed camera. However, we were able to measure the rebound velocity of the HDPE particles accelerated through the subsonic nozzle for forty of the particles yielding

the average value of V_r = 32 ± 23 m/s which is roughly consistent with the results from the micro-ballistic single particle impact experiments which calculated the HDPE particle rebound velocity as V_r = 20 ± 5 m/s.

7.2 Cold Spray Deposition of High-T_g Polymers

For both PA and PS particles, deposition was studied on substrates melt-cast from either the polystyrene or polyamide particles to test like-on-like deposition or substrates melt-cast from LDPE to study deposition on a substrate with a different modulus. In Table 1, the properties of polymer materials studied in this work are shown. SEM images of the feedstock powder particles for both PA and PS particles are shown in Figure 1c and d. It can be seen in Figure 1c and d that the PS particles are nearly spherical, but the PA are clearly more irregular with facetted surfaces and sharp edges which make them more challenging to process through the hopper of the cold spray system, a schematic diagram of which is shown in Figure 2b [13]. As described in the introduction section, this is a laboratory-scale cold spray system using a consumer grade single-stage air compressor with the capability of accelerating particles up to Mach 2. Both the PA and PS particles were easily accelerated in the micro-ballistic system shown schematically in Figure 3a. The particle shape did not play a significant role because the velocity of particles was measured directly from high speed photography of their flight as seen in Figure 3b.

A series of cold spray experiments were performed for PS and PA particles deposited on melt-cast PS, PA, and LDPE substrates. In all the experiments, the substrate temperature was fixed at T_s = 100 °C while the particle temperature and impact velocity were varied so that the deposition window for each particle/substrate combination could be determined. In Figure 29, the deposition windows of PA-on-LDPE, PA-on-PA, PS-on-LDPE and PS-on-PS are shown for the cold spray technique. At a given temperature, there exists a critical particle impact velocity above which deposition of PS and PA particles were found to be possible.

When depositing on the softer melt-cast LDPE substrate (Figure 29a and c), the critical impact velocity for the PS and PA particles, at room temperature was found to be just above 160 m/s. As the temperature was increased, the critical velocity was found to decrease roughly linearly with increasing temperature for both the PS and the PA particles to values close to 150 m/s at T_p =100°C. The same decreasing trend has been observed for cold spray of metals like aluminum, copper, steel, and tantalum for the critical velocity with increasing the particle temperature [5, 28, 47]. The deposition window for PA and PS on LDPE are similar in some ways. For instance, from Figure 29a and c, we note that the critical velocity decays with roughly the same temperature dependence for both the PA and PS particles deposited on LDPE. However, there are some important differences to be pointed out as well. At 120°C and above, the PS particles became tacky inside the powder feeding hopper, making powder delivery difficult and cold spray processing

impossible. This did not happen for PA particles which could be processed well above 120 °C. The other major difference is the existence of an upper velocity limit for PS particles above which particles rebound from the substrate leaving signs of erosion on the substrate surface. At room temperature, this upper limit was found to be 230m/s for the PS particles. It was found to increase linearly with increasing particle temperature resulting in a deposition window that expands with increasing temperature. The PA particles, on the other hand, appeared to deposit on LDPE even at the highest velocities studied in this work. It is possible that an upper limit would have been found for PA if higher velocity experiments were performed, however, here we chose to limit our study to velocities less than the speed of sound, $Ma = 1$, to avoid issues associated with shock waves. This upper limit has been observed before [13], and represents the limit where the incoming particles begin to remove particles that initially adhere through an ablation process.

For the case of like-on-like deposition shown in Figure 29b and d, the deposition boundaries were found to shift to higher critical velocity for a given particle temperature creating smaller windows of deposition than those deposited on LDPE. For example, at room temperature, the critical velocity for PA shifted from 161m/s on LDPE to 181m/s on PA (Figure 29a and b) while the critical velocity for PS shifted from 161m/s on LDPE to 170m/s on PS (Figure 29c and b). As the temperature was increased, the critical velocity was found to decay about 1.5 times more rapidly for deposition of PA-on-PA than that of PA-on-LDPE until it reached roughly the same critical velocity of about 155m/s at T_p =120 °C for PA on both substrates. The change in slope was not as great for the PS but can still be seen. It is well known that a mismatch in the modulus between the particle and substrate can lead to an increase in plastic deformation and thus an increased likelihood of adhesion [13, 19, 46]. These differences observed between the like-on-like deposition of PS and PA were unexpected as both PS and PA have roughly the same T_g and T_m. The differences could be linked to the stronger temperature dependence of the critical impact velocity of the PA particles than that of the PS particles. For PS particles, at room temperature, the critical velocity shifted from 161m/s on LDPE to 170m/s on PS (Figure 29c and d). As the temperature was increased, the critical velocity was again found to decrease for deposition on both LDPE and on PS, this time however, at a roughly same trend until at 100°C, it reached 155m/s for PS-on-LDPE and 170m/s for PS-on-PS.

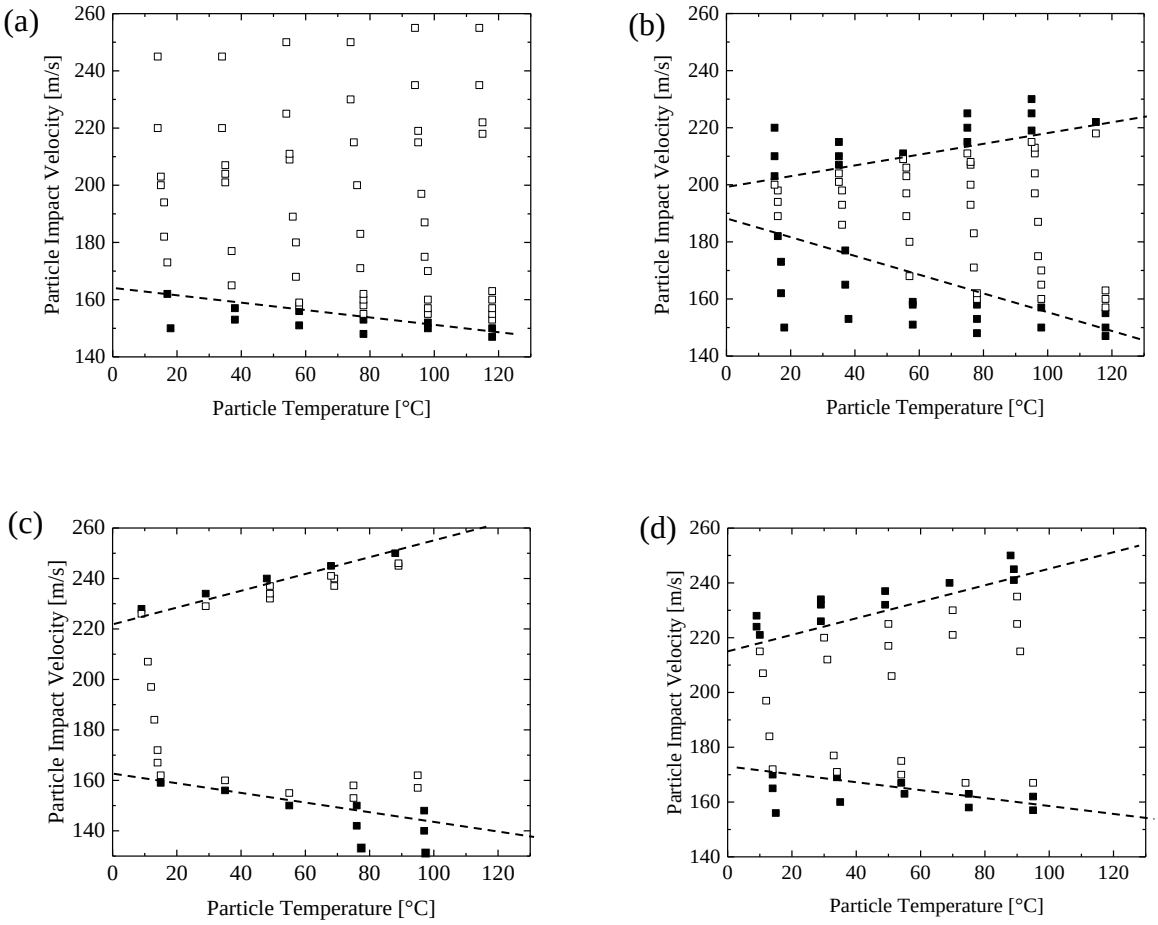

Figure 29 – Deposition window of (a) PA-on-LDPE, (b) PA-on-PA, (c) PS-on-LDPE and (d) PS-on-PS in cold spray experiment showing the transition from no deposition, (□) to deposition, (■). In all cases, the substrate was held fixed at T_s = 100°C and the stand-off distance was 10cm.

From Figure 29 (a-d), an upper limit of deposition can be observed in three of the four deposition windows. For PA particles, the upper limit of deposition was found when the substrate was changed from LDPE to melt-cast PA. Within the range of our experiments, no upper limit was found for PA-on-LDPE deposition. PA-on-PA deposition was found to fail for particle impact velocity above V_i > 210m/s for experiments performed at room temperature. This upper limit of deposition for PA-on-PA was found to increase slightly as the temperature increased reaching a value of V_i = 220m/s at 120°C. For the PS particles, an upper limit of the deposition window was found for both PS-on-PS and PS-on-LDPE depositions, although with slightly different rate of increase in the maximum impact velocity with increasing temperature. The dashed lines which have been superimposed over the deposition data in Figure 29

illustrates the trend of both the lower and upper limits of deposition with increasing temperature. The slope of these trendlines was found to range between 0.23 and 0.33. This is notably smaller than what was previously obtained for the cold spray deposition of HDPE particles on PVC and POM substrates where slopes were between 0.55 – 0.66 [13]. A similarly weaker temperature dependence of critical velocity for successful deposition of both the PA and PS particles was also observed for cold spray deposition compared to HDPE particles. These differences are likely due to differences in the thermal softening of the different polymers at high temperatures and high deformation rates of impact.

7.3 Micro-Ballistic Single Particle Impacts of High-T_g Polymers

In order to better understand the window of deposition achieved in cold spray, a series of micro-ballistic single particle impact experiments were performed under experimental conditions designed to mimic those experienced in the cold spray process. In all cases, the particle and substrate temperature were held constant at 100°C while the particle impact velocity was varied from 50 – 500m/s. In each case, the impact velocity was measured from the ultrafast photographs and, in the experiments where adhesion was not observed, the rebound velocity was also measured. After the successful adhesion experiments, electron microscopy was used to inspect the shape and deformation induced in the particle and substrate.

In Figure 30, the results from single particle impact experiments are shown. Included in this figure are the rebound velocity and the coefficient of restitution, $C_r = V_r/V_i$, for PS particles impacts on PS and LDPE substrates as well as PA particle impacts on PA and LDPE substrates. Here, V_i is the particle impact velocity and V_r is the particle rebound velocity. For particles that were found to adhere to the surface, $V_r = 0$. In

Table 5, the critical velocity obtained from both micro-ballistic single particle impact experiments and cold spray process for PS particles depositing on PS and LDPE and PA particles depositing on PA and LDPE is listed. The particles and substrates were kept at 100°C in both the cold spray and micro-ballistic impact experiments to make comparison possible. It can be seen from the data in

Table 5 that the micro-ballistic single impacts of PS particles depositing on LDPE yielded a critical velocity in the range of V_{cr} = 120m/s to 140m/s. this critical velocity compares favorably to the value obtained from the cold spray process, $V_{cr} = 160 \pm 7$m/s. The PA particles started depositing on LDPE at a slightly higher critical velocity range in the single impact experiments, V_{cr} = 170 to 180m/s. Again, this

critical velocity compares favorably with the value measured in the cold spray process, V_{cr} = 150 ± 30m/s. The larger standard deviations obtained for critical velocities of PA particles in the cold spray process compared to that of PS particles is due to the wider size distribution of PA particles ($50 \pm 25\mu m$) compared to that of PS particles ($44 \pm 4\mu m$). This size variation affects the calculation of the impact velocity as the particle velocity is not measured in the cold spray process but predicted from a series from the compressible flow calculations [13], where the particle diameter is an important input parameter.

The coefficient of restitution, $C_r = V_r/V_i$, is plotted against the impact velocity in Figure 30b. The coefficient of restitution, or more appropriately, one minus the square of the coefficient of restitution, $(1 - C_r^2)$, is indicative of the amount of kinetic energy dissipated by the impacting particles. From numerical simulation, it is known that in high speed collisions, a large portion of the kinetic energy is dissipated in the form of plastic deformation in regions adjacent to particle/substrate interface [16]. In the case of depositing on LDPE, the coefficient of restitution, C_r, was found to decrease with increasing the particle impact velocity, V_i, for both PS and PA in micro-ballistic single impact trials until it reached zero at the critical velocity when the particles began to adhere. Above the critical velocity, the coefficient of restitution remained zero indicating 100% deposition efficiency for PA and PS particles accelerated onto LDPE substrate through the micro-ballistic impact experiments. This observation also indicates that there is no upper velocity limit, at least, within the range of velocities tested here for deposition of PA and PS on LDPE in the single impact trials. This suggests that the impact of successive particles plays a role in the failure to successfully deposit PS and PA on LDPE at large velocities in cold spray. Perhaps the shear stress of successive impacts at a glancing angle as depicted in Figure 34b is enough to dislodge poorly adhered particles. We will come back to this discussion later in the paper.

In the case of micro-ballistic single particle like-on-like deposition, the coefficient of restitution was found to decrease for both the PS and PA particles with increasing impact velocity. The functional form was similar to that observed for impacts on LDPE. However, adhesion was not observed and as a result, the coefficient of restitution never reached zero. Instead, at impact velocities above V_i = 300m/s, the data in the coefficient of restitution plots appeared to approach an asymptotic value of C_r = 0.2 for both the PS and PA particles. Thus, successful like-on-like deposition was not achieved for either PS or PA particles in the micro-ballistic single impact method over the impact velocity range of 100 – 400m/s at 100°C. This represents a major discrepancy between the single particle impact results and the results of the cold spray deposition for which particle adhesion was achieved in like-on-like deposition above a critical velocity of approximately V_{cr} = 170m/s for both PS and PA.

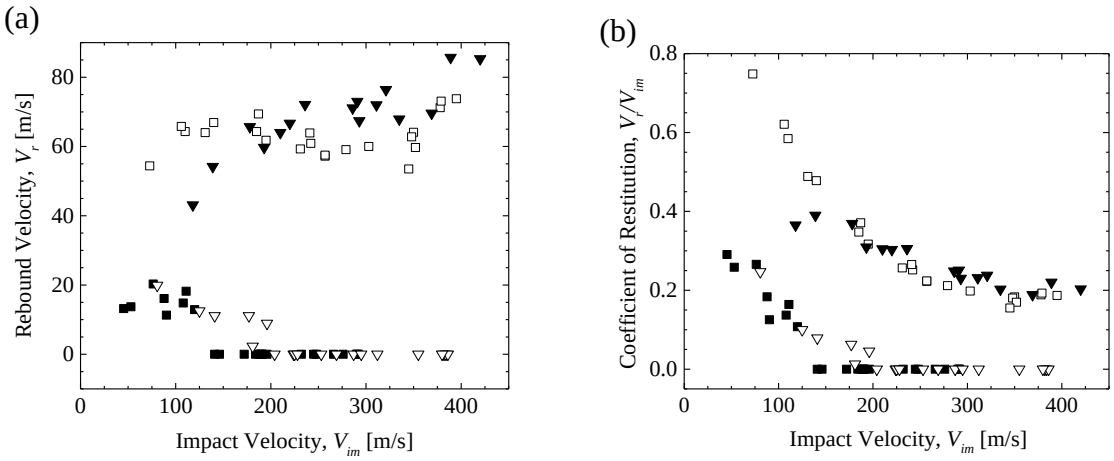

Figure 30 – Results for the micro-ballistic single particle impact experiment including (a) rebound velocity and (b) coefficient of restitution for PS-on-LDPE, (■), PS-on-PS, (□), PA-on-LDPE, (▽), and PA-on-PA, (▼), in the single particle impact test. Both particles and substrates were at the same temperature, $T_p = T_s = 100°C$. Data provided by W. Xie.

Table 5 – Critical velocity obtained from single particle impact test and cold spray process for polystyrene and polyamide-12 particles deposited on LDPE substrates. Particle and substrate temperature is kept at 100°C.

Particle/Substrate	Single Particle Impact Test Results	Cold Spray Process Results
PS-on-LDPE	120 – 140m/s	160 ± 7m/s
PA-on-LDPE	170 – 180m/s	150 ± 30m/s
PS-on-PS	No deposition	170 ± 7m/s
PA-on-PA	No deposition	160 ± 30m/s

For particles that do adhere to the substrate, SEM can be used to study their final shape and degree of deformation. A series of SEM images of PA particles absorbed on the LDPE substrate following micro-ballistic single particle impact at 100°C are shown in Figure 31. All of the SEM images presented in Figure 31 were at an 80° of angle. Some evidences of melting of the particles can be observed at the interface connecting the particle to the substrate where the surface roughness of the particle clearly changes from rough to smooth. As the impact velocity was increased, the degree of polymer melting, and flow clearly increased with liquid regions appearing to flow or climb up the side of the particle after or during deposition. During impact the particle elastically deforms the interface. If some of the particle or substrate melts, it could be pulled back up with the particle as some of the elastic deformation is recovered. It is not clear, however, if the melting originates from the particle or from the substrate. It is likely that the majority of the melt polymer has originated from the substrate rather than the particle because the melting point of LDPE

is more than 50°C less than that of PA. However, recent numerical simulations have shown that upon impact, the temperature at the interface should exceed the melting temperatures of both LDPE and PA [19]. If the melting did indeed originate from the substrate, then it follows that any volume of LDPE from the substrate that has wetted onto the particle, must have been displaced from the substrate leaving behind a crater. However, because no crater is visible adjacent to the deposited particles, any LDPE polymer present on the impacted particle must have been displaced from just beneath the particle. It is likely that the flow of the substrate material onto the particles is contributing to the particle/substrate bond.

The SEM images of PS single particles deposited on LDPE in the micro-ballistic experiment at different impact velocities are shown in Figure 32. Although significant differences are not observed between these SEM images in Figure 32a – f at various impact velocities, a small increasing trend is noticeable in the plastic deformation of the PS particles with increasing the impact velocity. Evidence of melting is also visible around the PS particle deposited on LDPE, more noticeably in Figure 32e at an impact velocity of V_i = 290m/s. The presence of the clear melted region might help explain the difference between the like-on-like and particle on LDPE results. LDPE is well above its T_g at the processing temperature and its melt temperature, T_m = 110 °C is just above the process temperature. As a result, local melting of the LDPE at the particle substrate interface is likely. This molten region likely helps dissipate energy and increase adhesion strength. For both the PS and PA particles, the melting temperature is well above the processing conditions and as a result melting is unlikely.

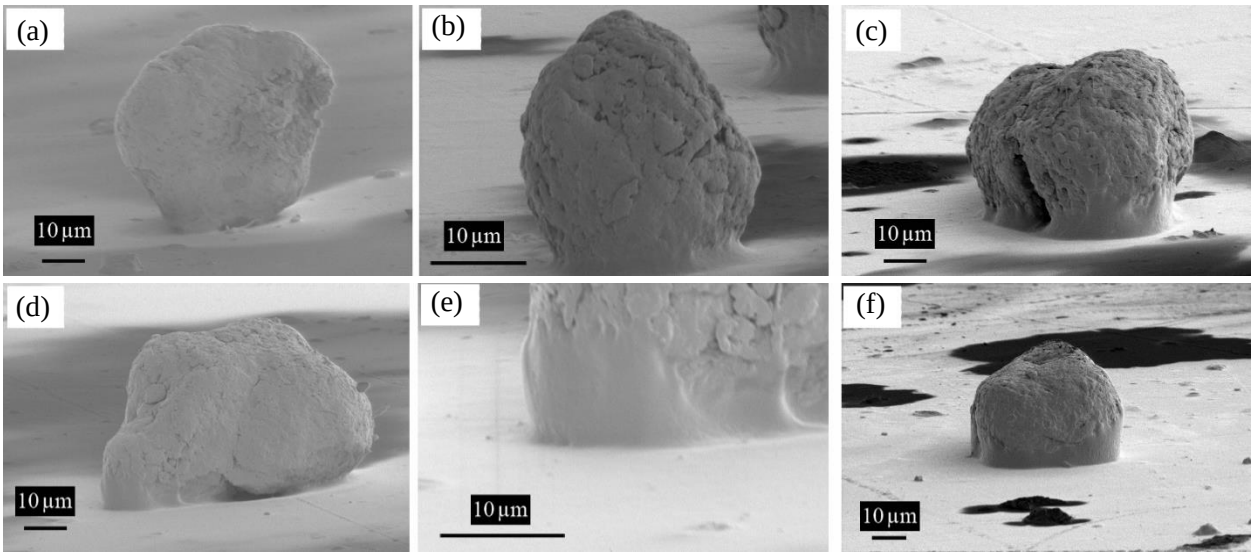

Figure 31 – SEM images of PA particles deposited on LDPE through a micro-ballistic impact experiment. The data include particles with impact velocities of a) V_i = 225m/s, b) 295m/s, c) 355m/s, d) 382m/s, e) higher magnification imaging of (d), and f) 384m/s. All experiments were performed at 100°C. All images are taken at 80° angle so that the interface between particle and substrate could be observed.

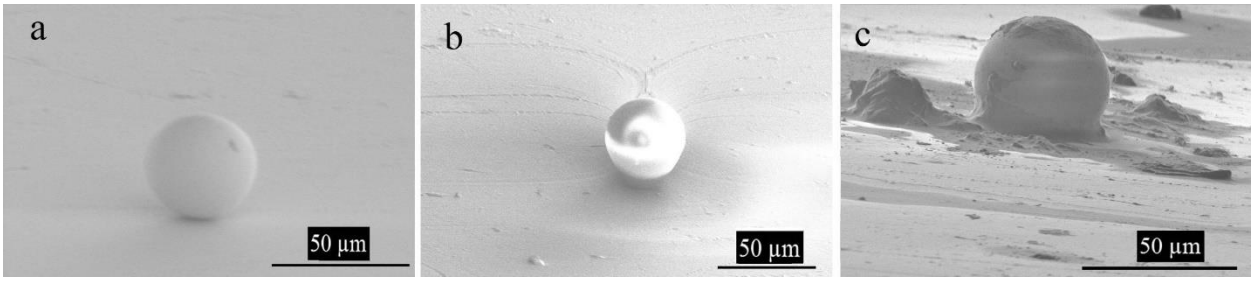

Figure 32 – SEM images of the individual particles of polystyrene deposited on a LDPE substrate at impact velocities of a) V_i = 140m/s, b) 230m/s, d) 290m/s. Both particles and substrates were at a temperature of $T_p = T_s$ = 100°C.

The plastic deformation measured following the successful deposition of the PS particles onto an LDPE substrate using the micro-ballistic single impact technique experiments are plotted against particle impact velocity in Figure 33. The plastic deformation of the particles was found to increase linearly with increasing impact velocity. Similar linear trends were observed between the plastic deformation and the impact velocity for aluminum particles depositing on either sapphire or aluminum in laser-induced single particle impact experiments [33, 48]. Unfortunately, the plastic deformation could not be quantified for the PA particles because, unlike the PS particles, they did not begin the experiment spherical and, as a result, it is unclear what initial condition the final deformed particle should be compared to in order to determine the plastic deformation.

The coefficient of restitution was used to infer the total energy dissipated for both the rebounding and adhering particles, $(1 - C_r^2)$, and it is included in Figure 33 to provide a direct comparison to plastic deformation data of the PS particles. For PS-on-LDPE, at impact velocities as low as V_i = 50m/s, the percentage of impact energy dissipation was above 90%. With increasing impact velocity, the dissipated portion of the impact energy was found to increase monotonically until it reached 100% at V_i = 140m/s. The compression ratio, $\Delta r(= r - r_0)/r_0$, of the particle needed for deposition of PS-on-LDPE in the single particle impact method was measured to be $\Delta r/r_0$ = 1.5%. Here, local strains which should clearly be much larger than this at the interface between the particle and the substrate and not be directly measured. A numerical simulation by Shah et al. [19] using a finite element analysis program, ABAQUS 6.14, with the Lagrangian field specification scheme for high density polyethylene (HDPE) on a HDPE substrate at room temperature showed that the compression ratio of the particle increases from 0.5% at impact velocity of V_i =150m/s to 1.5% at the impact velocity of V_i = 250m/s. This suggests that giving similar compression ratios that it is reasonable to use these simulations to probe in more details of the deformation and temperature

history of the particles and infer similar trend in our experimental impacts. Meanwhile, in the simulations of Shah et al. [19] the temperature at the particle/substrate interfacial region was shown to increase from 32°C to 47°C when the impact velocity was increased from V_i = 150 to 250m/s. The present single impact study for PS particles impacting on an LDPE substrate indicated an increase in compression ratio from 1.5% at the impact velocity of V_i = 140m/s to 7.2% at the impact velocity of V_i = 295m/s. Wanting et al. [33] studied the laser induced single particle impact of aluminum particles with an average diameter of D_{ave} = 19μm on sapphire and found an increase in the plastic deformation of the particles from $\Delta r/r_0$ = 15% to $\Delta r/r_0$ = 55% with increasing the impact velocity from V_i = 170m/s to V_i = 700m/s. Thus, the compression ratio we obtained here in the micro-ballistic single impact experiments for the PS particles on LDPE is an order of magnitude less than that of aluminum particles depositing on sapphire in a similar deposition technique. This implies another important difference between metals and polymers when applying these additive manufacturing techniques.

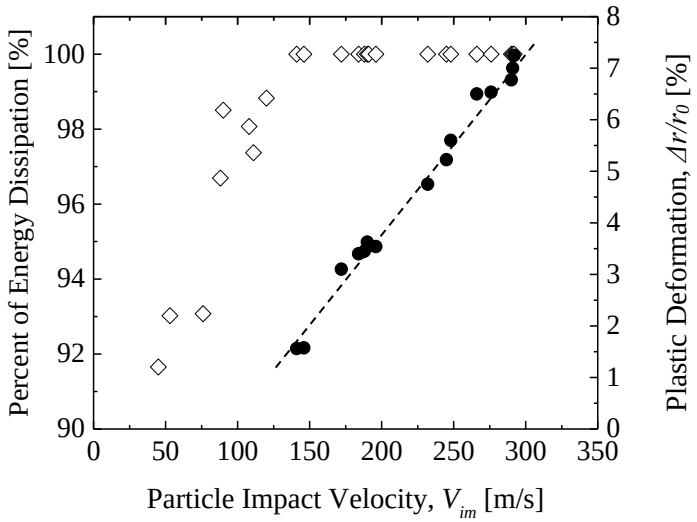

Figure 33 – Results for the micro-ballistic single particle impact experiment including the plastic deformation (●) and percent of energy dissipation upon impact (◊) for PS particles accelerated toward the LDPE substrate. All experiments were performed at 100°C.

The results of the single particle impacts, however, showed a 100% deposition for particles impacting the LDPE substrate at any velocities above the critical velocity. One possible reason for the differences between deposition efficiency of cold spray and that of micro-ballistic single impacts could be that the secondary impacts might be knocking off the initially deposited particles. The roughness of the substrate surface can also play a role in determining the deposition efficiency. In the cold spray process, only the first

layer of particles hit the smooth surface of the substrate and thereafter all other incoming particles impacted on the rough and bumpy surface of an already deposited layer of particles. This was not the case for the single particle impact experiments because secondary impacts were not examined in the micro-ballistic test and the single particle was always accelerated towards the smooth substrate surface rather than deposited particles.

The reasons behind the successful like-on-like deposition observed for cold spray of PS and PA and the failure to obtain successful deposition for micro-ballistic single impacts may also stem from multiple impacts. Successive impacts, if head on or nearly head on, can produce extra plastic deformation and melting in the initially deposited particle. Thus, it seems reasonable that multiple particle strikes can be both advantageous and disadvantageous depending on the angle of impact, θ, shown schematically in Figure 34. For a head on collision $\theta = 0$ while for the extreme case of a glancing collision $\theta = 90°$. If a second particle impacts the primary particle in a nearly head on collision, as seen in Figure 34a, the net result could be an enhanced plastic deformation in the primary particle and the substrate beneath the primary particle. This beneficial secondary collision could increase the likelihood of deposition. However, an impact at a more acute angle could be detrimental as it could dislodge a weakly adhered particle. Ganesan et al. [7] also confirmed the significance of the peening effect of secondary particles in the formation of a uniform coating on a polymeric substrate.

For simultaneous particle impacts to play a key role in the cold spray deposition process of polymers, there must be a non-zero probability of a second particle hitting the first particle within the time it is impacting the substrate. This impact time has been calculated to be about 30ns [19]. In order to assess this possibility, take for example, a specific set of process conditions in which the impact velocity of particles is 200m/s, the standoff distance from the nozzle exit is 10 mm, the particle flowrate is 50g/min, and the mean particle size is 40μm. Under these conditions, the probability of second particle striking the primary particle during its impact can be approximated to be about 1%. Although not large, this probability of hitting in cold spray is significant enough that it is reasonable to assert that multi-body impact could be playing a role in explaining the difference between these two methods. It is also important to note that in cold spray, the deposition efficiency was found to increase with increasing flowrate of particles up to a limit of 50g/min. Finally, we should note that the peening effect of other particles and their bombardment on an already impacted particle as well as reducing the roughness of the substrate can affect the particle/substrate bonding process.

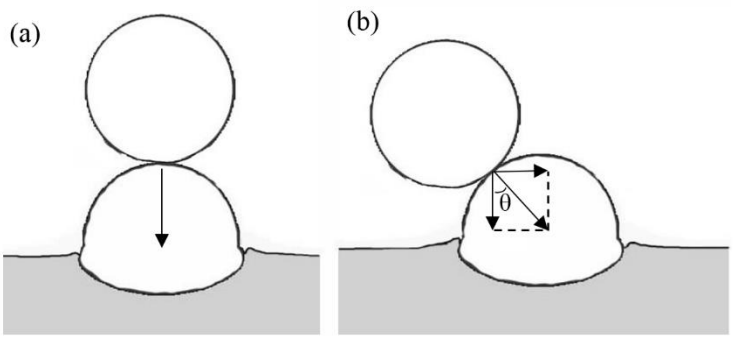

Figure 34 – a) Second particle hits the first particle right on top and b) second particle hits the first one at an angle θ.

Finally, we investigated whether particle size had a significant effect on adhesion. The rebound velocity and the coefficient of restitution are presented in Figure 35a and b for micro-ballistic single particle impacts of PS particles with sizes ranging from 40 – 47μm impacting on an LDPE substrate at 100°C. Within the size range studied, no significant effect of particle size was observed on either of the critical velocity or the coefficient of restitution. The same result was obtained for PA particles depositing on LDPE in single particle impact experiment. The critical velocity obtained for PA particles in the single impact method, didn't show significant dependency on particle size even though the variation in PA particles sizes (50 ± 25μm) was larger than PS particles (44 ± 4μm) presented in Figure 35.

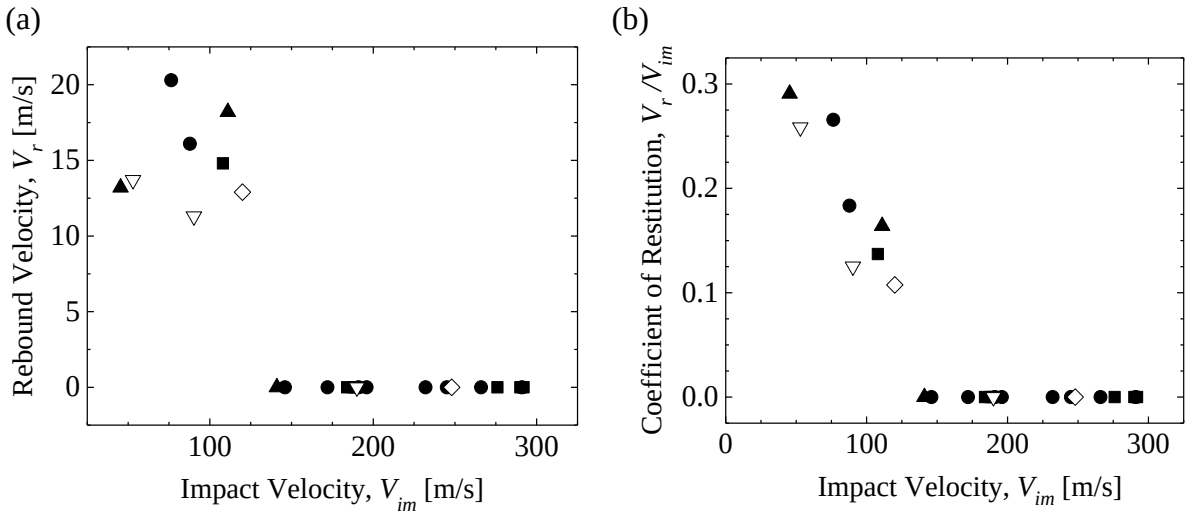

Figure 35 – Results for the micro-ballistic single particle impact experiment including (a) rebound velocity and (b) coefficient of restitution for single particles of polystyrene with the particle size range of 40 – 42μm, (■) , 42 – 43μm, (●), 43 – 44μm, (▲), 44 – 4μm, (▽), 45 – 47μm, (◊), on an LDPE substrate at 100°C.

7.4 Cold Spray Deposition of Low-T_g Polymers

In order to examine whether low-T_g polymers behave the same as high-T_g ones, we conducted similar sets of experiments for HDPE and polyurethane particles using both the micro-ballistic single particle impact tests and the cold spray process. HDPE and polyurethane particles were cold sprayed onto melt-cast HDPE, PU, and LDPE substrates. The deposition window for each particle/substrate combination was developed and are shown in Figure 36 as the particle temperature and impact velocity were varied over the 20 – 80 °C and 70 – 300 m/s ranges, respectively. In all the experiments, the substrate temperature was fixed at T_s =100 °C. The lower boundary of deposition represents the critical velocity above which deposition of HDPE and polyurethane particles were found to be possible at any of the studied temperatures. This critical impact velocity, V_{cr}, does not depend on the deposition efficiency such that any observed deposition was considered to be successful. To reach high deposition efficiency and quality, 1.5 V_{cr} is typically required in the metal cold spray systems. We will see that a similar rule-of-thumb criteria is not obviously applicable to polymeric cold spray as deposition efficiency was found to increase monotonically with increasing impact velocity.

The deposition window for HDPE and polyurethane particles on LDPE are similar in some ways. For instance, from Figure 36 a and c, we note that the critical velocity decays with roughly the same temperature dependence for both the HDPE and polyurethane particles deposited on LDPE. The same decreasing trend has been observed for cold spray of polymers like polyamide and polystyrene [25] and metals like aluminum, copper and steel for the critical velocity with increasing the particle temperature [10, 28, 49]. At 100 °C and above, both HDPE and polyurethane particles became tacky inside the powder feeding hopper, making powder delivery difficult and cold spray processing impossible. No upper limit was found for either HDPE and polyurethane depositing on LDPE and like substrates. In our previous study [25] we found a 230 m/s upper velocity limit for polystyrene depositing on LDPE which increased linearly with increasing particle temperature resulting in a deposition window that expanded with increasing temperature. This upper velocity limit represents the limit where the incoming particles begin to remove previously adhered particles through an ablation process. It is possible that an upper limit would have been found if higher velocity experiments were performed, however, here we chose to limit our study to velocities less than the speed of sound, $Ma<1$, to avoid issues associated with shock waves.

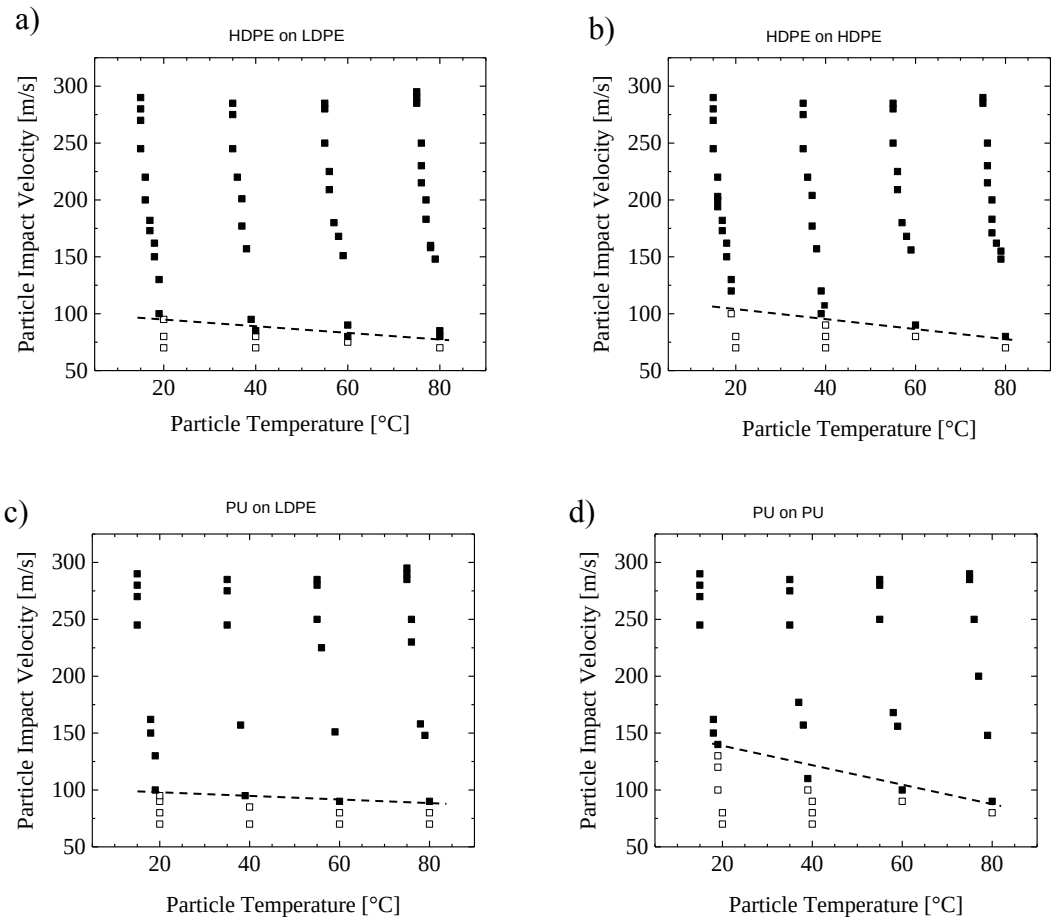

Figure 36 – Deposition window of (a) HDPE-on-LDPE, (b) HDPE-on-HDPE, (c) PU-on-LDPE and (d) PU-on-PU in cold spray experiment showing the transition from no deposition (□) to deposition (■). In all cases, the substrate was held fixed at T_s =100 °C and the stand-off distance was 10 mm. Above T_p > 80 °C, the particles became tacky in the hopper making cold spray impossible.

For the case of like-on-like deposition shown in Figure 36 b and d, the deposition boundaries were found to shift to higher critical velocity for a given particle temperature creating smaller windows of deposition than those deposited on LDPE. For example, at room temperature, the critical velocity for HDPE shifted from V_{cr} = 100 m/s on LDPE to V_{cr} = 110 m/s on HDPE (Figure 36 a and b) while the critical velocity for polyurethane shifted from 100 m/s on LDPE to 140 m/s on polyurethane (Figure 36 c and d). As the temperature was increased, the critical velocity was found to decay about 1.67 times more rapidly for deposition of HDPE-on-HDPE than that of HDPE-on-LDPE. This decay was about 5 times more rapidly for deposition of PU-on-PU decayed five times more rapidly with particle temperature, than for the

deposition of PU on LDPE. The weak dependence on particle temperature for PU or HDPE deposition on LDPE suggests that the deposition in this case results nearly entirely from the plastic deformation of the substrate [13, 25, 46]. Softening the particle has little impact as even at these elevated temperatures, the substrate is significantly softer. For like-on-like deposition, the strain is more evenly distributed between the particle and substrate and as a result particle softening has a significant impact on the critical deposition velocity and the deposition efficiency [13]. The differences observed between the like-on-like deposition of HDPE and PU could be linked to the mechanical properties of the PU particles compared to the HDPE particles. Interestingly, at T_p = 80 °C, the same critical velocity of V_{cr} = 85 m/s was reached for HDPE depositing on either HDPE or LDPE. At the particle temperature of T_p = 80 °C, polyurethane particles also deposited at a same critical velocity of V_{cr} = 90 m/s on either the LDPE or the polyurethane substrates.

In Figure 37, SEM images of the cold sprayed HDPE and polyurethane particles on the LDPE substrate are shown from the cross-sectional view. Considering the particle size of both feedstock materials, 48 µm for HDPE and 40 µm for polyurethane, no traces of the original particles can be seen at or above the grain boundaries in the SEM images.

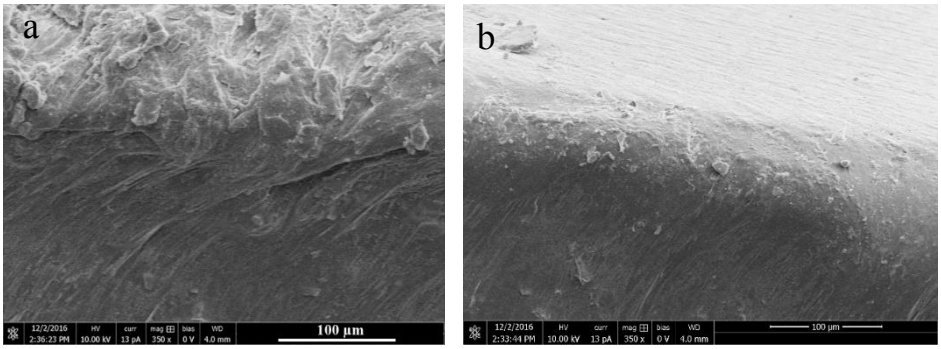

Figure 37 – SEM images of the cold sprayed particles of (a) HDPE and (b) polyurethane on the LDPE substrate with the cross-sectional view.

In Figure 38, deposition efficiency is presented as a function of particle impact velocity for HDPE and polyurethane particles for deposition on LDPE and the like-on-like cases. The deposition is quantified by measuring the change in mass of the substrate after deposition and dividing that by the mass of powder used during the experiment. The deposition efficiency of the HDPE particles was found to be larger than that of the polyurethane particles for both the case of cold spray deposition on LDPE and the case of like-

on-like deposition. These differences are likely due to the variations of their mechanical and viscoelastic properties at elevated temperatures and extremely high shear rates. In Figure 38, a monotonic increase in the deposition efficiency is observed with increasing the impact velocity of the HDPE and polyurethane particles in both like-on-like deposition cases and deposition on LDPE. At the maximum impact velocity tested, however, the deposition efficiency was found to approach 10% for HDPE-on-LDPE but remained between 5 – 6% in all other cases. For metals like copper and aluminum, the variation of deposition efficiency with particle impact velocity is more like a step function [1] rather than a continuous trend observed here for HDPE and polyurethane or our previous study on polystyrene and polyamide [25]. In metal cold spray, at impact velocities just above the critical velocity, a deposition efficiency of DE = 25% is observed, but then it abruptly increases to DE = 75–100% at impact velocities higher than $1.2V_{cr}$ [1]. Similar transitioning was not observed here. In fact, going to supersonic gas velocity was found to be detrimental on deposition efficiency as the shock waves appear to remove weakly-adhered particles.

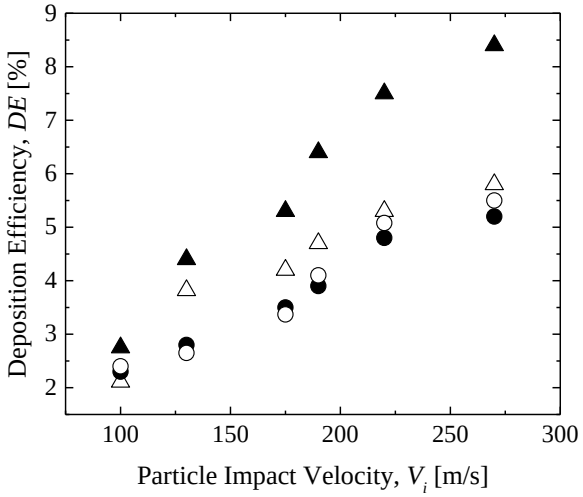

Figure 38 – Deposition efficiency as a function of particle impact velocity for HDPE-on-LDPE (▲), HDPE-on-HDPE (△), PU-on-LDPE (○), and PU-on-PU (●), in the cold spray process. Both particle and substrate were at T_p =80 °C and T_s = 100 °C.

7.5 Micro-Ballistic Single Particle Impacts of Low-T_g Polymers

In the second step of this study, a series of laser-induced single particle impact experiments were performed under experimental conditions designed to mimic those experienced in the cold spray process in

order to obtain additional insight into the deposition mechanism of HDPE and PU particles. In all cases, the particle and substrate temperatures were held constant at 100 °C while the particle impact velocity was varied from 100 to 500 m/s. In each case, the impact velocity was measured from the ultrafast photographs and, in the experiments where adhesion was not observed, the rebound velocity was also measured. After the successful adhesion experiments, SEM imaging was used to determine the shape and deformation created in the particle and substrate during impact.

PU particles indicated successful deposition on both LDPE and PU substrates, while HDPE was only observed to deposit on the LDPE substrate. No successful like-on-like deposition was achieved for HDPE in the laser-induced single particle impact experiments within the impact velocities studied. Similarly, single particles of polystyrene and polyamide 12 were found to deposit on LDPE, but did not show like-on-like deposition in a similar laser induced impact experiment [25]. In the cold spray process, on the other hand, like-on-like deposition was successful for HDPE, PU, PS and PA [25].

The optical microscopy and SEM images of three of the HDPE particles before and after the laser-induced single particle impact trials on the LDPE substrate are shown in Figure 39. All SEM images presented in Figure 39 are at an angle of 90°. The HDPE particles were found to strongly deformed during impact and some evidences of melting of the particles or the substrate can be observed at the interface connecting the particle to the substrate. As the impact velocity was increased, the degree of polymer melting and compression of the particle can be seen to increase. It is likely that the majority of the melted polymer originated from the substrate rather than the particle because the melting point of LDPE is 20 °C less than that of HDPE and the softer LDPE should experience more plastic deformation and heating during the impact [19]. If the melting did indeed originate from the substrate, then it follows that any volume of LDPE from the substrate that has wetted onto the particle, must have been displaced from the substrate leaving behind a crater. However, because no crater is visible adjacent to the deposited particles, any LDPE polymer present on the impacted particle must have been displaced from just beneath the particle. It is likely that the flow of the substrate material onto the particles is contributing to the particle/substrate bond.

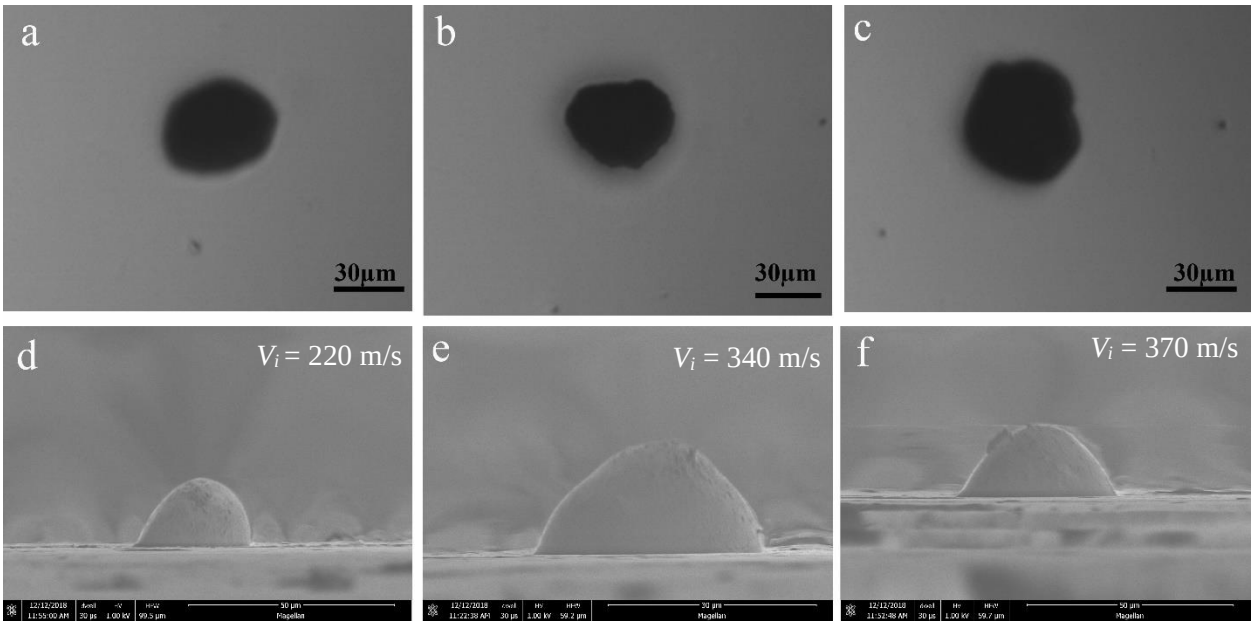

Figure 39- Single particles of HDPE before (a – c) and after (d – f) impacting the LDPE substrate in the laser-induced single particle impact experiment.

Xu and Hutchings [12] reported critical impact velocity of just over 100m/s which is an order of magnitude lower than for most metal sprays and a deposition efficiency less than 0.5%. They also noted that gross melting of the entire particle did not occur, but they could not localize melting near the point of impact. Numerical simulations of HDPE polymer particle impacting an HDPE substrate performed by Shah et al. [19] reinforced these experimental observations and showed that at these impact velocities, a large temperature jump in the polymer was observed at the interface between the particle at the substrate resulting from the large shear stresses and plastic deformation of the polymer. In some cases, the temperatures attained were large enough to induce a local melting of the semi-crystalline polymer and the mobilization of amorphous polymer chains in both the substrate and the particle. These thermal effects appear to be critical to aid inter-diffusion and bonding between the plastically deformed particle and the substrate as Shah et al. [19] showed that the interfacial tension effects alone was not large enough to explain particle adhesion.

In Figure 40, single particles of polyurethane are shown before and after impacting the LDPE substrate in the laser-induced single particle impact experiment. SEM images of both top view and view at 90 ° angle are presented for a better comparison of the shape before and after impact. Like HDPE particles, the plastic deformation is observed to increase for polyurethane particles depositing on LDPE with increasing the impact velocity in laser-induced single particle impacts.

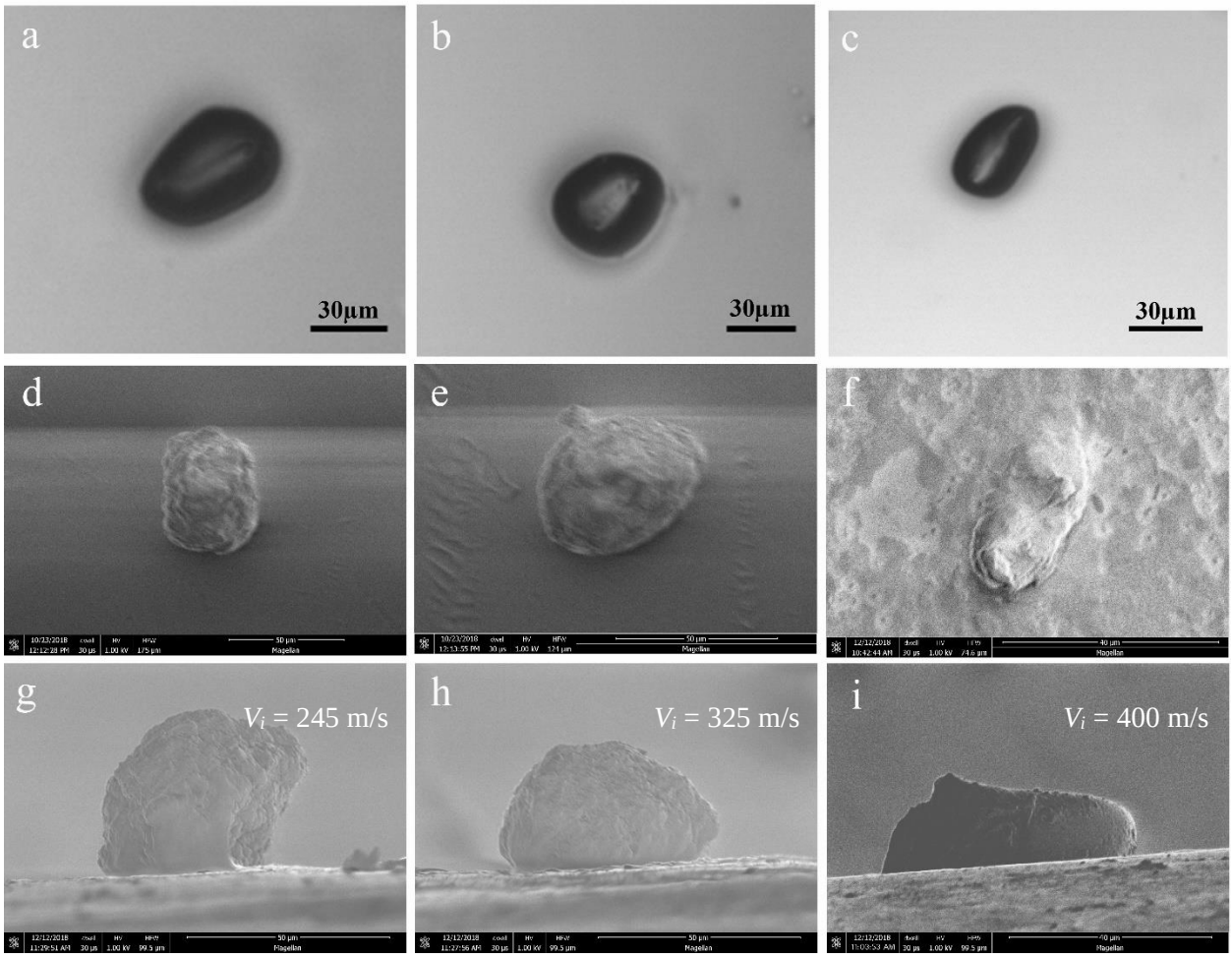

Figure 40 - Single particles of polyurethane before (a – c) and after (d – i) impacting the LDPE substrate in the laser-induced single particle impact experiment. SEM images of top view and view at 90 ° angle are presented in d – f and g – i, respectively.

Single particles of polyurethane before and after impacting the polyurethane substrate in the laser-induced single particle impact experiment are presented in Figure 41. Evidence of significant melting is visible around the polyurethane particle deposited on polyurethane, more noticeably in Figure 41 f at an impact velocity of V_i = 370 m/s. The presence of the clear melted region might help explain why we achieved like-on-like deposition for polyurethane but not for HDPE in the single particle impact experiment. Polyurethane is well above its T_g at the processing temperature and its melt temperature, T_m = 97 °C is just below the process temperature. However, even though PU is above its T_m, the PU has been chemically cross-linked during processing and as such it will not fully melt or liquify even at temperatures well above T_m. As a result, local melting of the polyurethane at the particle substrate interface is likely. This molten region likely helps dissipate energy and increase adhesion strength. For HDPE, the melting point

(T_m = 130 °C) is 30 °C above the processing temperature and as a result full scale melting of the particle upon impact is less likely.

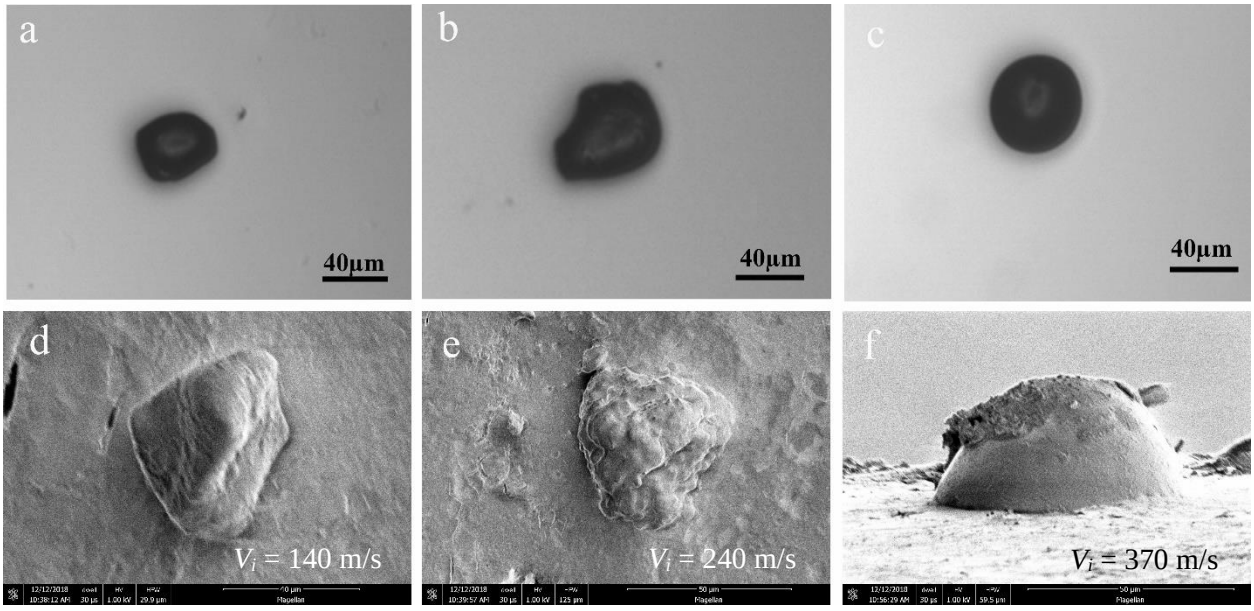

Figure 41- Single particles of polyurethane before (a – c) and after (d – f) impacting the polyurethane substrate in the laser-induced single particle impact experiment.

In Figure 42 and Figure 43, the results from single particle impact experiments are shown. Included in these figures are the rebound velocity, V_r, and the coefficient of restitution, $C_r = V_r/V_i$. Here, V_i is the particle impact velocity and V_r is the particle rebound velocity. For particles that were found to adhere to the surface, $V_r = 0$. In Figure 42, the rebound velocity and the coefficient of restitution are presented for laser-induced single particle impacts of HDPE particles on the LDPE and HDPE substrates at 100 °C. In Figure 43, the rebound velocity and the coefficient of restitution for polyurethane particles on the LDPE and polyurethane substrates are presented from the same process. Particle size is pointed out on top of each datapoint in Figure 42 and Figure 43. Within the particle size range studied for HDPE, D_p = 48 ± 18 µm, no significant variation was observed in the rebound velocity and thus in the coefficient of restitution. Similar to HDPE particles, the critical velocity obtained for polyurethane particles in the single impact method, did not show significant dependency on the particle size over the D_p = 50 ± 21 µm studied range. Thus, particle impact velocity appears to be the most important experimental variable governing particle deposition.

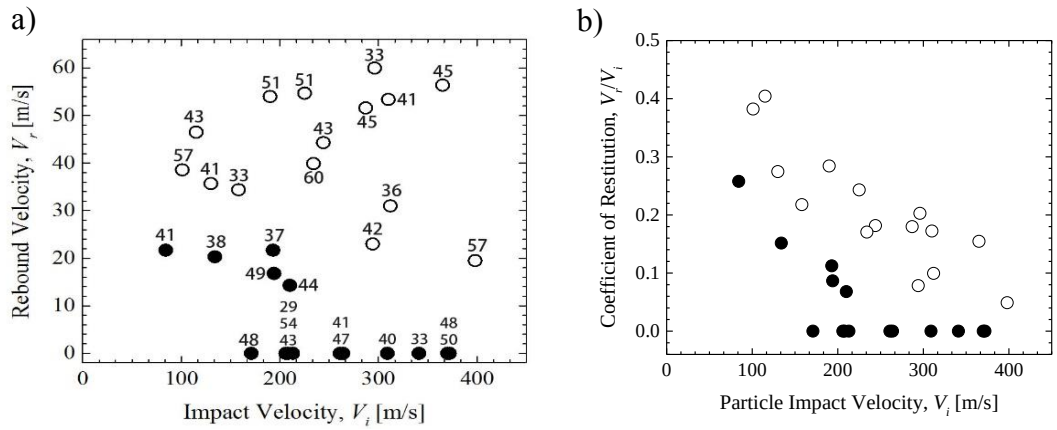

Figure 42 – Results for the laser-induced single particle impact experiments including (a) rebound velocity and (b) coefficient of restitution for single particles of HDPE accelerated onto the LDPE (●) and HDPE (○) substrates - Data provided by W. Xie.

The coefficient of restitution, $C_r = V_r/V_i$, is plotted against the impact velocity in Figure 42b and Figure 43c. One minus the square of the coefficient of restitution, $(1 - C_r^2)$, is indicative of the amount of kinetic energy dissipated by the impacting particles. From numerical simulation, it is known that in high speed collisions with velocities above 250 m/s, a large portion of the kinetic energy is dissipated in the form of plastic deformation in regions adjacent to particle/substrate interface [19]. In the case of depositing on LDPE, the coefficient of restitution was found to decrease with increasing the particle impact velocity, V_i, for both HDPE and polyurethane in the laser-induced single impact trials until it reached zero at the critical velocity when the particles began to adhere.

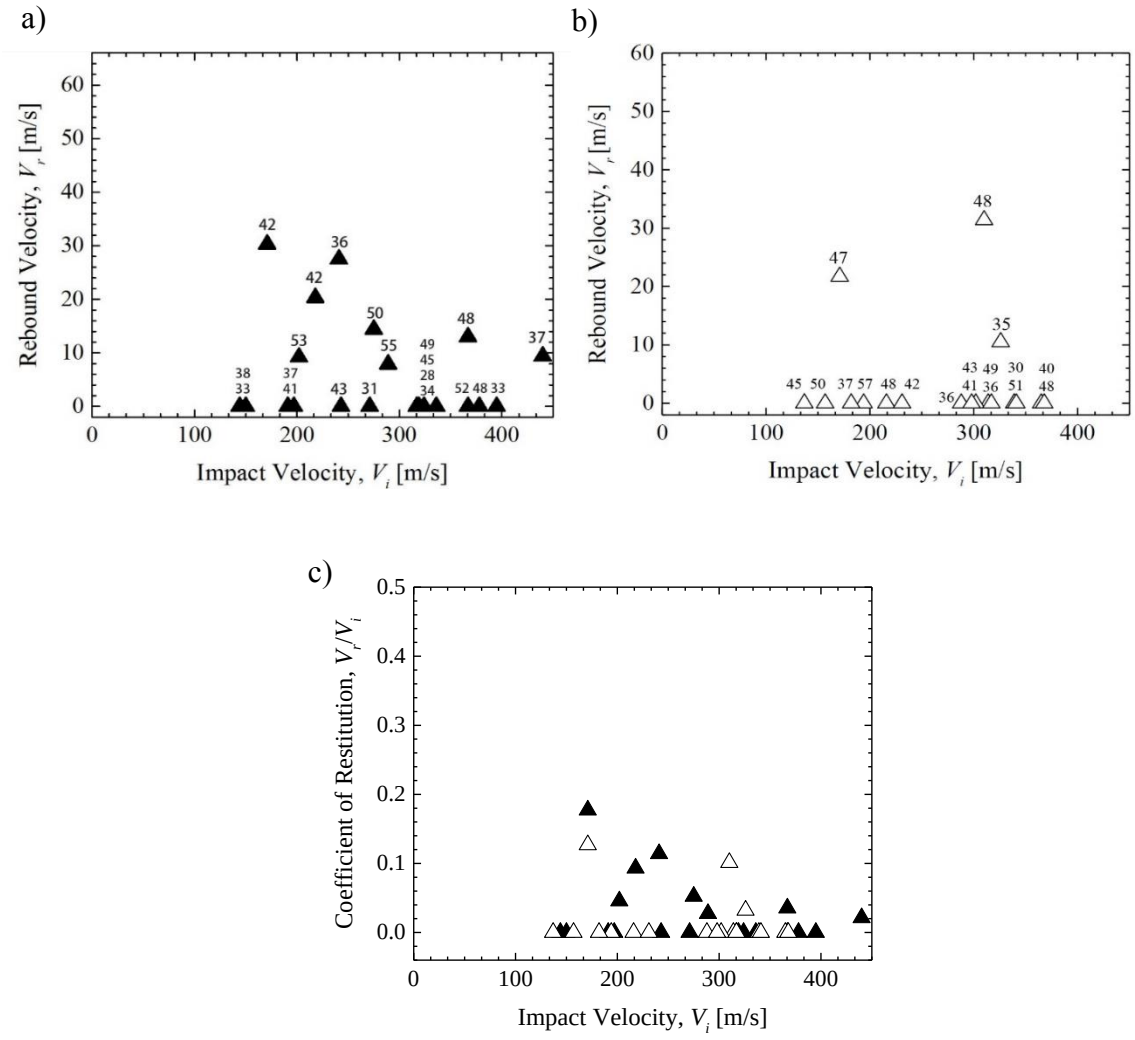

Figure 43 – Results for the laser-induced single particle impact experiments including rebound velocity of single particles of polyurethane accelerated towards (a) the LDPE (▲) and (b) polyurethane (△) substrates and (c) coefficient of restitution for all particle/substrate pairs for polyurethane single particles - Data provided by W. Xie.

In Table 6, the critical velocity obtained from both the laser-induced single particle impact experiments and the cold spray process for HDPE particles depositing on HDPE and LDPE and polyurethane particles depositing on polyurethane and LDPE are presented for comparison. The particles and substrates were kept at 100 °C in both the cold spray and laser-induced single impact experiments to make comparison possible. It can be seen from the data in Table 6, that the laser-induced single impacts of HDPE particles depositing on LDPE yielded a critical velocity in the range of V_{cr} = 140 m/s to 167 m/s. In the cold spray process, HDPE particles became sticky at T_p = 100 °C and thus we could not measure the

critical velocity at this temperature. Instead, we extrapolated the datapoints in Figure 36 a and b was extrapolated to 100 °C and a critical velocity of V_{cr} = 80 m/s for deposition of HDPE particles on LDPE and a critical velocity of V_{cr} = 76 m/s for the like-on-like deposition can be predicted. PU particles were observed to deposit on the LDPE and PU substrates from the very beginning of the laser induced single particle impact experiments at impact velocities as low as 140 m/s. As a result, the true value of the critical velocity for PU could not be determined. By extrapolating the datapoints for PU particles in Figure 36 c and d and reached a critical velocity of V_{cr} = 86 m/s, for deposition on LDPE and a critical velocity of V_{cr} = 73 m/s for deposition on polyurethane at T_p = 100 °C in the cold spray process can be predicted. The relatively large standard deviations obtained for critical velocities in the cold spray process in Table 6 is because the particle size variation affects the calculation of the impact velocity as the particle velocity is not measured in the cold spray process but predicted from a 1D inviscid compressible flow model [13], Even with the large standard deviation in the data, the cold spray process appears to predict deposition at velocities that are systematically lower than the laser-induced single impact experiment. This suggests that multiple particle interaction may be beneficial in increasing the likelihood of deposition and its overall efficiency.

Like-on-like deposition was not observed for HDPE at any impact velocity in the laser-induced single particle impact experiments. However, the coefficient of restitution, V_r/V_i, showed a decreasing trend as the impact velocity increased, suggesting that deposition might be possible at even higher impact velocities. HDPE particles did not deposit on LDPE in three out of thirteen trials as can be seen in Figure 43 a, in the laser-induced single particle impact experiment, resulting in a deposition efficiency of DE = 77%. For PU, Eight particles out of twenty (DE = 60%) and three out of eighteen trials, (DE = 83%) on LDPE and PU substrates failed to deposit as shown in Figure 43 a and b. Although this is not the 100% deposition efficiency observed for metal particles, the deposition efficiency for single particle impacts is significantly larger than in cold spray. Interestingly, although the maximum deposition efficiency for polystyrene and polyamide 12 was also found to be around 5% in the cold spray process [25], for these high-T_g polymers, 100% deposition efficiency was achieved above the critical velocity for PS and PA for laser-induced single particle impacts.

Table 6 – Critical velocity obtained from the laser-induced single particle impact experiments and the cold spray process. Results for polystyrene and polyamide 12 are included from another study [25] for comparison.

Particle and Substrate Pairs	Single Particle Impact Experiment	Cold Spray Process
HDPE-on-LDPE	140 – 167 m/s	80 ± 15 m/s
PU-on-LDPE	≤140 m/s	87 ± 20 m/s
HDPE-on-HDPE	No deposition	77 ± 15 m/s
PU-on-PU	≤130 m/s	73 ± 20 m/s

The coefficient of restitution was used to infer the total energy dissipated, $(1-C_r^2)$, for both the rebounding and adhering particles and is included in Figure 44. The results for polystyrene and polyamide 12 from the previous study [25] are also included in this figure for a better comparison. For HDPE-on-LDPE, at impact velocities as low as V_i = 80 m/s, the percentage of impact energy dissipation was above 90%. With increasing impact velocity, the dissipated portion of the impact energy was found to increase monotonically until it reached 100% at V_i = 167 m/s. For polyurethane, the percentage of impact energy dissipation was 100% for the lowest impact velocity V_i = 130 – 140 m/s, studied in the laser-induced single particle impact experiment for deposition on either LDPE or polyurethane. For unsuccessful like-on-like deposition cases included in Figure 44 b, the percentage of impact energy dissipation did not reach 100%, but did approach 100% asymptotically. The impact energy dissipation for HDPE and PU at all like-on-like impact velocities studied was significantly larger than that of PS and PA. These experiments show that low-T_g particles are more dissipative than high-T_g during the high deformation rates experienced during impact in cold spray resulting in more plastic deformation, more melting, better adhesion, easier deposition and a higher deposition efficiency.

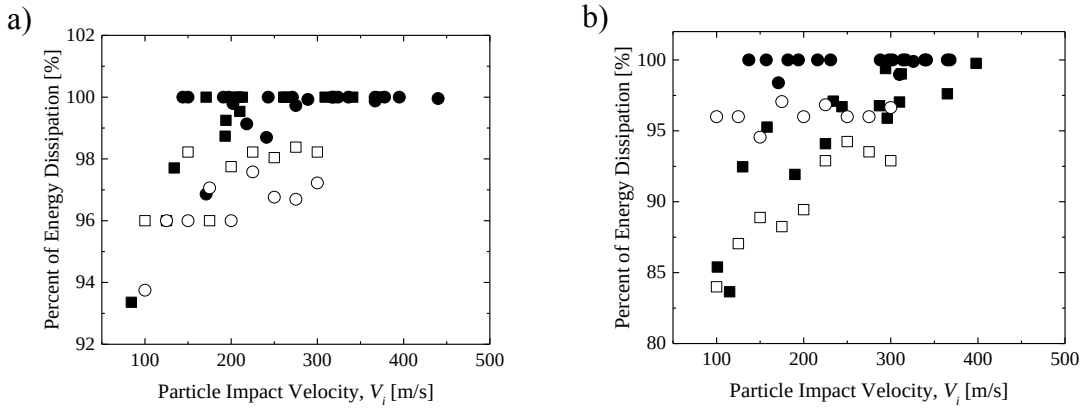

Figure 44 – Percent of kinetic energy dissipation, (1 − Cr2) for deposition of (■, □) HDPE and (●, ○) PU particles on (a) LDPE and in (b) like-on-like deposition cases. Solid symbols refer to single particle impact experiment results and hollow symbols correspond to the results from the cold spray process.

The plastic deformation after impacting the substrate in the laser-induced single particle impact trials was quantified by measuring the particle size before and after impact. The results for each particle/substrate pair as a function of particle impact velocity presented in Figure 45. SEM images of the HDPE and polyurethane particles after deposition in the laser-induced single particle experiments were analyzed using a software, ImageJ to measure the diameter, d, of the particle perpendicular to the substrate surface. The results were compared to the initial diameter, d_0, known from the ultrafast photography before impact and thus the plastic deformation could be quantified as $\Delta d/d_0$. The plastic deformation of the particles was found to increase linearly with increasing impact velocity. Similar linear trends were observed between the plastic deformation and the impact velocity for aluminum particles depositing on either sapphire or aluminum in laser-induced single particle impact experiments [33, 48]. Interestingly, the compression ratio of the particle needed for deposition of any of the studied particle/substrate pairs was measured to be only $\Delta d/d_0$ = 1.5%. However, with increasing the impact velocity, the plastic deformation increased with different slope for the various particle/substrate pairs. The compression ratio of HDPE-on-LDPE increased from 1.5% at the impact velocity of V_i = 167 m/s to 40% at the impact velocity of V_i = 370 m/s. The increase in the compression ratio for the PU particles was similar going from 1.5% at the impact velocity of V_i = 140 m/s to 50% at the impact velocity of V_i = 400 m/s.

For the like-on-like deposition case of PU, a similar increase in compression ratio was observed compared to PU-on-LDPE. In fact, all the low-T_g particle data can be fit relatively well with a single linear trendline. On the other hand, high-T_g polymers like PS and PA studied previously [25], showed significantly less compression, never reaching above 10% even at V_i = 400 m/s. In fact, the compression of the low-T_g particles during impact is much closer to that observed for metals like aluminum [33] than it is for high-T_g

particles like PS [25]. The increased plastic deformation of the low-T_g particles likely leads to better mixing with and adhesion to the substrate. In addition, the reduced profile of the particles decreases the roughness of the substrate after impact making subsequent impacts of the particles more likely to be successful thereby increasing the deposition efficiency of the cold spray process.

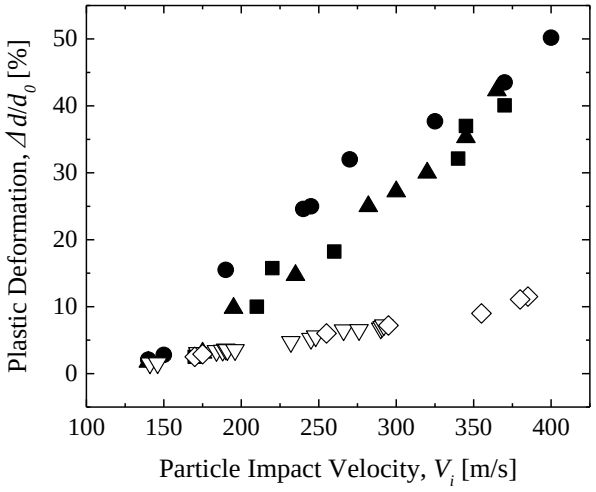

Figure 45– Plastic deformation of adhered single particles of HDPE-on-LDPE (■) and PU-on-LDPE (●), and PU-on-Pu (▲). Results from the previous work [25] are also included for Ps-on-LDPE (▽), and PA-on-LDPE (◊). The particles and the substrates are at 100 °C in all cases.

CHAPTER 8
PEENING EFFECT OF GLASS BEADS

8.1 Shot Peening

The study of the laser induced single particle impacts that successive particle collisions play a key role in making deposition possible. This observation brought the idea of adding some sacrificial non-adhesive particles like glass beads to the polymer particle batch in the powder feeding hopper. The objective was to add different amounts and sizes of glass beads to the polymer particle batch and investigate what effects it can have on deposition window, efficiency and quality.

The study of the laser induced single particle impacts for high-T_g polymers depositing on polymeric substrates in chapter 7 showed that successive particle collisions play a key role in making deposition possible. This observation brought the idea of adding some sacrificial non-adhesive particles like glass beads to the polymer particle batch in the powder feeding hopper. Therefore, the objective of the present study is to investigate the effects of adding different amounts and sizes of glass beads to the polymer particle batch on the deposition window, efficiency and quality in the cold spray process.

Shot peening is a mechanical treatment to improve surface properties of materials by bombarding the surface with high quality spherical media like steel, ceramic, or glass in a controlled operation. There are various types of shot peening including laser peening [50], wet shot peening [51], ultrasonic peening [52], micro-shot peening [52], all resulting in residual compressive stresses, grain refinement and grain size reduction. M. Chen et al [53] could induce about 900 MPa residual compressive stress at the 10 μm depth of steel by multiple shot peening processes with steel shots and ceramic beads. Kovaci et al. [54] improved corrosion resistance and electrochemical properties of steel by shot peening the surface in different intensities. Poongavanam et al. [55] increased heat transfer coefficient, Nusselt No., and friction factor in tubular heat exchangers by shot peening the copper inner tube. Ramos et al. [52] applied ultrasonic energy on an aluminum surface and showed that ultrasonic shot peening provides better surface finish and lower roughness values than micro-shot peening. Chen et al. [51], refined the microstructure of Ti6Al4V alloys into ultra-fine grains and increased its fatigue strength by 12.4%, by wet shot peening of the alloy surface with ceramic beads. B.K. Pant et al. [50] found laser peening more effective than shot peening in improving fatigue life of Ti6Al4V alloys.

Shot peening has applications in the treatment of ceramics and composites as well. The fatigue performance of SiC/Al [56] and WC/Co [57] cermet was notably improved after shot peening the composite surface with steel shots at the speed of 35 m/s.

In recent years, shot peening has been studied before [58], during [59], and after [58] the cold spray process for some metals and a few polymers. For instance in metallic cold spray, the shot peening process can eliminate the porosity [59] enhance the work hardening of the coating [60], or improve the fatigue performance of the cold sprayed material [58]. Luo et al. [59] added up to 70% large sized stainless-steel particles to the particle batch of pure metal and some alloys of titanium in a cold spray process and found that the peening effect from the steel shots decreased the porosity from 15% to 0.7% and increased the microhardness by 70%, although about 3 vol.% of the steel particles was found to incorporate into the cold sprayed coating. They reported that the plastic deformation of the previously deposited layers could get large enough due to the shot peening process to remarkably decline the porosities. They also reported a slightly lower deposition efficiency after adding the 70% steel particles to the titanium pure metal and alloy. Moridi et al. [58] found shot peening of cold sprayed specimens to be more effective when applied prior to the cold spray process. They increased the fatigue strength of aluminum by 26% with shot peening the aluminum substrate prior to cold spraying aluminum particles on it.

Additive particles in the cold spray process of polymeric materials may have other effects than the shot peening effect, for example to improve the surface activity of the cold sprayed polymeric particles to reinforce the bond between the particle and substrate [36]. Ravi et al. [36] studied the cold spray deposition of 45 – 63 µm UHMWPE particles on aluminum and found it impossible over the gas temperature of 190 – 500 °C and particle impact velocity ranging between 170 m/s and 220 m/s. The deposition efficiency of 0.014% was achieved in their work only after adding 10 wt.% fumed nano particles of alumina to the polymeric particle batch due to the hydrogen bonds created between the fumed alumina nano particles and the oxide layer on the aluminum surface. The bond between the UHMWPE particles and the fumed nano alumina was assumed to be due to the small size of the fumed nano alumina particles which allows them to pierce into the UHMWPE particles. They concluded that if UHMWPE particles with 10wt.% fumed nano-alumina particles undergo enough plastic deformation to cover a large area of the substrate surface, then they can form H-bonds that can act as bridge bonds between UHMWPE and the oxide layer on the Al substrate. As hydrogen bonds store about 4000–20000 J/mole of energy [61], Ravi et al. argued that the total energy of the H-bonds at the particle/substrate interface can surpass the non-dissipated portion of the particle kinetic energy which otherwise could lead to the particle rebounding.

8.2 Experiments

The cold spray process was performed for the five studied materials in this project as described in chapter 2. The flight of the HDPE particles was recorded using a Phantom VEO high speed camera S 640

at the framerate of 19,000 fps, resolution of 512 × 320, and the exposure time of 50 μs. In Figure 46, the schematic diagram of the high-speed camera set up is shown.

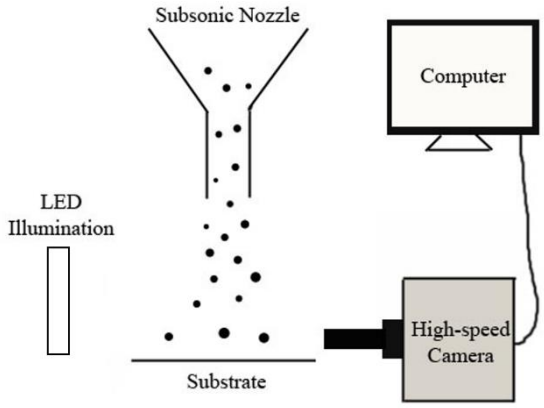

Figure 46 – The schematic diagram of the high-speed camera set up

Two different nozzle designs were used in the present study, a subsonic nozzle with a converging-straight geometry and a supersonic nozzle with a converging-diverging geometry. The geometry and the dimensions of the two studied nozzle designs are presented in Figure 47 and Table 7, respectively.

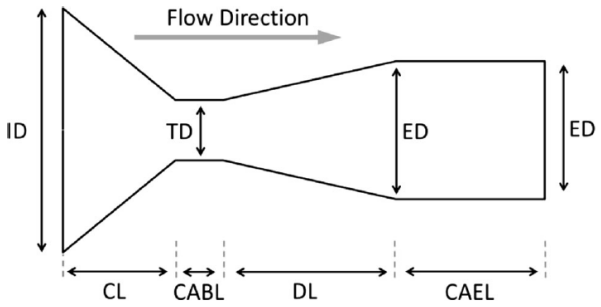

Figure 47 – Nozzle dimensions with a converging-straight geometry (the subsonic nozzle) and a converging-diverging geometry (the supersonic nozzle).

Table 7 – Nozzle dimensions for the subsonic supersonic nozzle.

Nozzle Dimensions	Subsonic Nozzle	Supersonic Nozzle
Inlet Diameter	0.95 cm	0.95 cm
Throat Diameter	0.16 cm	0.16 cm
Exit Diameter	0.19 cm	0.16 cm
Converging Length	2.99 cm	2.35 cm
Constant-Area Buffer Length	0.07 cm	N/A
Diverging Length	0.30 cm	2 cm
Constant-Area Extension Length	4.19 cm	1.15 cm
Exit to throat Area Ratio	1.45	1.57

Computational fluid dynamic (CFD) simulations of the two nozzle designs showing the velocity counters of the air flow are presented in Figure 48.

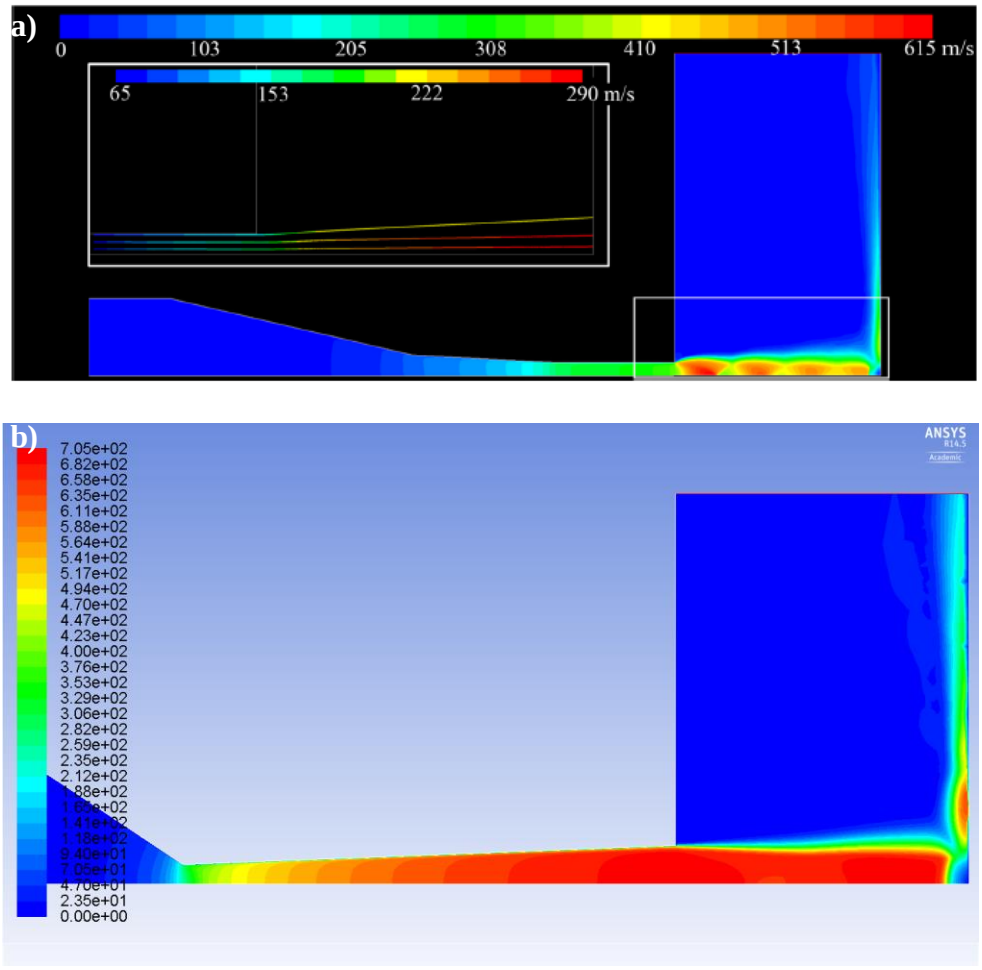

Figure 48 – CFD simulations showing velocity magnitude contours of the flow through (a) a subsonic nozzle and (b) a supersonic nozzle. The inset in (a) shows the particle paths with color scaled by particle velocity for a series of 23-μm-diameter particles released just upstream of the inlet with an initial velocity equal to flow at the location they were released - image provided by Trenton Bush

8.3 Effect of Peening particles on Deposition Efficiency

In the first set of experiments presented here, we will investigate the effect that the addition of glass bead peening particles has on the deposition efficiency of a number of different polymer powders including HDPE, PU, PA, PS and UHMWPE. The initial studies focus on the effect of glass bead size, concentration and impact velocity.

The cold spray deposition efficiency of HDPE particles on an LDPE substrate is presented in Figure 49. as a function of the percentage of the added glass beads under different spray conditions is depicted in. The glass beads and the HDPE particle had diameters of $D = 40 \pm 15$ µm and $D = 48 \pm 18$ µm, respectively. The variation in the diameter resulted in some uncertainty in the calculated particle velocities and temperatures presented in the results that follow.

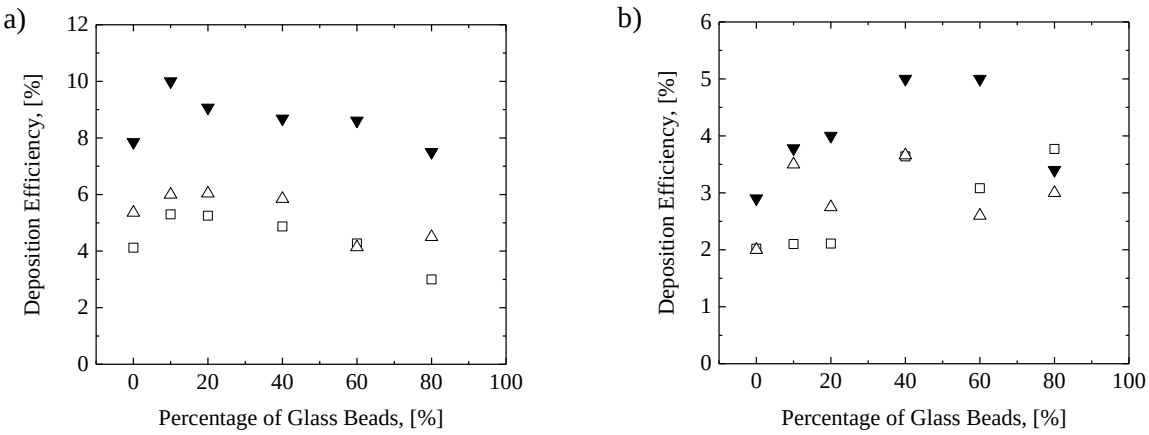

Figure 49 – Cold spray deposition efficiency of HDPE on an LDPE substrate as a function of the weight percentage of glass beads added. Data includes data from both (a) a subsonic nozzle with $V_{HDPE} = 275 \pm 15$ m/s and $V_{glass\ beads} = 265 \pm 15$ m/s, and (b) a supersonic nozzle with $V_{HDPE} = 375 \pm 20$ m/s and $V_{glass\ beads} = 360 \pm 20$ m/s. The data includes results for cold spray conditions (□) $T_P = T_S = 20$ °C, (Δ) $T_P = 80$ °C and $T_S = 20$ °C, and (▼) $T_P = 80$ °C and $T_S = 100$ °C.

For all the particle velocities studied, adding peening particles to HDPE powder at low concentration was found to increase the deposition efficiency above that of pure HDPE powders. However, increasing the glass bead concentration beyond 10% in the case of subsonic particle speeds, Figure 49 (a), and beyond 40% in the case of supersonic speeds, Figure 49 (b), was found to result in a decrease in deposition efficiency.

For the case of the subsonic nozzle, Figure 49 (a), adding 10 wt.% glass beads to the HDPE powder increased the deposition efficiency from below 7.7% for pure HDPE to 10% for the case of T_p = 80 °C and T_s = 100 °C. This notable 28% improvement in the deposition efficiency is a direct result of the peening effect of the added glass beads. Similar improvements were observed for processing conditions with room temperature particles and substrates. Beyond 10 wt.% the deposition efficiency begins to decay although remaining still larger than that of pure HDPE particles with as much as 60% or more of glass beads mixed into the HDPE powder. For the case of supersonic nozzle as shown in Figure 49 (b), the optimum weight percentage of the glass beads needed to maximize the deposition efficiency increased from 10% to about 40 wt.%. It should be noted here that SEM images of the HDPE coatings revealed no deposition of glass particles for the subsonic conditions presented in Figure 49 (a), however, for the case of supersonic conditions in Figure 49 (b), some glass beads were deposited. As the deposition efficiency is calculated by weighting the LDPE substrate before and after the spray process and comparing the increase in weight to the weight of polymer sprayed, the adhesion of glass particles can affect the results of the deposition efficiency in Figure 49 (b). The true value is slightly lower than what is reported. Similar trends with weight percent of glass beads were observed for all polymers studied.

8.4 Size Effect

In order to study the effect of the size of the glass bead peening particles, four different glass bead sizes of 20 ± 10 μm, 40 ± 15 μm, 70 ± 25 μm, and 120 ± 25 μm were added to the HDPE, PU, PA, and PS particles. The deposition efficiency was measured for each size of glass beads paired with each polymer particle and the results are plotted in Figure 50. In this figure, the data is for 10% by weight addition of glass beads and under processing conditions where the HDPE polymer powder temperature was held fixed at T_p = 80 °C and the LDPE substrate was held at T_s = 100 °C. The pressure drop was optimized for a polymer particle velocity of 275 m/s. However, because the glass bead size was changing, the glass bead impact velocity is not consistent across the figure but decreases from 370 m/s to 340 m/s as the size of the particles increase from 20 μm to 120 μm. additionally, it should also be noted that as the size of the particles increases, the kinetic energy of each particle on impact increased/decreased due to the change in velocity and mass. Finally, note that increasing the glass bead size of the same weight fraction means fewer particles are in the powder blend and fewer peening impacts will be experienced along the substrate.

For any of the four studied polymer particles, a slight increasing trend was seen in the deposition efficiency with increasing the glass bead size, with the largest effect being observed for the PU particles for which an increase of more than 3% was observed in the *DE* from 2% to 5%. For all other polymers, the

variation of the deposition efficiency with the size of the glass beads was found to be much smaller and not significant when the error in the measurements was accounted for. The increase in *DE* with peening particle size is likely the result of the increased kinetic energy of the particle, however, as seen with most polymers, this effect is mitigated to great extent by simultaneous reduction in the number of impacts.

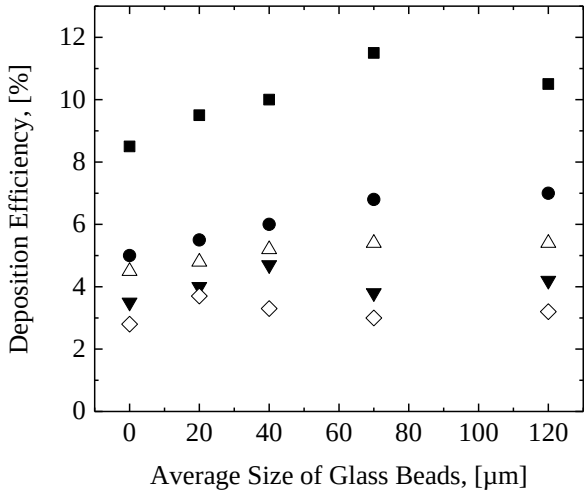

Figure 50 – Cold spray deposition efficiency as a function of the average size of the glass beads added as peening particles. In all cases, 10 wt.% of glass beads were added to (■) HDPE, (●) PU, (Δ) PA, (▼) PS, (◊) UHMWPE. The substrate was LDPE, the particle temperature was T_P = 80 °C, substrate temperature was T_S = 100 °C, and the polymer particle velocity was 275 ± 15 m/s.

8.5 Deposition of Glass Beads

In analyzing the effect of glass beads on the deposition efficiency, it is necessary to make sure that the glass beads are non-adhesive and are not depositing on the substrate surface thereby changing the composition of the desired deposited film. In order to ensure that the glass beads did not adhere to the surface, batches of 100% glass beads were sprayed at the processing conditions used above on an LDPE substrate. In Figure 51, the deposition percentage of the glass beads are plotted against the glass bead average size after accelerating the pure glass beads to the subsonic velocity range of V_i = 245 – 310 m/s and the supersonic velocity range of V_i = 340 – 370 m/s. The glass beads did not adhere to the LDPE substrate when traveling below $Ma < 1$. However, above $Ma > 1$, some glass beads did in fact deposit on the LDPE

substrate. The deposition percentage of the glass beads was found to decrease from 2.25% to 1% as the average glass bead size increased from 20 μm to 120 μm. The speed of the glass beads calculated using the 1D inviscid model of gas and particle dynamics [31] predicts a linear decrease in velocity from 370 m/s to 340 m/s as the glass bead size increased from 20 μm to 120 μm in the supersonic flow conditions in Figure 51 which might account for the reduced percentage of deposition of the glass beads.

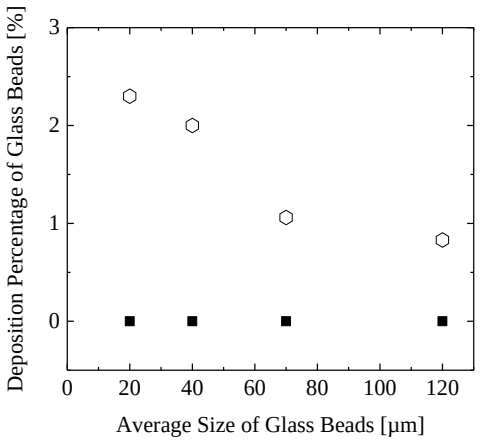

Figure 51 – (a) Deposition percentage of the glass beads cold sprayed on an LDPE substrate at room temperature using both a subsonic nozzle (■), and a supersonic nozzle (⬡), (the glass beads velocity ranges between 100 m/s and 260 m/s in the subsonic condition and between 340 m/s and 370 m/s in the supersonic conditions, both particle and substrate are at room temperature, $T_P = T_S = 20$ °C.

8.6 Microstructural studies

Evidence for glass bead adhesion can also be seen in the SEM images of cold sprayed depositions of HDPE and other polymers mixed with glass beads when they are processed at supersonic velocities. An SEM image of a cold spray deposition of HDPE particles with the addition of 10 wt.% glass beads on an LDPE substrate is presented in Figure 52. The presence of glass beads is clearly evident in Figure 52. The glass beads have been deposited and incorporated into the HDPE layer deposited on the LDPE substrate. SEM image of top view and cross-sectional view of the cold sprayed HDPE and PU particles on an LDPE substrate under subsonic conditions are presented in Figure 53. In contrast to the case for the supersonic nozzle in Figure 52, no traces of the glass beads are visible in either the top views or the cross-sectional views of the cold sprayed HDPE and PU deposited layer in Figure 53. A smooth and dense deposition is visible in the top views in Figure 53 a and c showing little porosity and a mixed and homogeneous interface between the deposited layer of HDPE and PU and the LDPE substrate can be seen in the cross-sectional views in Figure 53 b and d. Similar results were observed in SEM studies of PA, PS and UHMWPE deposited layers.

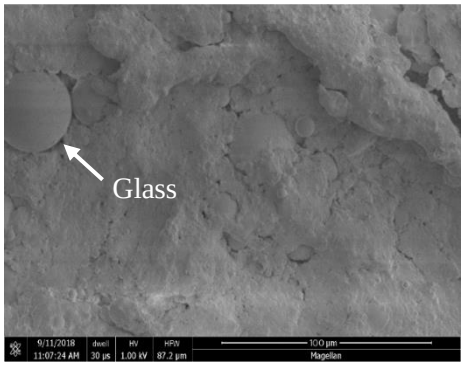

Figure 52 – SEM images of cold sprayed glass beads which deposited into the LDPE substrate after being accelerated to supersonic speeds of about 370 m/s. Cold spray deposition of HDPE particles with the addition of 10 wt.% glass beads on an LDPE substrate using the supersonic nozzle. The average glass bead size was $D = 20 \pm 10$ µm.

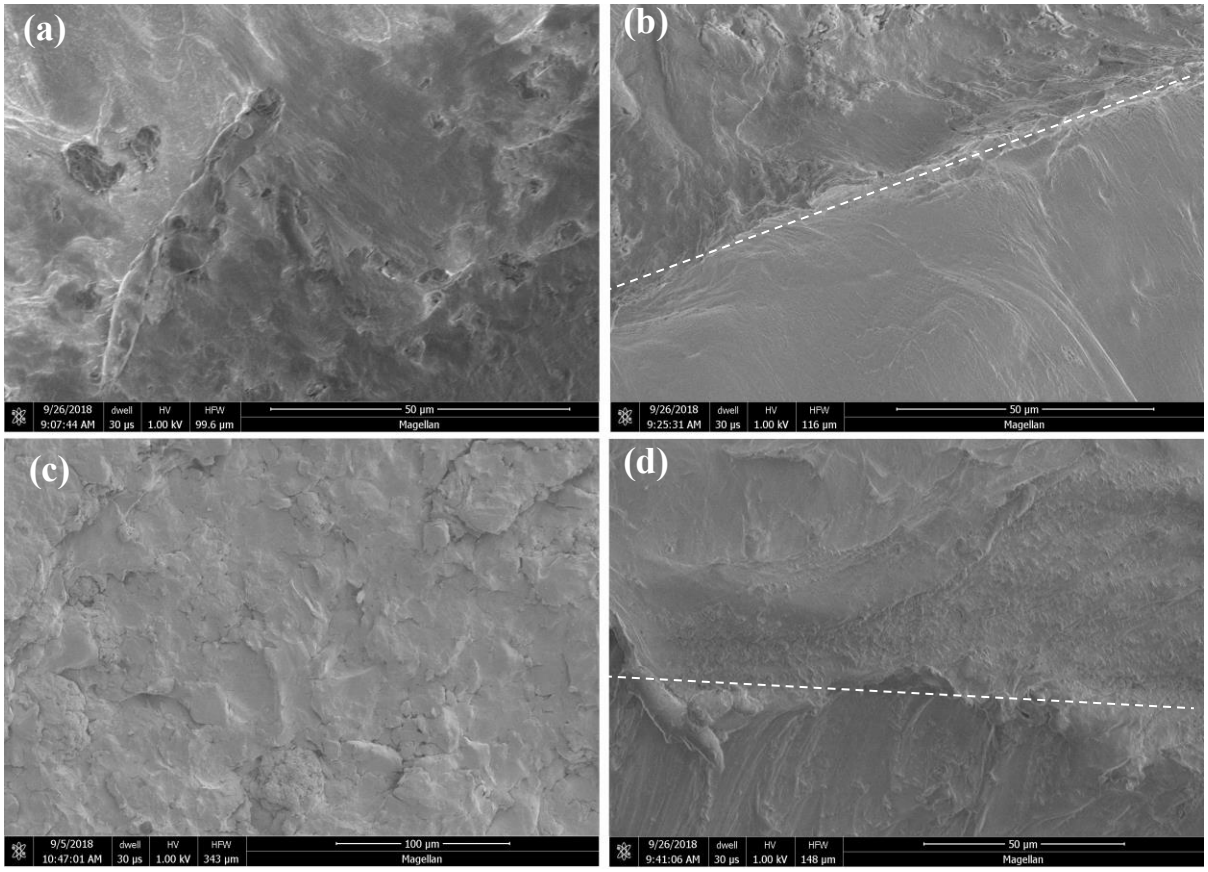

Figure 53 – SEM images of (a) the top view and (b) the cross-sectional view of HDPE particles and (c) the top view and (d) the cross-sectional view of polyurethane particles deposited on an LDPE substrate at particle temperature of T_p = 60 °C, substrate temperature of T_s = 100 °C and particle impact velocity of V_i = 270 m/s. 10 wt.% glass beads were added to the particle batch and a subsonic nozzle was used to accelerate particles.

8.7 Deposition Windows

In addition to increasing the deposition efficiency of polymer powders, the secondary goal of adding peening particles was to expend the deposition window for polymer powders especially the hard-to-deposit polymers like UHMWPE. The effect of adding glass beads to the polymer particles on the deposition window is shown in Figure 54 – Figure 56. It can be seen from these three figures that the deposition window of a number of different polymers is expanded through the addition of peening particles. In all cases, the minimum particle impact velocities needed for deposition was shifted lower over all the particle temperatures studied here. For example, as seen in Figure 54, for the HDPE particles the critical impact velocity was found to decrease from 100 m/s to 75 m/s at room temperature and from 80 m/s to 65 m/s at the particle temperature of T_p = 80 °C. The slope of the dashed lines connecting the critical impact velocity at the bottom of the deposition windows in Figure 54 – Figure 56 shows little variation between the case of pure polymer particle cold spray results and the case of polymer/glass beads cold spray depositions.

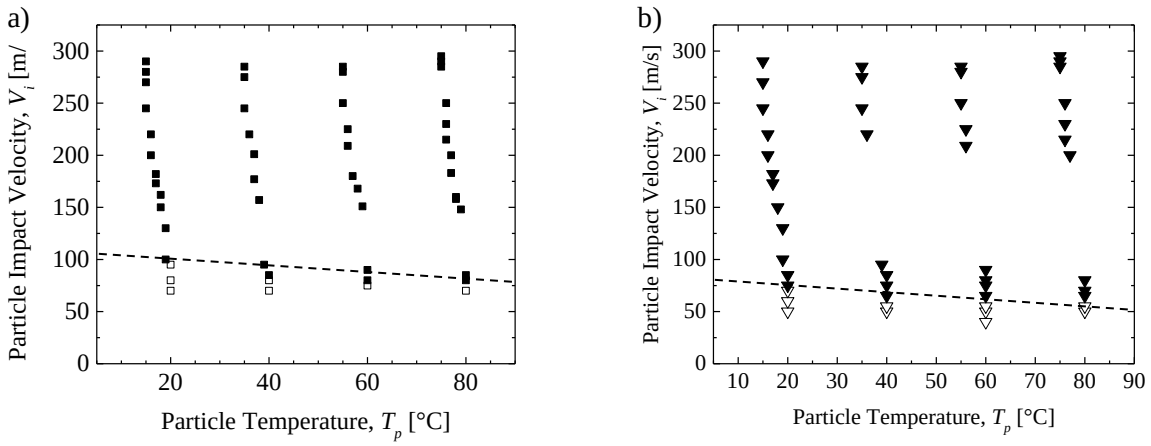

Figure 54 – Cold spray deposition window for HDPE particles (a) with and (b) without the addition of glass beads. The ratio of HDPE particles to the glass beads is 9:1 in terms of weight percent. The substrate temperature is T_s = 100 °C in all experiments. The plots show a transition from no deposition (hollow symbols) to deposition (solid symbols).

The cold spray results shown in Figure 55, indicate that for PS particles, the minimum impact velocity for successful deposition was only shifted down by 5 – 10 m/s after adding 10 wt.% glass beads. However, it can be seen from Figure 55 that the maximum impact velocity for successful deposition was shifted up by 15 m/s resulting in an improved deposition window on both ends.

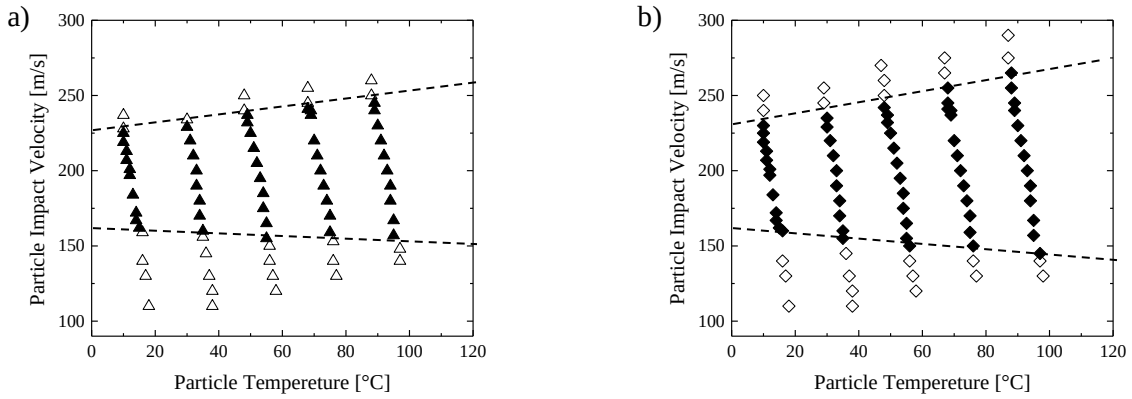

Figure 55 – Cold spray deposition window for polystyrene particles (a) with and (b) without the addition of glass beads. The ratio of HDPE particles to the glass beads is 9:1 in terms of weight percent. The substrate temperature is T_s = 100 °C in all experiments. The plots show a transition from no deposition (hollow symbols) to deposition (solid symbols).

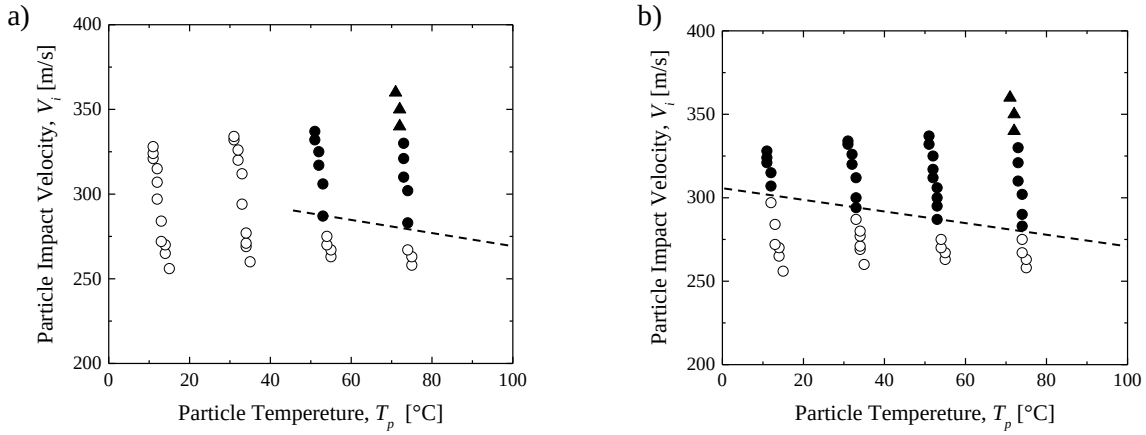

Figure 56 – Cold spray deposition window of UHMWPE particles (a) without and (b) with 10 wt.% glass beads with the average size of D = 20 ± 10 µm on an LDPE substrate showing the transition from no deposition (o) to deposition (●, ▲). The solid triangle symbols (▲) correspond to the results from using the supersonic nozzle. In all cases, the substrate was held fixed at T_s = 100 °C and the stand-off distance was 10 mm. The dashed lines are not meant to be quantitative but are simply there to guide the reader's eye. The plots show a transition from no deposition (hollow symbols) to deposition (solid symbols).

Finally, the deposition window for the UHMWPE particles for both the pure UHMWPE particles and the polymer plus 10% glass bead blend are shown in Figure 56. Here the most stark contrast can be observed after the addition of glass beads. Without peening glass beads, the deposition of UHMWPE at room temperature was not possible, however, after the addition of 10 wt.% glass beads to the UHMWPE, deposition was achieved. This deposition occurred at subsonic velocities meaning that deposition was viable over a range of velocities where the glass beads were not incorporated into the UHMWPE coating.

Interestingly, unlike the other polymers tested, the deposition windows in Figure 56 was not expanded to lower impact velocities with the addition of the 10 wt.% glass beads to the UHMWPE powder.

8.8 AFM Studies

In the peening of metals, often one of the goals is to smooth the surface and decrease its surface roughness. The surface roughness of the pure HDPE deposition was about 1.2 μm which is twice the surface roughness of the melt cast HDPE sample which was 0.6 μm, Figure 57. After adding 10 wt.% glass beads to the HDPE particle batch, the surface roughness of the cold sprayed deposition was reduced to 0.5 μm. As a result, the deposited surface when peening particles were included, was even smoother than the melt cast sample. This result shows that the addition of peening particles is reducing the roughness of the cold sprayed substrate. This has positive implications for the final finish of the deposited layer, but it also likely helps explain the increased deposition efficiency. Our previous work suggested that deposition occurred for polymer powders only below a critical particle-substrate impact angle. Surface roughness can cause failure of particle deposition if the impact is at too acute an angle to the local roughness. In addition, single particle impact measurements show very little, 1.5 %, plastic deformation of successfully deposited particles meaning that they can be easily sheared off by secondary particles, but also cause a dramatic increase in the surface roughness. Peening particles clearly help smooth the overall surface and flatten already deposited particles making them more strongly adhered and more conductive for successful deposition of the successive polymer particle during impact.

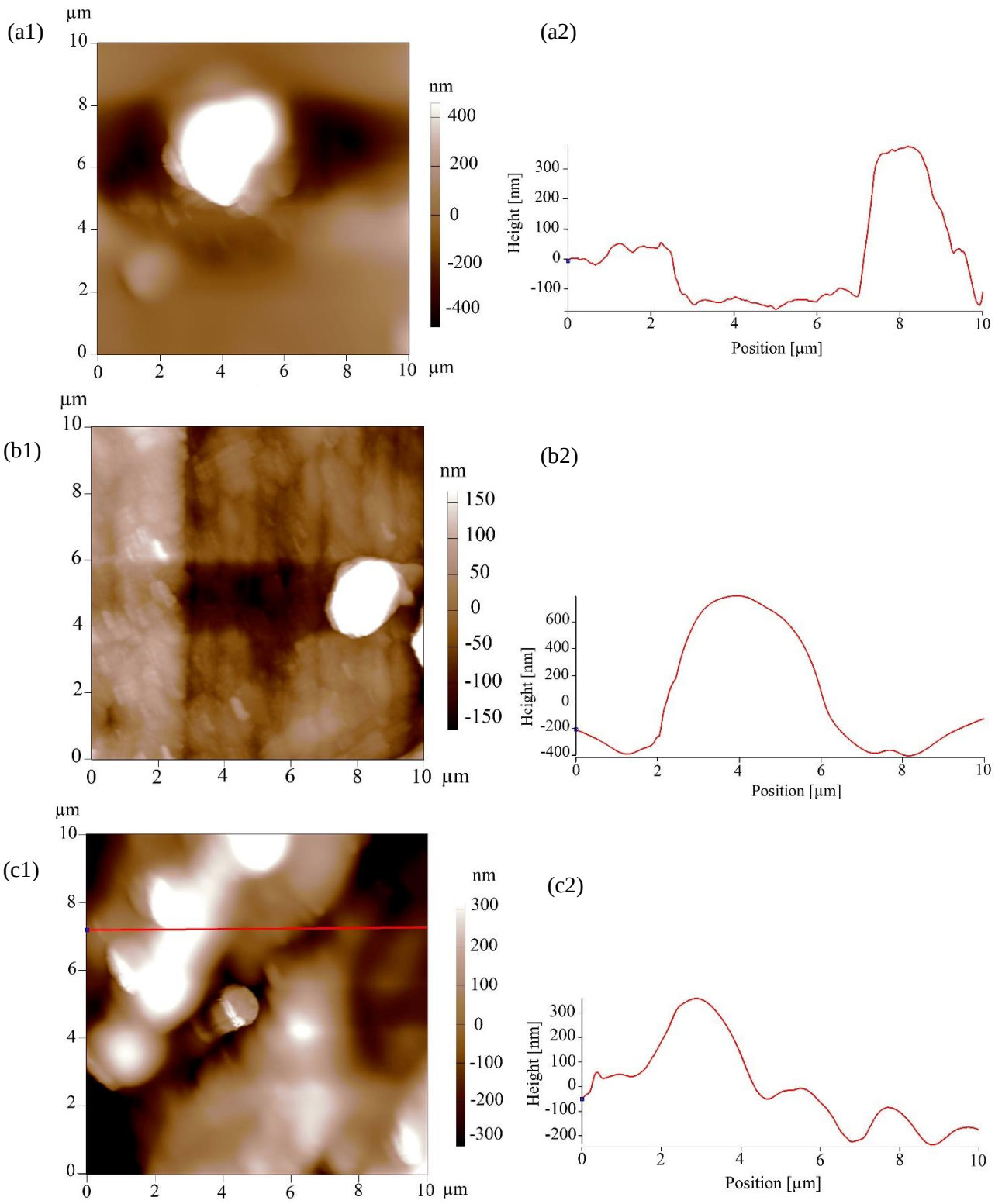

Figure 57 – 2D AFM images of (a1) a melt cast HDPE substrate, (b1) a cold sprayed HDPE sample on an LDPE substrate, and (c1) a cold sprayed HDPE deposition with 10 wt.% added glass beads, and (a2), (b2), c2) the section analysis of 2D images. The particle temperature, substrate temperature, and particle impact velocity were T_p = 60 °C and T_s = 100 °C and V_i = 275 m/s in the cold spray process – Provided by Z. Zhu.

CHAPTER 9
COLD SPRAY DEPOSITION OF CORE-SHELL PARTICLES

This chapter is a collaborative work with two other research groups. The synthesis and development of the core-shell particles have been performed by Gouzhen Yang and Yuan Liu, the two postdocs from Professor Klier and Professor Schiffman's research group. The cold spray process has been done by me in the Non-Newtonian Fluid Dynamic Lab. The single particle impact experiments are implemented by Wanting Xie from Professor Lee's group and finally the characterization of the cold sprayed coatings is done by Yuan Liu from Professor Schiffman's research group.

In this chapter, the study of the cold spray deposition of a particular polymer particle with a core-shell structure, as depicted in Figure 58 is presented. The core is a combination of a reactive component and a carrier component. Bisphenol A diglycidyl ether (commonly abbreviated as BADGE or DGEBA) acts as the reactive component and poly butyl acrylate (PBA) is the carrier component in this study. Non-crosslinked polyurea is used to form the 7-17 μm thick shell for this particle and is made of poly methyl methacrylate (PMMA) which is a brittle material that melts at T_m = 160 °C. The glass transition temperature for BADGE and PBA is T_g = -19°C and T_g = -39°C, respectively. The core compound melts slightly above room temperature and thus could undergo severe plastic deformation under the high strain rates in the cold spray process. The brittle shell breaks at the particle impact on the substrate surface letting out the reactive and liquid-like core material which splashes to form coatings on the substrate. As described in previous sections, plastic deformation is critical to the particle/substrate bonding process. Therefore, this material was a promising choice for the cold spray process which eventually could improve the deposition efficiency to above 50%. This core-shell powder material was provided by Yuan Liu from Professor John Klier's research lab and was synthesized through a suspension polymerization process. The related setup is shown in Figure 59. Suspension polymerization is a heterogeneous polymerization process that uses mechanical agitation to mix a monomer or mixture of monomers in a liquid phase while the monomers polymerize, forming spheres of polymer. In the suspension polymerization process that led to the production of the core-shell particles for this study, the oil phase consisted of DGEBA, acrylate monomer (DGEBA diluent), and hydrophobic shell reactant and the aqueous phase included polyvinyl alcohol (PVA) solution and hydrophilic shell reactant.

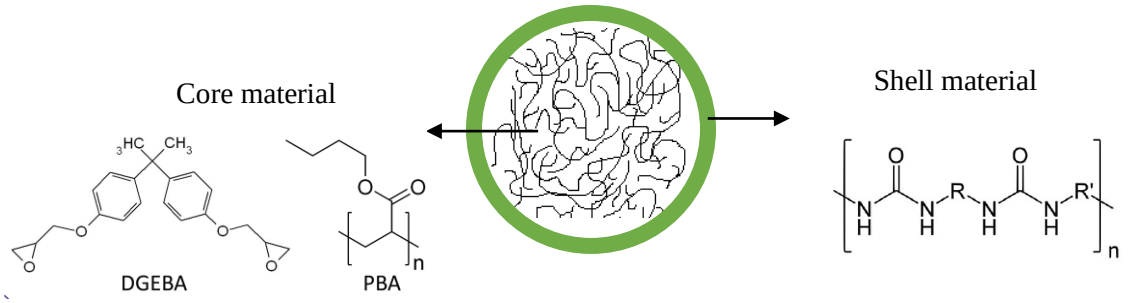

Figure 58 – the core-shell structure- image provided by Yuan Liu


Figure 59 – the setup for the suspension polymerization process - image provided by Yuan Liu

The particle size was controlled through the critical micelle concentration (CMC) of sodium dodecyl sulfate (SDS) and the oil phase viscosity. The spheres produced through the suspension polymerization process have zero volatile organic compounds (VOC) and are thus environmentally friendly. The rigid shell stabilizes the liquid-like core material during the suspension polymerization process. For the following experimental results The DGEBA/PBA ratio was 71 : 29 wt.%. Cold spray deposition of the core-shell particles on galvanized steel under air pressure of 90 psi, the air speed of 370 m/s and particle flowrate of 30-50 g/min was studied using the supersonic nozzle in the cold spray setup. An example of a cold sprayed sample can be seen in Figure 60.

Figure 60 – Cold spray deposition of the core-shell particles on galvanized steel

Cold spray deposition results including the deposition efficiency, the particle size, and the shell thickness are presented in Figure 61 as functions of the critical micelle concentration (CMC) of sodium dodecyl sulfate (SDS). As seen from this figure, deposition efficiency increased from 2% for the 260 µm particle size and 16 µm-thick shell to 8.2% for the 100 µm particle size and 7 µm-thick shell. Thus, it is obvious that smaller particle size led to higher impact speed. The shell was also thinner for smaller particles and a thinner shell thickness was easier to break.

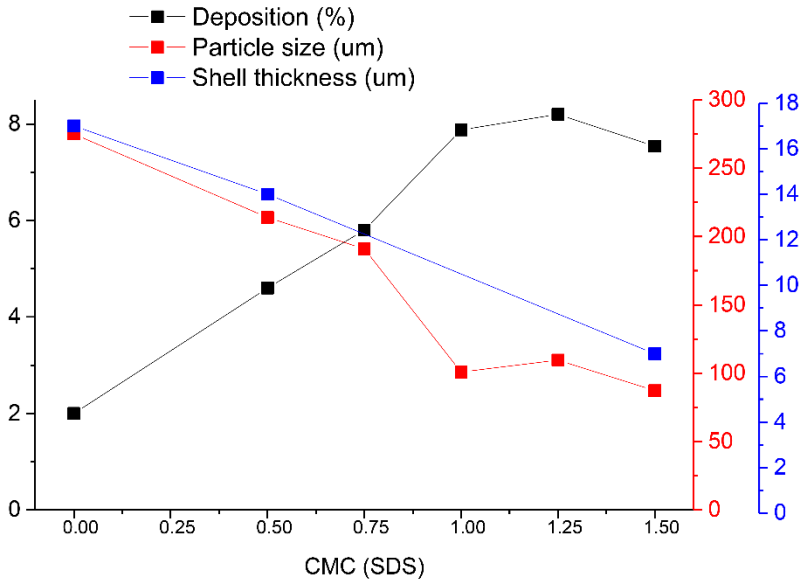

Figure 61 – Cold spray deposition results for the core-shell particle. The data include the deposition efficiency, particle size, shell thickness as functions of the critical micelle concentration (CMC) of sodium dodecyl sulfate (SDS)- image provided by Yuan Liu

In Figure 62, SEM image of a multi-layer cold spray deposition of the core-shell particles on galvanized steel is presented. It is seen from this figure that the early incoming particles that hit the hard surface of the metal substrate have been broken and have formed a good coalescence with each other and with the substrate surface. Other particles deposited visible on the top layers, on the other hand, show that secondary layers of the core-shell particles did not break to form a uniform coating on the top deposited layers.

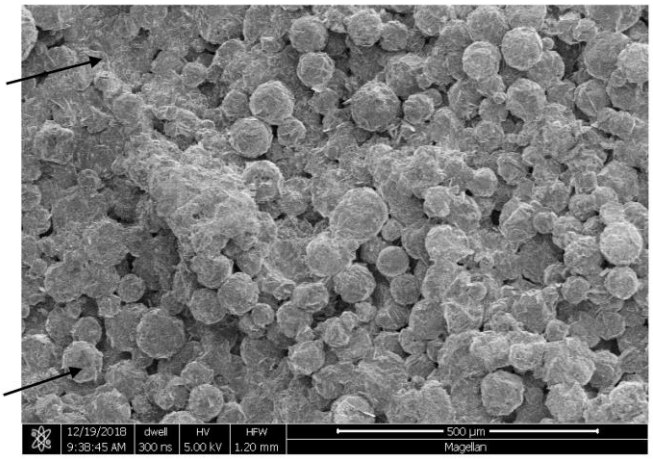

Figure 62 – SEM image of a multi-layer cold spray deposition of the core-shell particles on galvanized steel- image provided by Yuan Liu

In another trial, Yuan Liu increased the fluidity of the core material by including only the DGEBA component in the core and removing the PBA component from it. For this purpose, she mixed a combination of DGEBA, methylene chloride (DGEBA diluent), and hydrophobic shell reactant as the oil phase and a combination of polyvinyl alcohol (PVA) solution and hydrophilic shell reactant as the aqueous phase in a suspension polymerization process to form the core-shell particles with the average size of about 90 µm. These particles were cold sprayed on a galvanized steel substrate under the same process conditions as the previous one. The SEM image of the coating can be seen in Figure 63.

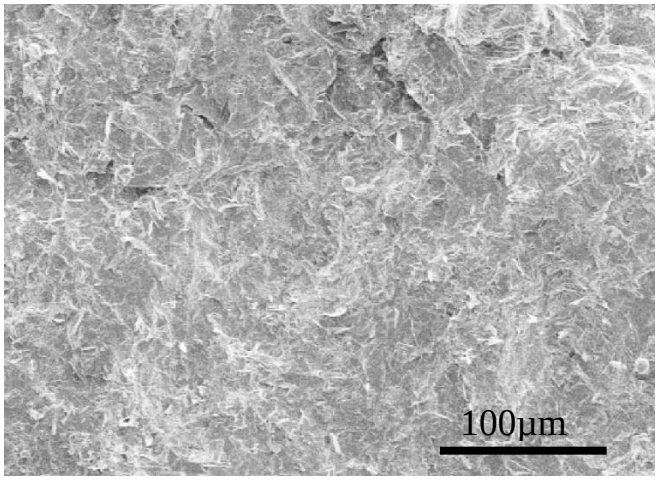

Figure 63 – SEM image a cold sprayed sample of the core-shell particles with the core material with the lower viscosity- image provided by Yuan Liu

The deposition efficiency increased by a factor of 4 to about 28% for the core shell particles with the core material which only had the DGEBA component and thus a lower viscosity. In another trial with a much lower flowrate of 7 g/min, these particular core-shell particles exhibited a remarkable deposition efficiency of 57% as the particles were accelerated with the air flow with the pressure of 90 psi and velocity of 370 m/s through the supersonic cold spray.

The effect of particle flowrate on the deposition efficiency was also investigated and the results are shown in Figure 64. It is seen from this figure that the 40 g/min particle flowrate works best for the particle size range of 100 – 110 µm and 30 g/min works best for the finer core-shell particle of the size of 87 µm. The substrate was again galvanized steel in all experiments and the cold spray conditions included the air pressure at 90 psi and air speed at 370 m/s at room temperature.

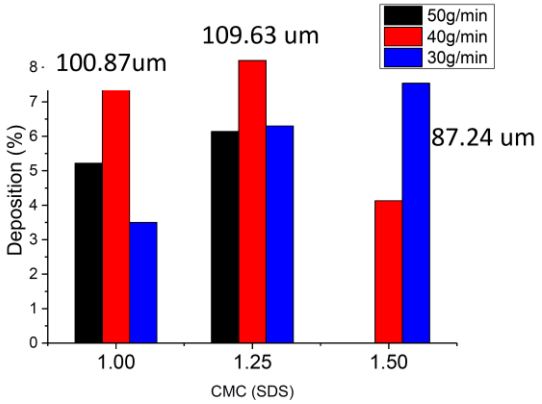

Figure 64 – Cold spray results for the core-shell particles deposited on a galvanized steel at different particle flowrates from the nozzle- image provided by Yuan Liu

Laser induced single particle acceleration experiments were also conducted on the core-shell particles to directly monitor single particles during flight, impact, and either rebounding or depositing on the galvanized steel surface at room temperature. The rebound velocity of the particles was plotted against the impact velocity over the 100 – 700 m/s impact velocity studied in this set of laser induced single particle impact experiments and is shown in Figure 65. It is seen from this figure that as the glass transition temperature of the core material decreases from T_g = 20 °C to -39 °C, the critical velocity also decreases from V_{cr} = 430 m/s to 308 m/s. It is also seen in this figure that the rebound velocity for a core material with the glass transition temperature of T_g = 20 °C is about 30 m/s more than that with the glass transition of T_g = -39 °C.

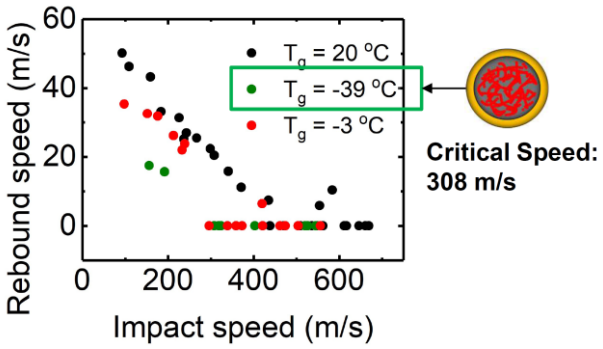

Figure 65 – the rebound speed of the core-shell particles as a function of particle impact speed in the laser induced single particle impact experiment. The particle size was 70 – 90 µm- image provided by Yuan Liu

The SEM studies of the deposited particles are also presented in Figure 66 for three different particle impact velocity in the laser induced single particle impact experiments. It is obvious from this figure that as the particle impact velocity increases the shell material breaks to much more pieces and the core material splashes to cover a larger area on the substrate surface leading to a stronger bonding with the substrate material.

Figure 66 – SEM images of the core-shell particles deposited on a galvanizes steel substrate at different impact velocities

CHAPTER 10

A MESSAGE TO THE NEXT STUDENT

In this research project, several polymer particles were studied as the feedstock powder for the cold spray deposition process. However, the effect of size was only explored for one of the polymers, HDPE. Shape and size of the sprayed particles are important parameters which could significantly affect the flowability of the particles through the powder feeding hopper and out of the nozzle, the angle of impact on the substrate and the final deposition efficiency. From my own experience, particles with good flowability were not very adhesive as were sprayed on the substrate. On the other hand, particles with less flowability through the powder feeding hoper, were more ready to adhere onto the substrate, but were more difficult to be released outside the vibrating hopper. Therefore, an appropriate start for the next student who is going to investigate cold spray for polymers using the setup in NNFD lab, could be the analysis of the effect of size and shape of the feedstock powder on final results and to find a reliable balance between flowability and the bonding procedure.

In chapter 8 of this dissertation, where I studied the effect of adding glass beads to the polymer powder on properties like deposition efficiency and deposition window, I kept the polymer particle size fixed and varied other parameters such as the size and amount of the added glass beads and the temperature and velocity of particles in each experiment. The effect of polymer particle size was not investigated there. Therefore, the next student can extend these experiments by studying the cold spray deposition of different particle size of polymer powders with added glass beads or metal beads. This way the correlation between particle size and deposition behavior could be further understood. In addition, this could also be worthwhile to study the adhesion/cohesion strength of the coated polymers with the 10 wt.% added glass beads to see whether or not the peening effect of the sacrificial glass beads could also affect the bonding strength either adhesively or cohesively.

Another promising approach could be the study of adding nano-particles to the polymer powders. These nano-particles could be ceramic or metal. For instance, ceramic nano-particles like titanium oxide and alumina [36] are proven to enhance the likelihood of hydrogen bonds between the particles and the substrate in the cold spray process. Metal nanoparticles such as cupper, on the other hand, can improve deposition efficiency simply by increasing the density of the polymer particles and thus the kinetic energy at impacting the substrate which can eventually result in an improved deposition efficiency. Cupper nanoparticles could also bring some antibacterial properties to the coated surface and thus could be an

important research area from the application viewpoint. Therefore, the next student can investigate the deposition of nanocomposites on a variety of substrates.

My final recommendation for the next student is to study the cold spray process from the application viewpoint. For example, High-density polyethylene has been widely used in marine antifouling surfaces [20] and as the embedded materials for fibers in pipeline networks coatings [21]. In oil/water separation systems, it has been used as a favorable coating with good self-cleaning property, corrosion resistance, thermal and wear stability along with superoleophilicity [23]. Polyurethane-based coatings are also used universally in the aviation, automotive, and medical industries due to their relative resistance to abrasion and degradation and high impact strength at low temperatures [24]. Polyurethane, as the organic phase in organic/inorganic hybrid coatings improves flexibility and mechanical properties, while the inorganic phase protects the surface from corrosion [25]. Thus, polyurethane/polysiloxane hybrid coatings has recently been successfully studied as candidates for replacement of chromate conversion coatings in aerospace industry to address health and environmental challenges associated with the later coatings. Acrylic polyurethane is a widely used coating for engineering equipment due to its significant antiaging properties [26]. UHMWPE is utilized in the applications demanding high wear resistance, high impact resistance and high cavitation erosion resistance. UHMWPE is a comparably efficient (high strength to weight ratio), inexpensive and an easily procurable option to hard alloys and intermetallic compounds which are often used in such applications [36]. Other polymers, either studied in this research project or not, all have broad applications as coatings. None of these coatings, however, has been created by the cold spray technique yet. Therefore, it is worth to cold spray these polymer particles and then begin to study the properties such as corrosion resistance, thermal stability, wear resistance, hydrophobicity, oleophilicity, impact resistance and cavitation erosion resistance and compare the results to the required standards for each of these applications. This way, the cold spray technique might even become a primary additive manufacturing technique for polymers in wide range of industrial applications.

CHAPTER 11

CONCLUSIONS

A laboratory-scale cold spray setup was used in this research to study the deposition of several polymeric materials on polymeric substrates. A material-dependent window of successful deposition was determined for each particle/substrate combination as a function of particle temperature and impact velocity. These deposition maps allowed for a deeper comparison between the deposition mechanisms of the studied polymers with reported metal cold spray results.

The critical impact velocity, above which successful deposition was observed, was shown to decrease with increasing temperature of the depositing particles. Additionally, like metals, a mismatch between the modulus of the particle and the substrate was found to be beneficial for particle deposition, resulting in a decrease in the critical impact velocity. Unlike the cold-spray deposition of metallic particles, the empirical model used to predict the critical impact velocity for metallic particles was found to vastly over-predict the particle velocities and kinetic energy necessary to achieve deposition. For the HDPE particles used in these studies, the critical impact velocity was found to be in the range of V_{pi} = 100 m/s to 150 m/s while the predictions of the empirical model used in metal cold-spray predicted a value that was a factor of three larger between 300m/s and 450m/s.

Despite the reduced particle velocity and kinetic energy demands, the maximum deposition efficiency reported by the literature on polymer cold spray was less than 1% [12]. This deposition efficiency is much smaller than what has been reported for metallic cold-spray. In the present research, a detailed investigation into the deposition efficiency over a wide range of processing conditions was performed. The processing conditions varied included the particle temperature, particle impact velocity, particle size, substrate material, substrate temperature and the standoff distance between the nozzle and the substrate. The present study revealed that increasing particle temperature, particle impact velocity, and substrate temperature, all had a positive effect on deposition efficiency. Additionally, reducing particle size was also shown to have a significant effect on deposition efficiency. The stand-off distance between the nozzle and the substrate had a non-monotonic effect. An optimal distance was observed that balances the acceleration of the particle with its cooling during its time of flight. By optimizing operational parameters, deposition efficiency of almost 10% was achieved for the cold-spray deposition of HDPE particles. This represents an order of magnitude improvement on the best results presented in the literature.

A comparison between the cold spray results and those of a laser-induced single particle impact experiment was carried out for HDPE, polyurethane, polystyrene and polyamide 12. In the laser-induced

single particle impact experiments, the impact, critical and rebound velocities were measured through direct ultrafast laser photography. The plastic deformation and the percent of kinetic energy dissipation were quantified after studying the optical images and scanning electron microscopy of the single particles deposited through the laser-induced single particles impact experiments. Particle size did not seem to affect deposition in the laser induced single impacts within the size ranges studied here. However, the choice of substrate had a large effect on the adhesion process in both deposition techniques. The softer LDPE substrate was found to reduce the critical velocity for cold spray deposition by about 20 m/s for HDPE particles compared to deposition on HDPE. In the laser-induced single particle impact experiment, changing the substrate from LDPE to HDPE made deposition impossible. The lack of like-on-like deposition in the single particle impact experiments was also seen previously for high- T_g polymers like PS and PA. This observation suggests that multiple particle impacts or sequential particle impacts that heat, deform and smooth out the substrate are necessary to make cold spray deposition possible. Multiple particle impacts may also be a reason that the deposition efficiency in cold spray is significantly lower than the single particle impact experiment. Secondary impacts may strip weakly adhered particles from the substrate, especially in the case of the low velocity depositions where plastic deformation of the adhered particle is relatively small. Comparing low-T_g particle impacts to high-T_g particle impacts, a number of trends can be observed. First, low-T_g particles appear to dissipate more energy than high-T_g particles of the same impact velocities. Second, upon successful deposition, the low-T_g particles were found to undergo significantly more plastic deformation at the same impact velocities resulting in a better adhered particle and a smoother resulting substrate for further impacts. These differences likely account for the higher deposition efficiencies of low-T_g as compared to high-T_g polymer powders.

In the micro-ballistic single particle impact experiments, the plastic deformation of polystyrene particles was an order of magnitude smaller than that of metals depositing on sapphire in a same process but at considerably higher impact velocities. The cold spray process showed a monotonic increase in deposition efficiency of the studied polymer materials with the impact velocity which is quite different from that of metals which more looks like a step function. Although like-on-like deposition was not possible for HDPE in the single particle acceleration experiments, the percent of energy dissipation was still higher than those of polystyrene and polyamide 12 in like-on-like cases over the 50 – 500 m/s impact velocity range. Plastic deformation plotted against particle impact velocity for the low-T_g polymers fell on a steep line (slope = 0.18) while those of high-T_g polymers increased at a much lower slope, 0.046, as impact velocity increased. The plastic deformation as a function of impact velocity for aluminum particles depositing on either sapphire or aluminum in laser-induced single particle impact experiments showed similar linear trends to that of the low-T_g polymers studied in this work. The critical velocity obtained from the two deposition methods were roughly in the same range for each particle/substrate pair. No upper limit velocity

was found over the 50 – 500 m/s and 50 – 300 m/s impact velocity ranges for the laser-induced single impacts and the cold spray process, respectively. The modulus mismatch between the particle and substrate proved favorable in both deposition techniques. The enhanced plastic deformation in both the primary particle and the substrate beneath the primary particle due to the successive head on particle collisions might explain why we achieved like-on-like deposition in the cold spray process but not in the micro-ballistic single particle impacts for HDPE, polyamide and polystyrene particles. Adding about 10 wt.% sacrificial glass beads to the particle batch could improve the deposition efficiency and broaden the deposition maps. However, these glass beads should be same size or larger than the particles and should not exceed the speed of sound. Addition of the 10 wt.% glass beads also made deposition of UHMWPE possible at room temperature.

Finally, the study of the maximum tilting angle for successful deposition, revealed that when the particle impacts take place on a tilted substrate, the normal component of the impact velocity on the substrate surface should equal or surpass the critical velocity obtained from deposition on a flat substrate. This finding indicates that in creating a conformal coating on 3D objects, it is essential that the robotic arm holding the nozzle continuously changes its position with regard to the 3D object to ensure a high enough normal component for the particle impact velocity.

BIBLIOGRAPHY

[1] H. Assadi, T. Scmidth, H. Richter, J.-O. Kliemann, K. Binder, F. Gartner, T. Klassen, and H. Kreye, "On Parameter Selection in Cold Spraying," *Thermal Spray Technology,* p. 1161-1176, 2011.

[2] M. Gardon, A. Latorre, M. Torrell, S. Dosta, J. Fernandez, J.M. Guilemany, "Cold gas spray titanium coatings onto a biocompatible polymer," *Materials Letters,* vol. 106, p. 97-99, 2013.

[3] X.L. Zhou, A.F. Chen, J.C. Liu, X.K. Wu, J.S. Zhang, "Preparation of metallic coatings on polymer matrix composites by cold spray," *Surface & Coatings Technology,* no. 206, p. 132–136, 2011.

[4] H. Assadi, H. Kreye, F. Gartner, T. Klassen, "Cold spraying: A materials perspective," *Acta Materialia,* vol. 116, p. 382-407, 2016.

[5] V.K. Champagne, D. Helfritch, P. Leyman, S. Grendahl, B. Klotz, "Interface Material Mixing Formed by the Deposition of Copper on Aluminum by Means of the Cold Spray Process," *Thermal Spray Technology,* vol. 14, no. 3, p. 330-334, 2005.

[6] V.K. Champagne, The Cold Spray Materials Deposition Process: Fundamentals and Applications, Woodhead Publishing, Cambridge: Woodhead Publishing, 2007.

[7] A. Ganesan, J. Affi, M. Yamada, M. Fukumoto, "Bonding behavior studies of cold sprayed copper coating on the PVC polymer substrate," *Surface & Coatings Technology,* no. 207, p. 262–269, 2012.

[8] R. Lupoia, C. Stensona, K.A. McDonnellb, D.P. Dowlingb, E. Ahearne, "Antifouling coatings made with Cold Spray onto polymers: Process characterization," *CIRP Annals - Manufacturing Technology,* vol. 65, p. 545–548, 2016.

[9] G. Archambault, B. Jodoin, S. Gaydos, M. Yandouzi, "Metallization of carbon fiber reinforced polymer composite by cold spray and lay-up molding processes," *Surface & Coatings Technology,* vol. 300, p. 78–86, 2016.

[10] A.S. Alhulaifi, G.A. Buck, W.J. Arbegast, "Numerical and Experimental Investigation of Cold Spray Gas Dynamic Effects for Polymer Coating," *Thermal Spray Technology,* vol. 21, p. 852-862, 2012.

[11] K. Ravi, Y. Ichikawa, T. Deplancke, K. Ogawa, O. Lame, J.-Y. Cavaille, "Development of Ultra-High Molecular Weight Polyethylene (UHMWPE) Coating by Cold Spray Technique," *Thermal Spray Technology,* vol. 24, no. 6, p. 1015-1025, 2015.

[12] Y. Xu, I.M. Hutchings, "Cold spray deposition of thermoplastic powder," *Surface & Coatings Technology,* vol. 201, p. 3044–3050, 2006.

[13] T.P. Bush, Z. Khalkhali, V.K. Champagne, D.P. Schmidt, J.P. Rothstein, "Optimization of Cold Spray Deposition of High-Density Polyethylene Powders," *Thermal Spray Technology,* vol. 26, no. 7, p. 1548–1564, 2017.

[14] H. Che, P. Vo, S. Yue, "Metallization of carbon fibre reinforced polymers by cold spray," *Surface & Coatings Technology,* vol. 313, p. 236–247, 2017.

[15] F. Meng, D. Hu, Y. Gao, S. Yue, J. Song, "Cold-spray bonding mechanisms and deposition efficiency prediction for particle/substrate with distinct deformability," *Materials and Design,* vol. 109, p. 503–510, 2016.

[16] M. Grujicic, J.R. Saylor, D.E. Beasley, W.S. DeRosset, D. Helfritch, "Computational analysis of the interfacial bonding between feed-powder particles and the substrate in the cold-gas dynamic-spray process," *Applied Surface Science,* no. 219, p. 211-227, 2003.

[17] M. Grujicic, C.L. Zhao, W.S. DeRosset, D. Helfritch, "Adiabatic shear instability based mechanism for particles/substrate bonding in the cold-gas dynamic-spray process," *Materials and Design,* no. 25, p. 681–688, 2004.

[18] R. Nikbakht, S.H. Seyedein, S. Kheirandish, H. Assadi, B. Jodoin, "Asymmetrical bonding in cold spraying of dissimilar materials," *Applied Surface Science,* vol. 444, p. 621–632, 2018.

[19] S. Shah, J. Lee, J.P. Rothstein, "Numerical Simulations of the High Velocity Impact of a Single Polymer Particle during Cold Spray Deposition," *Thermal Spray Technology,* vol. 26, no. 5, p. 970-984, 2017.

[20] W.-Y. Li, C. Zhang, H.-T. Wang, X.P. Guo, H.L. Liao, C.-J. Li.,, "Significant influences of metal reactivity and oxide films at particle surfaces on coating microstructure in cold spraying," *Applied Surface Science,* vol. 253, no. 7, p. 3557-3562, 2007.

[21] W.-Y. Li, C. Zhang, X. Guo, C.-J. Li, H. Liao, C. Coddet, "Study on impact fusion at particle interfaces and its effect on coating microstructure in cold spraying," *Applied Surface Science,* vol. 254, no. 2, p. 517-526, 2007.

[22] T. Hussain, "Cold Spraying of Titanium: A Review of Bonding Mechanisms, Microstructure and Properties," *Key Engineering Materials,* vol. 533, p. 53-90, 2013.

[23] S.V. Klinkov, V.F. Kosarev, M. Rein, "Cold spray deposition: Significance of particle impact phenomena," *Aerospace Science and Technology,* vol. 9, no. 7, p. 582–591, 2005.

[24] T. Hussain, D.G. McCartney, P.H. Shipway, D. Zhang, "Bonding Mechanisms in Cold Spraying: The Contributions of Metallurgical and Mechanical Components," *Thermal Spray Technology,* vol. 18, p. 364-379, 2009.

[25] Z. Khalkhali, W. Xie, V.K. Champagne, J.-H. Lee, J. P. Rothstein, "A comparison of cold spray technique to single particle micro-ballistic impacts for the deposition of polymer particles on polymer substrates," *Surface & Coatings Technology,* vol. 351, p. 99-107, 2018.

[26] C. Chen, X. Xie, Y. Xie, X. Yan, Ch. Huang, S. Deng, Z. Ren, H. Liao, "Metallization of polyether ether ketone (PEEK) by copper coating via cold spray," *Surface & Coatings Technology,* vol. 342, p. 209–219, 2018.

[27] A. Papyrin, V. Kosarev, S. Klinkov, A. Alkhimov, V.M. Fomin, Cold Spray Technology, Elsevier, 2007.

[28] T. Schmidt, F. Gartner, H. Assadi, and H. Kreye, "Development of a Generalized Parameter Window for Cold spray Deposition," *Acta Materialia*, vol. 56, no. 3, p. 729-742, 2006.

[29] W. O. N. R. Lupoi, "Deposition of metallic coatings on polymer surfaces using cold spray," *Surface and Coatings Technology*, vol. 205, no. 7, p. 2167–2173, 2010.

[30] C.R.C. Lima, N.F.C. de Souza, F. Camargo, "Study of wear and corrosion performance of thermal sprayed engineering polymers," *Surface and Coatings Technology*, vol. 220, p. 140 - 143, 2013.

[31] V.K. Champagne, D.J. Helfritch, S.P.G. Dinavahi, P.F. Leyman, "Theoretical and Experimental Particle Velocity in Cold Spray," *Thermal Spray Technology*, vol. 20, p. 425–431, 2011.

[32] A.H. Shapiro, The Dynamics and Thermodynamics of Compressible Fluid Flow, The Ronald Press Company, 1953.

[33] W. Xie, A.A. Dehkharghani, Q. Chen, V.K. Champagne, X. Wang, A.T. Nardi, S. Kooi, S. Muftu, J.-H. Lee, "Dynamics and extreme plasticity of metallic microparticles in supersonic collisions," *Scientific Reports*, vol. 7, no. 5073, p. 1-9, 2017.

[34] G.M. Swallowe, Mechanical Properties and Testing of Polymers an A-Z Reference, Netherlands: Springer, 1999.

[35] H. Suzuki, J. Grebowicz, B. Wunderlich, "The Glass Transition of Polyoxymethylene," *British Polymer Journal*, vol. 17, no. 1, p. 1-3, 1985.

[36] K. Ravi, T. Deplancke, K. Ogawa, J-Y. Cavaille, O. Lame, "Understanding deposition mechanism in cold sprayed ultra high molecular weight polyethylene coatings on metals by isolated particle deposition method," *Additive Manufacturing*, vol. 21, p. 191–200, 2018.

[37] W.C. Oliver, G.M. Pharr, "An improved technique for determining hardness and elastic modulus using load and displacement sensing indentation experiments," *Materials Research*, vol. 7, p. 1564–1583, 1992.

[38] W.C. Oliver, G.M. Pharr, "Measurement of hardness and elastic modulus by instrumented indentation: advances in understanding and refinements to methodology," *Materials Research*, vol. 19, pp. 3-20, 2004.

[39] "Standard Test Method for Adhesion or Cohesion Strength of Thermal Spray Coatings'', C633, Annual Book of ASTM Standards, ASTM, 2013, P. 8.

[40] K. Petrackova, J. Konda, M. Guagliano, "Mechanical Performance of Cold-Sprayed A357 Aluminum Alloy Coatings for Repair and Additive Manufacturing," *Thermal Spray Technology*, vol. 26, p. 1888–1897, 2017.

[41] J.H. Lienhard, A heat transfer textbook, Prentice-Hall, 1981.

[42] T.G. Mezger, Applied Rheology, Austria: Anton Paar GmbH, 2015.

[43] A. Groisman, V. Steinberg, "Elastic turbulence in a polymer solution flow," *Nature,* vol. 405, p. 53-55, 2000.

[44] B. Yildirim, S. Muftu, A. Gouldstone, "Modeling of high velocity impact of spherical particles," *Wear,* vol. 270, no. 9-10, p. 703-713, 2011.

[45] K.L. Johnson, Contact Mechanics, Cambridge: Cambridge University Press, 1985.

[46] G. Bae, Y. Xiong, S. Kumar, K. Kang, C. Lee, "General Aspects of Interface Bonding in Kinetic Sprayed Coatings," *Acta Materialia,* vol. 17, p. 4858-4868, 2008.

[47] M. Strantza, D.V. Hemelrijck, P. Guillaume, D.G. Aggelis, "Acoustic emission monitoring of crack propagation in additively manufactured and conventional titanium components," *Mechanics Research Communications,* vol. 84, p. 8-13, 2017.

[48] Q. Chen, A. Alizadeh, W. Xie, X. Wang, V.K. Champagne, A. Gouldstone, J-H. Lee, S. Muftu, "High-Strain-Rate Material Behavior and Adiabatic Material Instability in Impact of Micron-Scale Al-6061 Particles," *Thermal Spray Technology,* vol. 27, no. 4, p. 641-653, 2018.

[49] H. Assadi, F. Gartner, T. Stoltenhoff, H. Kreye, "Bonding mechanism in cold gas spraying," *Acta Materialia,* vol. 51, p. 4379–4394, 2003.

[50] B.K. Pant, A.H.V. Pavan, R.V. Prakash, M. Kamaraj, "Effect of laser peening and shot peening on fatigue striations during FCGR study of Ti6Al4V," *International Journal of Fatigue,* vol. 93, p. 38-50, 2016.

[51] G-Q. Chen, Y. Jiao, T-Y. Tian , X-H. Zhang , Z-Q. Li , W-L. Zhou, "Effect of wet shot peening on Ti−6Al−4V alloy treated by ceramic beads," *Transactions of Nonferrous Metals Society of China,* vol. 24, p. 690−696, 2014.

[52] R. Ramos, N. Ferreira, J.A.M. Ferreira, C. Capela, A.C. Batista, "Improvement in fatigue life of Al 7475-T7351 alloy specimens by applying ultrasonic and microshot peening," *International Journal of Fatigue,* vol. 92, p. 87–95, 2016.

[53] M. Chen, H. Liu, L. Wang, C. Wang, K. Zhu, Z. Xu, C. Jiang, V. Ji , "Evaluation of the residual stress and microstructure character in SAF 2507 duplex stainless steel after multiple shot peening process," *Surface & Coatings Technology,* vol. 344, p. 132–140, 2018.

[54] H. Kovaci, Y.B. Bozkurt, A.F. Yetim, M. Aslan, A. Celik, "The effect of surface plastic deformation produced by shot peening on corrosion behavior of a low-alloy steel," *Surface and Coating Technology,* vol. 360, p. 78-86, 2019.

[55] G.K. Poongavanam, V. Ramalingam, "Effect of shot peening on enhancing the heat transfer performance of a tubular heat exchanger," *International Journal of Thermal Sciences,* vol. 139, p. 1-14, 2019.

[56] Q. Wu, D-J. Xie, Z-M. Jia, Y-d. Zhang, H-Z. Zhang, "Effect of shot peening on surface residual stress distribution of SiCp/2024Al," *Composites Part B,* vol. 154, p. 382–387, 2018.

[57] C. Wang, C. Jiang, F. Cai, Y. Zhao, K. Zhu, Z. Chai, "Effect of shot peening on the residual stresses and microstructure of tungsten cemented carbide," *Materials and Design,* vol. 95, p. 159–164, 2016.

[58] A. Moridi, S.M. Hassani-Gangaraj, S. Vezzu, L. Trsko, M. Guagliano, "Fatigue behavior of cold spray coatings: The effect of conventional and severe shot peening as pre-/post-treatment," *Surface and Coatings Technology,* vol. 283, p. 247-254, 2015.

[59] X-T. Luo, Y-K. Wei, Y. Wang, C-J. Li, "Microstructure and mechanical property of Ti and Ti6Al4V prepared by an in-situ shot peening assisted cold spraying," *Materials and Design,* vol. 85, p. 527–533, 2015.

[60] H. Lee, H. Shin, S. Lee, K. Ko, "Effect of gas pressure on Al coatings by cold gas dynamic spray," *Materials Letters,* vol. 62, no. 10-11, p. 1579-1581, 2008.

[61] J.W. Larson, T.B. McMahon, "Gas-phase bihalide and pseudobihalide ions: an ion cyclotron resonance determination of hydrogen bond energies in XHY- species (X, Y=F, Cl, Br, CN)," *Inorganic Chemistry,* vol. 23, no. 14, p. 2029–2033, 1984.

[62] Y. Liu, X. Shao, J. Huang, H. Li, "Flame sprayed environmentally friendly high density polyethylene (HDPE)–capsaicin composite coatings for marine antifouling applications," *Materials Letter,* vol. 238, p. 46–50, 2019.

[63] H.T. Draghicescu, D. Scarlatescu, Sorin Vlase, M.L. Scutaru, C. Nastac, "Advance high-density polyethylene used in pipelines networks," *Procedia Manufacturing,* vol. 22, p. 27–34, 2018.

[64] Y. Cheng, B. Wu, X. Ma, S. Lu, W. Xu, S. Szunerits, R. Boukherroub, "Facile preparation of high density polyethylene superhydrophobic/superoleophilic coatings on glass, copper and polyurethane sponge for self-cleaning, corrosion resistance and efficient oil/water seperation," *Colloid and Interface Science,* vol. 252, p. 76-85, 2018.

[65] C.-S. Hung, D.E. Barlow, V.A. Varaljay, C.A. Drake, A.L. Crouch, J.N. Russell Jr., L.J. Nadeau, W.J. Crookes-Goodson, J.C. Biffinger, "The biodegradation of polyester and polyester polyurethane coatings using Papiliotrema laurentii," *International Biodeterioration & Biodegredation,* vol. 139, p. 34-45, 2019.

[66] M.M. Alrashed, S. Jana, M.D. Soucek, "Corrosion performance of polyurethane hybrid coatings with encapsulated inhibitor," *Progress in Organic Coatings,* vol. 130, p. 235–243, 2019.

[67] J. Gao, C. Li, Z. Lv, R. Wang, D. Wu, X. Li, "Correlation between the surface aging of acrylic polyurethane coatings and environmental factors," *Progress in Organic Coatings,* vol. 132, p. 362–369, 2019.

[68] S. Chong, G.-T. Pan, M. Khalid, T.C.-K. Yang, S.-T. Hung, C.-M. Huang, "Physical Characterization and Pre-assessment of Recycled High-Density Polyethylene as 3D Printing Material," *Polym Environ* , vol. 25, p. 136–145, 2017.